DE-FE0029085

FINAL REPORT

Long-Term Methane Emissions Rate Quantification and Alert System for Natural Gas Storage Wells and Fields

)

Principal Investigator: Ann P. Smith, P.E., BCEE
P: 512.346.4474 | F: 512.346.4476
Email: apsmith@gsi-net.com

Issued: 18 June 2019
Revised: 29 January 2020

Prepared for: David P. Cercone
U. S. Department of Energy
National Energy Technology Laboratory
Email: david.cercone@netl.doe.gov

GSI ENVIRONMENTAL

GSI Environmental Inc.

9600 Great Hills Trail, Suite 350E, Austin, TX 78759 ■ P: 512.346.4474

TABLE OF CONTENTS

TABLES

FIGURES

APPENDICES

ACRONYMS & ABBREVIATIONS

BLM.....Bureau of Land Management
DOE .....Department of Energy
EF .....emission factor
ft.....feet
GHGI.....Green House Gas Inventory
GHGRP.....Green House Gas Reporting Program
GPS .....global positioning system
GSI.....GSI Environmental Inc.
IR .....infrared
KS .....Kolmogorov-Smirnov
LGR.....Los Gatos Research
m .....meter
MET .....meteorological station
MMcf .....million cubic feet
MQI .....method quality indicator
NETL.....National Energy Technology Laboratory
OEL.....open-ended line
OGI .....optical gas imaging
OP-FTIR.....open-path Fourier transform infrared
OTM .....other test method
ppm .....parts per million by volume (e.g., ml/m^3)
PRV.....pressure relief valve
psi .....pounds per square inch
scf/hr .....standard cubic feet per hour
SF_6 .....sulfur hexafluoride
TASC .....Technical Advisory Steering Committee
TFN.....transfer function-noise
TOC .....total organic carbon
TPH.....total petroleum hydrocarbons
USU .....Utah State University
USEPA.....U.S. Environmental Protection Agency

EXECUTIVE SUMMARY

The Department of Energy (DOE) National Energy Technology Laboratory (NETL) and other critical stakeholders (e.g., U.S. Environmental Protection Agency (USEPA), state regulators, and industry) seek to more accurately characterize and quantify methane emissions from natural gas storage wells. These efforts will reduce uncertainties in estimates of these emissions in USEPA's current Green House Gas Inventory (GHGI) under their Greenhouse Gas Reporting Program (GHGRP; EPA, 2016). Emission factors currently used to estimate methane emissions from gas storage wells are the same factors used for onshore natural gas production wells (USEPA, 2016). This study has developed a robust and representative dataset of emissions from disaggregated gas station wellhead components and related emission factors that will inform future enhancements to the GHGI and GHGRP.

Extensive methane emissions measurements and meteorological data were collected from three active storage facilities representing two of the three types of storage facilities (i.e., depleted gas reservoir and salt cavern) to support development of emissions factors specifically for gas storage wells and associated components. Methane emissions were quantified from both above-ground components (e.g., pipe fittings and valves) and seepage from the ground surface in proximity to gas storage wellheads.

Component Emissions Quantification: Large valves exhibited the highest observed emission rates followed by small valves, flanged connectors and "other" (non-flanged, e.g., threaded) connectors. Statistical tests showed no significant difference in the mean emission rates of large vs. small valves or flanged vs. other connectors. However, emissions were observed with greater frequency from large vs. small valves; therefore, subdividing storage wellhead valves by size may be important with respect to population emission factors.

Emission Factors: Disaggregated, component-specific emission factors (EF) for gas storage wellheads were developed to align with existing EF and component categories for natural gas production wells in the EPA GHGRP (40 CFR Part 98, Subpart W).

a) *Leaker EFs:* Compared to existing values used in Subpart W, the leaker EFs calculated in this study are smaller for flanged connectors and open-ended lines and similar for 'other (non-flanged) connectors' and valves. There was no statistical difference between leaker EFs for the two connector subcategories or between leaker EFs for small vs. large valves.

b) *Population EFs:* The values calculated in this study range from one sixth of the corresponding Subpart W EFs for open-ended lines to equivalence with the Subpart W EFs for undifferentiated valves. The results of this study do not support the subdivision of flanged vs. other and connectors for population EFs. However, there is a substantial difference between the population EFs for small vs. large valves.

Table ES-1. *Leaker and Population Emission Factors*

Component Type	Leaker EF (scf/hr/component)		Population EF (scf/hr/component)	
	This study	Subpart W [a]	This study	Subpart W [b]
Connector, all	0.88	n/a	0.0023	0.01
Connector, other	1.2	1.1	0.0029	n/a
Connector, flanged	0.49	3.4	0.0013	n/a
Valve, all	3.6	4.1	0.10	0.1
Valve, small	0.96	n/a	0.016	n/a
Valve, large	5.65	n/a	0.46	n/a
Pressure relief valve	nd	3.7	0.10	0.17
Open-ended line	0.27	2.3	0.0053	0.03
Gauge	nd	n/a	0.027	n/a
Regulator	0.11	n/a	0.0092	n/a

nd = not enough data, n/a = not available. [a] Values from Table W-4A, Storage Wellheads, Subpart W (USEPA, 2016). [b] Values from Table W-4, Storage Wellheads, Subpart W (USEPA, 2011).

Ground-Level Emission Fluxes: Ground-level soil emissions near the wellheads represented less than 4% of total observed per-well emissions. These exhibited large amounts of spatial and temporal variability and no significant correlations with gas storage type (depleted reservoir vs. salt cavern), operational conditions (reservoir/cavern pressures, gas injection or withdrawal rates, well temperatures, etc.) or meteorological conditions, including barometric pressure. Elevated methane fluxes were observed at one salt cavern well and five depleted reservoir wells and varied over several orders of magnitude among samples collected approximately 1 m apart from one another. The maximum estimated soil emission rate observed at any well was approximately 2 kg/day or 4 scf/hr, which is roughly equivalent to the leaker EF value for a single valve. The average estimated per-well soil emission rate was 0.1 kg/day or 0.2 scf/hr (for perspective, this value is less than the per-head enteric fermentation emission factor for most U.S. beef and dairy cattle (EPA, 1998)).

High-Resolution Below-ground Emissions Monitoring: Modeling analyses of over a year's worth of hourly monitoring data, including surface soil conditions and related meteorological and operational parameters potentially related to subsurface methane seepage, have produced a variety of expected, unexpected, and contradictory results. Consistent with the adopted conceptual model, localized daily increases in soil temperatures indicative of elevated methane degradation were observed as expected during a short-term controlled release experiment. However, when averaged over longer periods, observed temperature differentials exhibited behavior opposite to what is predicted by the conceptual model and contrary to short-term observations. Consequently, the findings are of this portion of the study are inconclusive and warrant further evaluation.

1.0 PROJECT OVERVIEW

1.1 Background and Project Description

Knowledge of methane seepage from underground natural gas storage wells is currently limited and not fully represented in the United States Green House Gas Inventory (GHGI; Zimmerle et al., 2015). The current Green House Gas Reporting Program (GHGRP; 40 CFR Part 98 Subpart W) specifies emission factors for storage wellheads based on emissions measured from above-ground components (e.g., valves and fittings) at a small population of gas production wells (EPA, 40 CFR Part 98 Subpart W; GRI, 1996). While, to date, attention has been paid to quantifying methane leakages from above-ground equipment, several investigations have shown clear evidence of methane seepage from the ground surface near gas storage wells (Lyman et al. 2016; Stolp et al., 2006). The contribution of subsurface methane leaks to the GHGI remains unknown.

For underground storage, natural gas is injected down a wellbore and into a subsurface geological formation. As gas is injected, pressure builds within the formation. Higher reservoir pressures allow higher gas flow volume during the extraction (withdrawal) part of the storage cycle to help ensure suitable production gas flow rates (Niska, 2010). Natural gas is stored in three types of underground reservoirs: depleted oil and gas (petroleum) reservoirs, aquifers, and salt caverns (see **Figure 1-1**). Ultimately, the type of a given storage facility depends on local geology, energy demand, and required reservoir capacity. Regardless of type, a typical underground natural gas storage facility contains well heads, transmission lines, a compressor station, and in some cases other equipment such as dehydrators. Most emissions associated with underground natural gas storage operations are associated with compressor-related equipment and have been quantified in previous studies (Zimmerle et al., 2015, Subramanian et al., 2015).

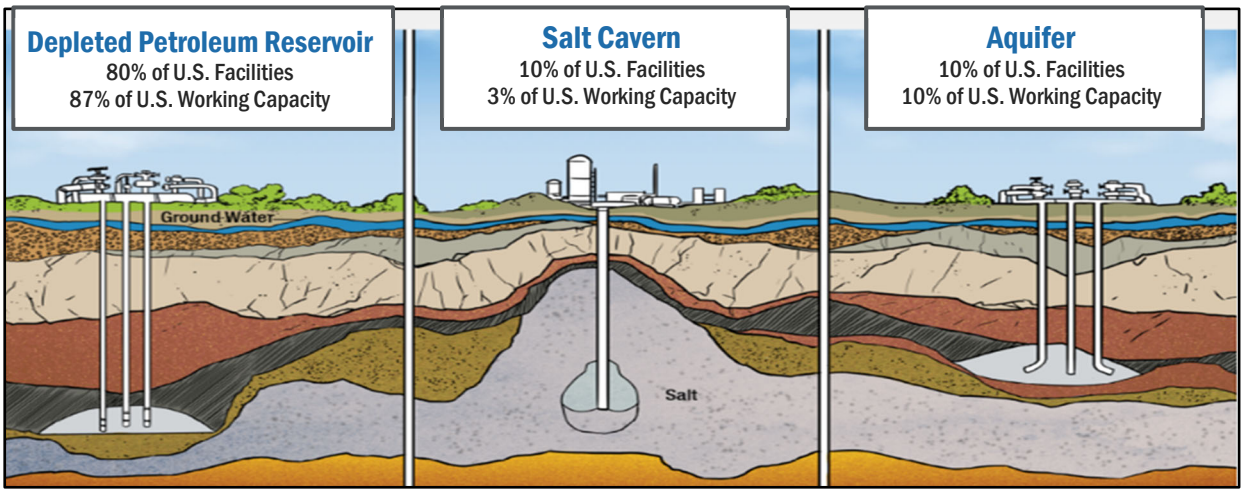

(Image source: API, 2013; Labels modified, annotations added. Data source: EIA, 2015)

Figure 1-1. *Types of Natural Gas Storage*

1.2 Project Approach

The present work aimed to quantify methane emissions both from above-ground components (e.g., pipe fittings, valves, etc.) and ground-level seepage at natural gas storage wellheads. A combination of complementary measurement methods and technologies was employed to detect and accurately quantify average annual methane emissions from a variety of underground natural gas storage wells located at multiple U.S. facilities.

The study contains two main subparts: 1) Field Wide Leak Detection and Quantification, and 2) High-Resolution Below-ground Emissions Monitoring. Field Wide Leak Detection and Quantification, or Task 4.0, as described in the project Work Plan, (issued December 30, 2016) was conducted in March (Field Campaign 1) and October (Field Campaign 2) 2017. Extensive methane emissions measurements and meteorological data were collected from three active storage facilities representing two of the three types of storage facilities (i.e., depleted gas reservoir and salt cavern) to support development of emissions factors specifically for gas storage wells and associated components. Site access and activity data, including reservoir pressures and temperatures, well casing pressures and temperatures, and well injection or extraction flow rates, were provided by the owners/operators of each participating facility. Above-ground equipment leaks and fugitive emissions were identified and measured using a combination of infrared optical gas imaging (OGI), high-flow sampling, and open path Fourier transform infrared (OP-FTIR) spectroscopy. Potential underground leaks occurring in the immediate vicinity of the well head were assessed using dynamic flux chambers on the ground surface.

High-Resolution Below-ground Emissions Monitoring involved the implementation of a novel approach to continuously monitor methane emissions over a year-round cycle of injections and extractions at storage wells where elevated ground-level methane seepage was observed during the Field Wide Leak Detection and Quantification portion of the study. The purpose of the monitoring systems was to measure—relative to background conditions—the magnitude, rate and significance of changes in soil temperature over time and space based on measurements of the heat released by microbial reactions, which intensify in the presence of elevated subsurface methane concentrations. Monitoring systems were installed at three wells, two in a depleted gas reservoir and one at a salt cavern. The depleted reservoir systems were installed in November 2017 and the salt cavern well system was installed in March 2018. Soil temperature and moisture sensors were installed 19 to 75 inches below ground and connected to a solar-powered weather station providing wireless communications, data logging, and a remote camera. Soil sampling and environmental and geotechnical laboratory analyses were conducted to characterize existing in-situ soil conditions at each in-ground sensor location. Background sensors were also placed to measure background soil conditions and to characterize the influence of ambient conditions.

1.3 Participating Field Sites

1.3.1 Clay Basin, Utah – Depleted Gas Reservoir Wells

The gas storage reservoir at Clay Basin (**Figure 1-2**) is a depleted gas reservoir in an anticlinal dome approximately four miles long and two miles wide that is tapped by 43 injection and withdrawal wells. The facility is owned by the U.S. Bureau of Land Management (BLM) and

leased/operated by a private operator. During the injection season (May through October), the average injection volume is ~300 million cubic feet (MMcf), and during the withdrawal season (November through March), the average withdrawal volume is ~500 MMcf.

1.3.2 Gulf Coast Region – Salt Cavern Gas Storage Wells

The Gulf Coast region sites consisted of two facilities with a total of nine active natural gas storage wells completed in salt caverns (**Figure 1-2**). These facilities are privately owned and operated, and permission to conduct field measurements for this study was granted on condition that the site identities, specific location information, and operational details not be disclosed.

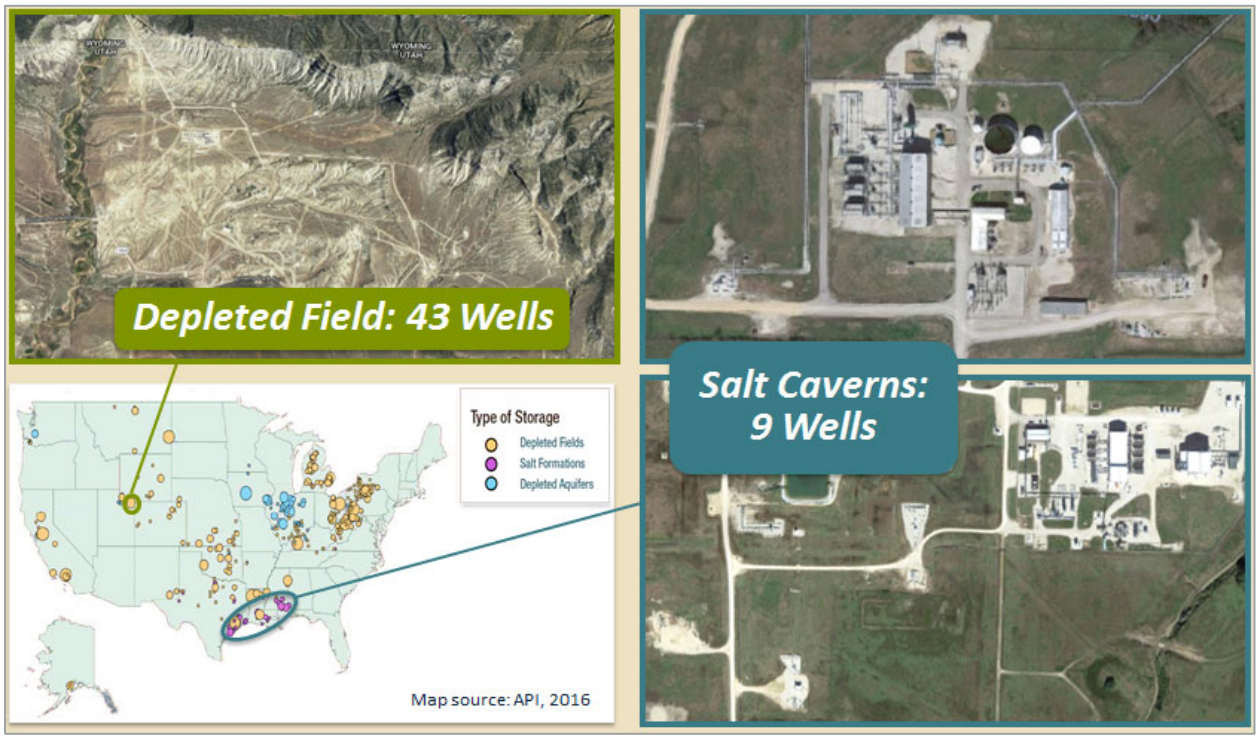

Figure 1-2. *Field Investigation Sites*

2.0 LEAK DETECTION AND MEASUREMENT

2.1 Introduction

Leak Detection and Measurement involved using a variety of techniques to quantify multiple types of wellhead-related methane emissions: 1) leaks, or fugitive emissions, were measured directly from wellhead components (e.g., valves and connectors, **Figure 2-1**); 2) total wellhead emissions were indirectly estimated by way of upwind and downwind measurements of ambient methane and tracer concentrations; 3) ground-level seepage adjacent to wellheads was quantified using short-term (15 minute) and long-term (4-8 day) soil flux measurements.

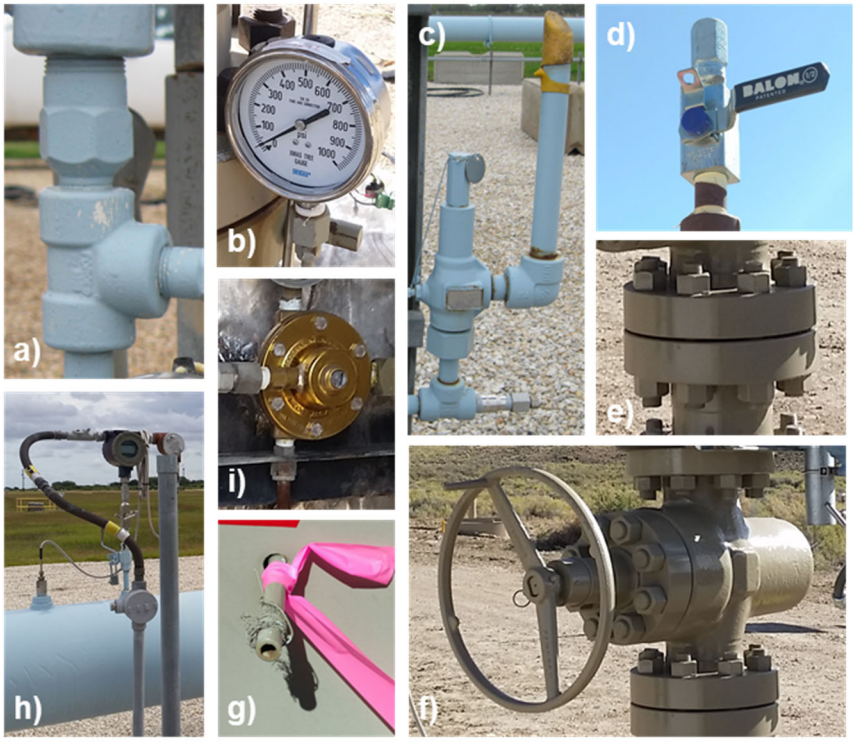

Figure 2-1. *Examples of Measured Components on Wellheads. Components are: a) connector, other (than flanged), b) gauge, c) pressure relief valve, d) small valve, e) connector, flanged, f) large valve, g) open-ended line, h) meter, i) regulator*

Fugitive emission screening and subsequent measurements of component-level emissions and short-term ground-level seepage were conducted during two field campaigns (Field Campaigns 1 and 2) at both the depleted gas reservoir facility in Clay Basin, Utah and two salt cavern storage facilities in the Gulf Coast region. Upwind and downwind measurements were conducted in conjunction with component-level emissions during Field Campaign 1. The longer-term soil flux tests were taken during separate field events denoted Field Campaigns 3 and 4. The dates of each field campaign are presented in **Table 2-1.**

***Table 2-1**. Leak Detection and Measurement Field Campaigns*

Field Event	Dates	Location	Reservoir Type	Measurements
Field Campaign 1a	Mar 20-31, 2017	Utah	Depleted Reservoir	Component-level Upwind and downwind Short-term soil flux
Field Campaign 1b	Mar 6-10, 2017	Gulf Coast	Salt Cavern	Component-level Upwind and downwind Short-term soil flux
Field Campaign 2a	Oct 2-13, 2017	Utah	Depleted Reservoir	Component-level Short-term soil flux
Field Campaign 2b	Oct 30-Nov 3, 2017	Gulf Coast	Salt Cavern	Component-level Short-term soil flux
Field Campaign 3a	Jan 16-26, 2018	Utah	Depleted Reservoir	Long-term soil flux
Field Campaign 3b	Mar 12-16, 2018	Gulf Coast	Salt Cavern	Long-term soil flux
Field Campaign 4a	Nov 1-9, 2018	Utah	Depleted Reservoir	Long-term soil flux

2.2 Methods

2.2.1 Field Site Operational Conditions

Two primary field venues were visited for methane emissions measurement: a depleted reservoir-type facility with 43 gas storage wells at Clay Basin, Utah, and two facilities representing a total of 9 salt cavern wells in the Gulf Coast region (see Section 1.3 for site details).

Depleted Reservoir Wells, Clay Basin, Utah

During Field Campaign 1a (March 2017), the facility was alternately engaged in gas injection and withdrawal in response to fluctuating demands for gas storage. As a result, the measured emissions from the field program represent both injection and withdrawal conditions. Reservoir pressures at the well heads ranged from approximately 1200 to 1600 psi, reflecting a seasonally low condition for the facility following the winter extraction season. Emissions were screened at all 43 wells and quantified at 24 randomly selected wells.

During Field Campaign 2a (October 2017) the facility was primarily engaged in gas injection or conducting a shut-in pressure test of the reservoir. The wells were split between injection and static conditions during this time, except for two wells that were under withdrawal conditions. Reservoir pressures were higher than the March field campaign and ranged from approximately 2000 to 2200 psi. Emissions were screened at all 43 wells (the same as in Field Campaign 1) and quantified at 20 randomly selected wells.

During the long-term soil flux measurements at two selected wells, reservoir pressures ranged from 960 to 1182 psi during Field Campaign 3a (January 2018) and from 1580 to 2131 psi during Field Campaign 4a (November 2018).

Salt Cavern Wells, Gulf Coast Region

These wells were engaged alternately in gas injection and withdrawal at different times during all field campaigns. Since these facilities are located in the Gulf Coast region where there is less demand for gas during winter and a higher demand for gas during the summer (e.g., to generate electricity for air conditioning), less seasonal variation in reservoir pressures is expected at these facilities compared to the Utah facility.

At one facility (5 wells), cavern pressures ranged from 1450 to 1625 psi during Field Campaign 1b and from 2200 to 2450 psi during Field Campaign 2b. At the other facility (4 wells), cavern pressures ranged from 1050 to 2150 psi during Field Campaign 1b, from 1300 to 2300 psi during Field Campaign 2b, and from 1300 to 2300 psi during Field Campaign 3b.

2.2.2 Fugitive Emissions Screening

A FLIR GF320 infrared (IR) optical gas imaging (OGI) camera and a Bascom-Turner Gas Rover gas "sniffing" device were used as screening tools to locate (but not quantify) leaking components of each gas storage well and associated above-ground component (**Figure 2-2**; details in Appendix A). Fugitive emissions screening was performed in accordance with 40 CFR part 60, subpart A, §60.18 of the *Alternative Work Practice for Monitoring Equipment Leaks*. All instruments were calibrated according to manufacturer recommendations.

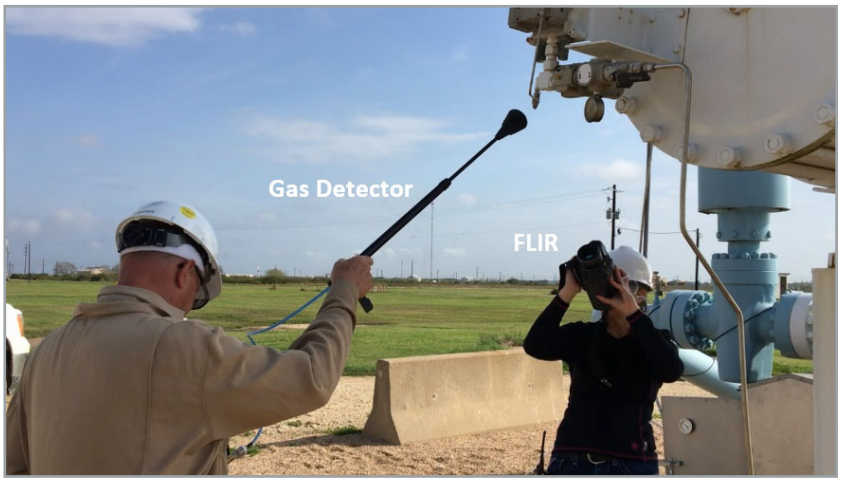

Figure 2-2. *Leak Detection with FLIR and Gas Detector*

The same populations of potentially emitting components were screened during Field Campaigns 1 and 2. This included over 6500 individual components at the 43 depleted reservoir wells in Utah and over 2200 individual components at 9 Gulf Coast salt cavern wells.

2.2.3 Component Classification and Count

Disaggregated underground storage wellhead components were classified and counted according to a detailed protocol to ensure consistent component counts among the field sites.

Key aspects of the component counting and classification system are summarized below, and the protocol is provided in **Appendix B**.

Components were classified into seven major categories: connectors, valves, pressure relief valves, meters, gauges, regulators, and open-ended lines. Where possible, these categories were subdivided into smaller groups and the function of the component was noted (**Table 2-2**). For example, connectors could be flanged or other (e.g., threaded, compression), and the function of a gauge could be to measure pressure or temperature. Component counts for each wellhead included aboveground piping connected to the wellhead. Photos of each of the component types are shown on **Figure 2-1**. Components associated with non-wellhead equipment, such as dehydrators, were not included.

Table 2-2. *Component Categories and Subcategories from the Component Classification Protocol*

Major Component Categories	Major Component Subcategories	Component Specifics
Connector	Other or flanged; Size of other connector (d=0.5", 0.5" < d < 6", d ≥ 6); Size of flanged connector (d < 1', 1' ≤ d < 3', d ≥ 3')	• Within pneumatic loop? • Function (e.g. pressure, temperature, ESD, etc.) • Other (visibility limitations)
Valve	Size (small, large); type (ball, gate, needle); and operating mechanism (manual, pneumatic, electronic)	
Pressure Relief Valve	n/a	
Meter	n/a	
Gauge	n/a	
Regulator	n/a	
Open-Ended Line	n/a	

2.2.4 Wellhead Component Emissions Measurements

Where emissions from individual wellhead components (valve, connector, etc.) were identified by the fugitive emission screening procedures described above, emission rates were quantified using a high flow sampling system customized by the Bingham Research Center at Utah State University (USU) (see **Appendix C** for details). This system was designed and configured to be able to distinguish between methane and other organics—a limitation of typical commercially-available high-flow sampling systems.

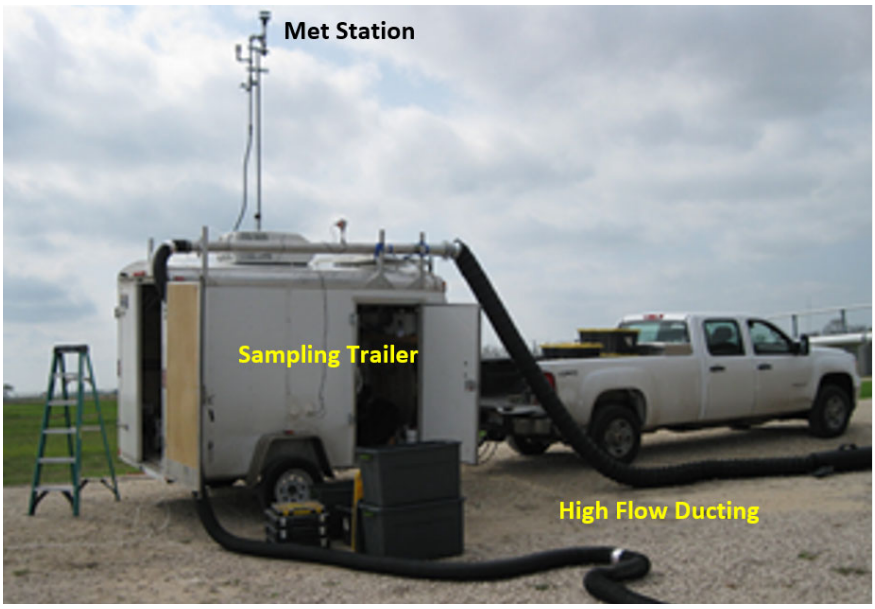

Figure 2-3. *USU Sampling Trailer, Showing High Flow Ducting and Met Station*

The customized sampling system, housed in a generator-powered trailer (**Figure 2-3**), includes a Los Gatos Research Ultraportable Greenhouse Gas Analyzer (LGR) to measure methane concentrations in sample gas and a Fox Thermal Instruments Model FT1 mass flow meter to measure total flow. The trailer also houses a custom-built air scrubber system to generate methane-free air, a global positioning system (GPS) to record its location, and meteorological instruments for measuring atmospheric conditions. An explosion-proof blower, attached to the trailer, generates flow from the bagged component to the trailer. All components of the high-flow system are grounded to the trailer, which is attached to a ground rod to dissipate buildup of static electricity.

Methane emissions from gas storage wells components were measured directly using the high-flow sampling system in accordance with 40 CFR Part 98 Subpart W. Individual components were either taped with aluminum tape or bagged off with an antistatic polymer bag to isolate them from ambient air and ensure all emissions were captured (**Figure 2-4**). A hose was then inserted into the bag or taped around the component to sample the leak, and the blower pulled a high volume of gas from the partitioned component through antistatic ducting and into a flow measurement tube to an analyzer for sample collection and analysis. Background air concentrations were measured by a sample port that was positioned next to each partitioned component to ensure an accurate background concentration measurement. If a known leak was near the background port, care was taken to ensure that background sampling was of ambient air and not influenced by elevated concentrations from any nearby emitting component.

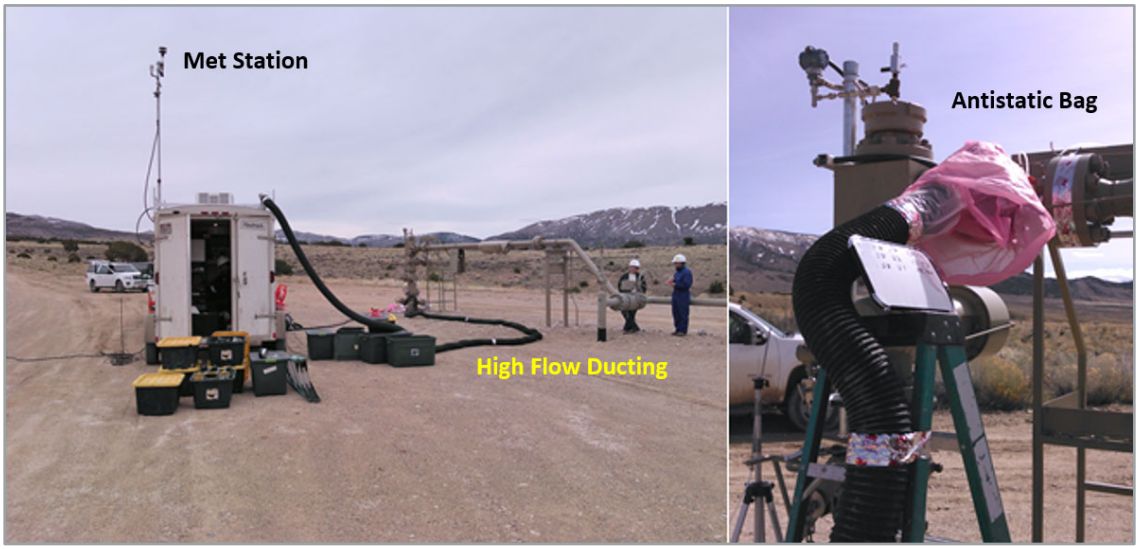

Figure 2-4. *High Flow Sampling System in Operation*

Methane concentrations were measured in 15-minute intervals to allow for 2-3 minutes of calibration between sampled components and ensure 12 minutes of usable data were recorded. Data was collected in 15- or 20-second intervals, and the average emission rate was reported (see Appendix C for details). During sampling, a set of pumps continuously pulled air from the sample hose and ambient air port through Teflon lines. An automated switching unit allowed the methane analyzer to alternately measure concentrations from the sample and background lines. A Fox Thermal Instruments Model FT1 mass flow meter measured total system flow, and the flow was corrected for temperature, pressure, water vapor, and methane concentration. A data logger recorded methane concentrations, sample flow rate, and sample temperature as well as meteorological conditions (wind speed and direction, air temperature, barometric pressure, relative humidity)

The LGR Greenhouse Gas Analyzer was able to detect methane concentrations of up to 10% in air, but if concentrations exceeded this threshold, a mass flow controller was used to dilute the analyzer flow with methane-free air to stay within the analyzer's range. This methane-free air was generated with a custom-built air scrubber system.

During all gas measurements with the high-flow sampler, field technicians ensured that data were complete and component location and type were accurately documented and backed up as soon as practical (no less frequently than daily). To confirm sample locations and IDs on field notes, photos were taken at each component showing a labeled whiteboard listing sample ID and time next to the sampled component.

2.2.5 Ground-level Seepage Measurements

Flux chamber sampling measured chemical emission rates from the ground surface (soil-air interface) before emissions were diluted and dispersed into the overlying air. The flux chamber sampling for both field sites was conducted by researchers from the Bingham Research Center

at USU. Details of the flux chamber sampling system and emissions measurement tests are presented in Appendix D.

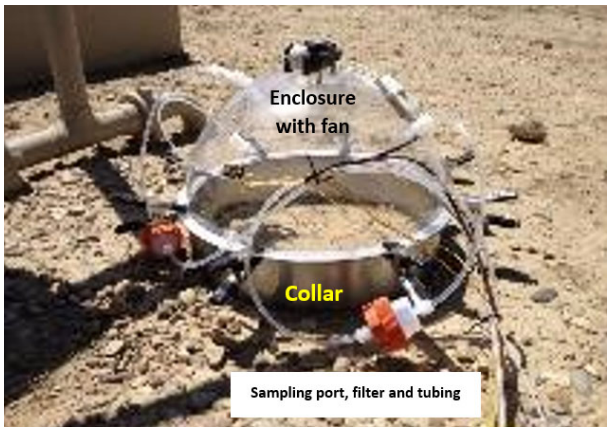

Figure 2-5. *USU Flux Chamber and Sampling Ports*

Measurements were collected using a modified version of the EPA emission isolation dynamic flux chamber that is widely used for air toxics emissions (**Figure 2-5**). Flux chamber tests were performed at discrete distances from the wellhead to quantify methane seepage due to wellbore imperfections. The chamber rested on a stainless-steel collar that was pressed or hammered into the soil. Collars were set into the soil as soon as possible prior to sampling to allow emissions to equilibrate after soil disturbance. The system collected measurements with high temporal resolution (as low as one minute for methane). The gas analysis system used for high-flow measurements was also used for flux chambers (**Figure 2-4,** see Sections 2.2.4 and 2.2.5 for details).

The dynamic flux chamber measured chemical emissions based on the difference in concentrations inside and outside the chamber. This differential concentration was multiplied by the flow rate and divided by the surface area covered by the chamber to calculate the emission (or deposition) flux.

Short-Term Soil Flux Measurements

At the two natural gas storage facilities in the Gulf Coast region, soil fluxes were measured over 15-min periods at every well at each facility. At the Utah facility, 15-min soil flux measurements were taken at 36 of the 43 wells at the facility. At each well, flux chambers were placed at three locations on the ground surface within 4 feet (ft) of the evaluated wellhead. Ideally, the locations were configured in a well-spaced triangle pattern to ensure spatial coverage around the wellhead; however, wellhead and equipment configuration dictated ultimate chamber placement.

Methane and carbon dioxide concentrations were measured for approximately 12 minutes after rates stabilized at each chamber location. Detailed meteorological data were also collected during all 12-minute emission measurement periods (solar radiation, wind speed, wind direction, ambient temperature, pressure, and relative humidity). In addition, air temperatures inside and outside the chamber were measured at 2-minute intervals.

At two wells in Utah and one in the Gulf Coast region exhibiting the highest soil fluxes, between 9 and 16 additional 15-min flux measurements were collected during Field Campaign 2 to evaluate the extent and spatial distribution of ground-level methane seepage around each wellhead. These wells were selected for soil flux measurements over longer periods during Field Campaigns 3 and 4 in conjunction with high resolution below-ground emissions monitoring (detailed in Section 3).

Long-Term Soil Flux Measurements

Long-term soil flux measurements were conducted over four days at two Utah wells in January 2018, over four days at one Gulf Coast well in March 2018, and again over eight days in November 2018 at one of the two Utah wells. During each of these tests, a manifold with solenoid valves was used to cycle among hourly measurements from flux chambers placed at 5 locations where short-term seepage was observed and one background location where seepage was not detected. The first 30 minutes of each hour-long measurement period was discarded to allow for equilibration of gas concentrations within the chamber.

As detailed in Section 3.1, clusters of subsurface soil gas sampling probes were installed at depths ranging from 0.6 to 1.7 m at multiple locations around each of the three wellheads. Through these, total combustible soil gas concentrations were measured daily using a Bascom Turner Gas Rover. The soil gas analyzer was allowed to sample for 30 sec (flow rate of ~1 L/min) before its output was recorded.

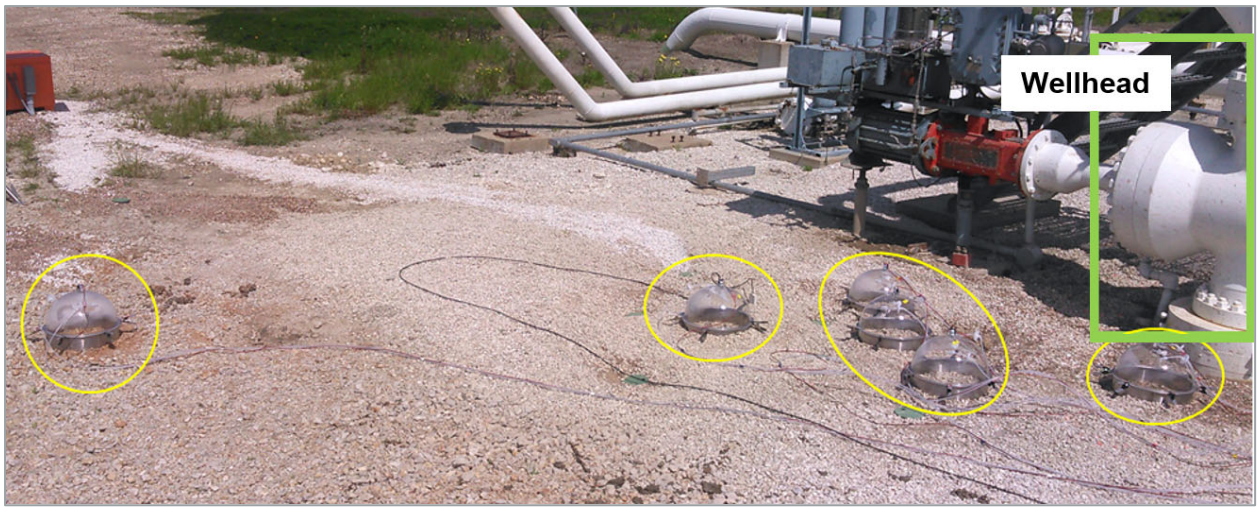

Figure 2-6. *Longitudinal Flux Chamber Setup. The wellhead is outlined in green, flux chambers are circled in yellow.*

2.2.6 OP-FTIR and Inert Tracer Release Sampling

As part of Field Campaign 1, upwind (background) and downwind concentrations of methane and an inert tracer were measured at each wellhead by Kassay Field Services, Inc., using a

RAM2000™ monostatic OP-FTIR spectrometer with a corner cube retroreflector (**Figure 2-7**). This optical spectroscopy technology was adapted to perform real-time monitoring of gaseous compounds in ambient air. A controlled stream of gas-phase sulfur hexafluoride (SF_6) was released at each wellhead as a tracer following protocols recommended by Lamb et al. (1995). The SF_6 emission rate was controlled and monitored, and the emission rate of other compounds were determined based on the ratio of their concentrations to the measured SF_6 concentration. The general layout of the OP-FTIR and tracer release configuration at each wellhead is shown on **Figure 2-8**. The OP-FTIR was employed during Field Campaign 1. Due to poor correlations between the methane plume and tracer gas, the OP-FTIR system was not used in subsequent field campaigns. A detailed description of OP-FTIR methodology is provided in **Appendix E**.

Figure 2-7. *OP-FTIR Spectrometer*

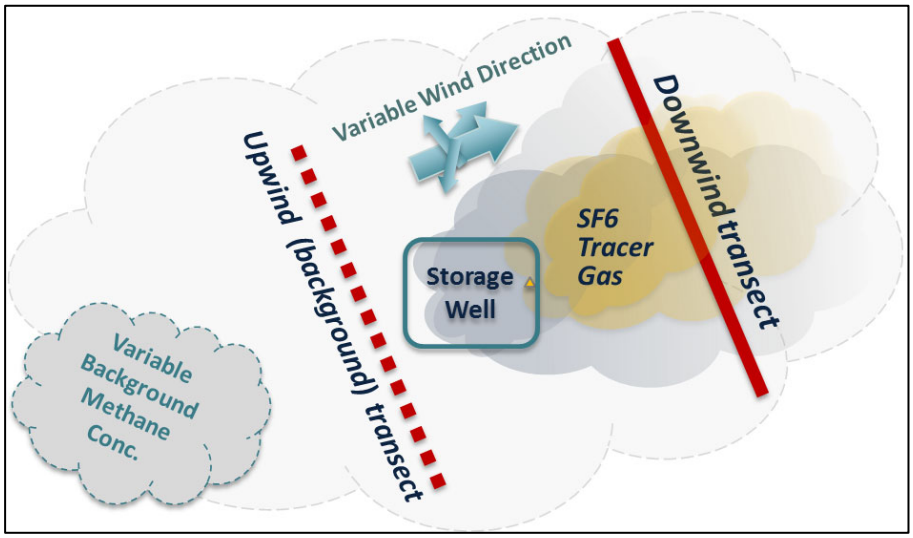

Figure 2-8. *OP-FTIR and Tracer Sampling Schematic*

The OP-FTIR spectrometer was used to detect and quantify the mixed plumes of SF_6 and methane. Measurements were taken with a sampling rate of 5 minutes and path lengths ranging from 50 to 130 meters (m) (165 – 430 ft). Path-integrated concentrations of methane and SF_6, were determined using standard infrared spectra of known concentrations for these gases and converted to parts per million (ppm) by dividing by the path length. The onboard computer software and a spectral library allowed for real time determination of concentrations for each compound. On-site data including start time, end time, weather, location of reflector, location of OP-FTIR, site conditions, and other field parameters were recorded during sampling. The spectrometer was calibrated in accordance with manufacturer specifications. Synchronous meteorological data, including wind speed, wind direction, and ambient temperature, were collected at 5-minute intervals during OP-FTIR sampling at all transect locations. These data were collected using a portable, tower-mounted weather station positioned 6 m above ground level (affixed to the high-flow sampler trailer). All meteorological and tracer release data were logged

in conjunction with the high-flow sampling data collected by USU for wellhead component emissions.

2.2.7 Wellhead Component-Specific Emission Factor Calculations

Disaggregated, component-specific emission factors (EF) for gas storage wellheads were developed to align with existing EF and component categories for natural gas production wells in the EPA GHGRP (40 CFR Part 98 Subpart W).

Leaker EFs were calculated as the average emission from samples positively identified with the FLIR (consistent leak identification with 40 CFR part 60, subpart A, §60.18).

$$Leaker\ EF_i = ER_{avg,F,i} \qquad \textit{(Equation 1)}$$

Where:

$ER_{avg,F,i}$ = average emission rate of component type i when detected with the FLIR

Population EFs were calculated by summing all emissions from a component type over both field campaigns and dividing by the population count of the component. Not all components for which emissions were indicated by screening with either the FLIR or Gas Explorer could be measured. Therefore, emissions for such components were estimated by multiplying the average emission rate for a given component type by the number of emitting components identified but not measured (Equation 2). As the sensitivity of the Gas Explorer was greater than the FLIR, estimated emissions from components positively identified with only the Gas Explorer were handled separately than the components also positively identified with the FLIR.

$$Population\ EF_{,i} = \frac{\sum Emissions_{M,i} + n_{NM,E,i} FP_{E,i} ER_{avg,E,i} + n_{NM,F,i} FP_{F,i} ER_{avg,F,i}}{n_{pop,i}} \qquad \textit{(Equation 2)}$$

Where:

- $Emissions_{M,i}$ = measured emissions from component type i
- $n_{NM,E,i}$ = number of emitting components type i, detected only with the Gas Explorer but not measured with the high flow sampler
- $n_{NM,F,i}$ = number of emitting components type i, detected with the FLIR but not measured with the high flow sampler
- $F_{PE,i}$ = False positive detection rate for the Gas Explorer for component type i
- $F_{PF,i}$ = False positive detection rate for the FLIR for component type i
- $ER_{avg,E,i}$ = average emission rate of component type i when detected only with the Gas Explorer
- $ER_{avg,F,i}$ = average emission rate of component type i when detected with the FLIR
- $n_{pop,i}$ = population of component type i

The false positive detection rates were determined with blank and control data and are discussed in the Results and Discussion.

2.3 Screening and Measurement Summary

Over 17,000 components were screened with the FLIR during Field Campaigns 1 and 2 (**Table 2-3)**. Among these, a total of 330 components, including controls (components not identified as emitting by the screening process), were sampled with the high-flow system. An additional 28 blank samples were collected in ambient air.

Table 2-3. *Screened Population and Measurement Counts*

Component Type	Depleted Reservoir		Salt Caverns	
	Screened Population	Measurement Count [a]	Screened Population	Measurement Count [a]
Valve, Large	433	46	142	31
Valve, Small	1,833	69	672	14
Connector, Flanged	1,376	38	854	13
Connector, Other	8,128	23	2,618	47
Pressure Relief Valve	0	0	20	2
Open-Ended Line	369	12	2	1
Meter	0	0	10	0
Gauge	522	23	138	6
Regulator	242	3	36	3
Total	**12,903**	**214**	**4,492**	**117**

[a] Measurement counts include control samples

2.4 Results and Discussion

2.4.1 False Negative and Positive Screening Rates

The accuracy of the screening methods was determined by comparing the results of the high flow measurements for blank, control, and detected samples. Samples falsely identified as not emitting (i.e., controls with methane emissions greater than blank samples) were used to determine the false negative screening rate. Samples falsely identified as emitting (i.e., detected samples with methane emissions less than blank or control samples) were used to determine the false positive screening rate.

Blank and control data sets were compared to each other to determine if there was a statistical difference between the two (**Figure F-1** in Appendix F). Both data sets were not normal (Shapiro-Wilk, $p<0.05$), and skewed to the right (skewness of blank data was 3.1 and of control data 2.8). The distributions of the two data sets were not statistically different (Kolmogorov-Smirnov [KS], $p = 0.64$). This indicated components with negative screening results (i.e., controls) were not significantly different from field blanks, and the screening methods successfully identified emissions.

The control data had five data points that fell outside of the range of the blanks (**Figure F-1** in Appendix F). Two of these points were negative (-0.018 and -0.087 standard cubic feet per hour [scf/hr]) and, when summed, were similar in magnitude to two positive values (0.046, 0.063 scf/hr). The last control data point that fell outside of the blank data range was 0.12 scf/hr. Due to the similar values and distributions of the blank and control data, all control data except the largest value (0.12 scf/hr) was considered to be similar to blank data and was not included in the emission

factor development. Of the 125 control samples that were taken, only 1 was determined to be a possible emission; thus, the screening methods resulted in 0.8% chance of a false negative.

Figure 2-9 compares the histograms of detected samples, controls, and blanks. Although the distributions are different, there is consistently a small peak in the same bin (0-0.0052 scf/hr). Due to the presence of this peak in all three sample types, it was concluded that detection data within this peak range was likely to be due to variation in the field (i.e., blank or control) and not a true emission (i.e., a false positive detection). Detection data that fell above the peak area (>0.01 scf/hr) but below the maximum filtered control value (0.063 scf/hr) was classified as a probable small emission and was included in emission factor development. Detection data that fell above 0.063 scf/hr was classified as an emission.

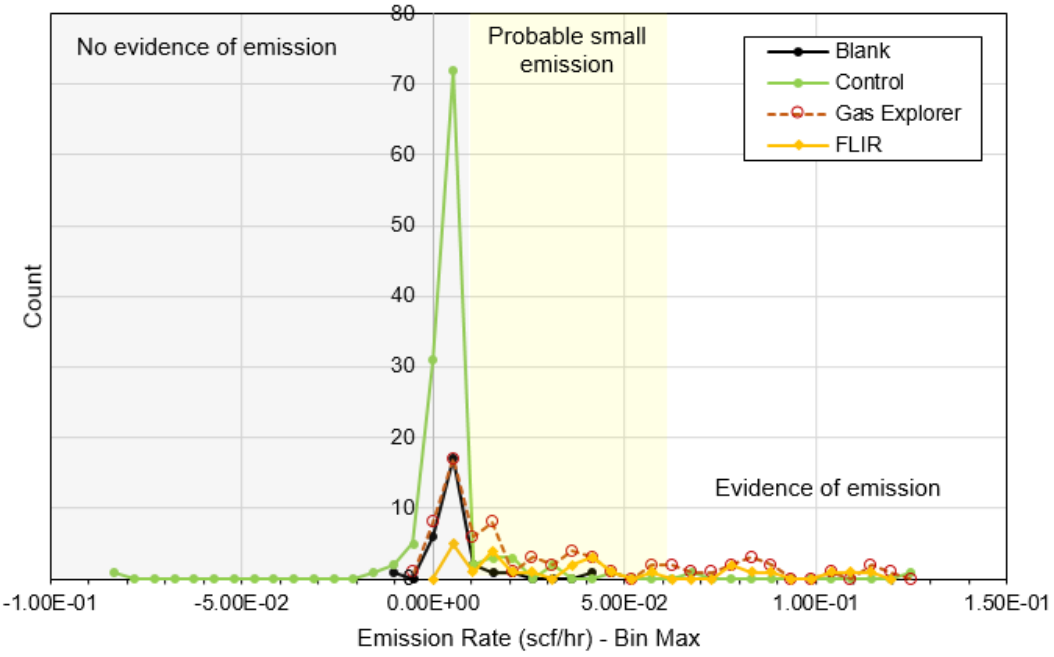

Data within range of control was less than 0.12 scf/hr. Values less than 0.01 scf/hr show no evidence of emission, values between 0.01 and 0.063 scf/hr show probable evidence of emission, values greater than 0.063 scf/hr show evidence of emission.

Figure 2-9. *Histogram of Emission Rate Data within Range of Control Data.*

Dividing detection samples into these categories filtered out 38 of the 191 detection samples. Of these 38 samples, 32 were positively identified as emissions with only the Gas Explorer and 6 with both the Gas Explorer and FLIR. The Gas Explorer screening method resulted in a 20% false positive rate (39 out of 192) and the FLIR method in a 6.5% false positive rate (6 out of 92). The greater false positive rate of the Gas Explorer may be a result of its higher sensitivity compared to the FLIR. To reduce the rate of false positive detections with the Gas Explorer, setting a threshold for detection may be useful.

Component screening was not immediately followed by high flow sampling, which may have contributed to the false positive rate. At the depleted reservoir, high flow sampling was conducted

over a period of two weeks, but component screening was completed within the first four days. Therefore, a component identified with the FLIR on day one may not have been measured with the high flow sampler until day 14, during which changing conditions at the wellhead (e.g., natural gas injection or extraction rate) may have affected the component emissions. This was not a concern at the salt caverns, as high flow sampling was conducted over 2 to 2.5 days and component screening was completed in 1 to 2 days

2.4.2 Component Counts

Wellheads at the salt caverns had higher average component counts for almost all component types compared to wellheads at the depleted reservoir (**Table 2-4**). The exceptions were open-ended lines and regulators, which were more common on the pneumatic loops at the depleted reservoir than the salt caverns. Contributing to the higher average component count by wellhead at the salt caverns was the larger size of the wells and greater amount of above ground piping near the wellhead compared to the wellheads at the depleted reservoir. Component counts were conducted only on wells that were sampled with high flow. As not all wells were sampled at the depleted reservoir, component counts needed to be estimated for a portion (14 out of 43) of the wells. For wells that were not counted, average component counts from sampled wells were used.

Small valves, pressure relief valves, open-ended lines, gauges, regulators, and 'other connectors' were commonly found on the wellhead pneumatic loops. Components within the pneumatic loop were included in the population counts when the pneumatics were run on methane. Four of the nine salt caverns wells had pneumatic loops run on system air. This resulted in almost half of the salt cavern wells having no pneumatic-associated components in the population count. The ratio of sampled wellheads with pneumatics run on methane compared to system air may not be representative of the national average. More information regarding wellhead pneumatic operations would be helpful in determining national average wellhead component counts, particularly for other connectors, small valves, pressure relief valves, open-ended lines, gauges, and regulators.

Table 2-4. *Component Count and Screening Results by Component Type*

Component Type	Avg. Count by Wellhead		% Emitting [a]		% Leaking [b]	
	Reservoir	Salt	Reservoir	Salt [c]	Reservoir	Salt
Connector, all	111	193	0.19	0.52	0.21	0.27
Connector, other	95	145	0.20	0.76	0.21	0.21
Connector, flange	16	47	0.073	0.00	0.15	0.47
Valve, all	26	45	1.2	1.9	2.7	2.6
Valve, small	21	37	0.76	0.75	1.7	0.86
Valve, large	5.0	7.9	2.8	7.9	7.0	11
Pressure relief valve (PRV)	0.0	1.1	-	10	-	5.0
open-ended line (OEL)	4.3	0.1	1.8	0.00 [d]	1.63	33 [d]
Gauge	6.1	7.7	0.57	0.00	0.19	0.00
Regulator	2.8	2.0	0.00	11	2.1	2.8

[a] Percent of the screened population that was positively detected to be emitting only with the Gas Explorer corrected for false positive detection rate. [b] Percent of the screened population positively detected to be emitting with the FLIR corrected for false positive detection rate. [c] Gas Explorer was not used at the salt caverns during Field Campaign 1, assumes the same number of Gas Explorer detections as Field Campaign 2. [d] Based on a sample size of one.

The percentage of components 'emitting' (i.e., detected with only the Gas Explorer) and 'leaking' (detected with the FLIR) were calculated using the number of detections and false positive detection rates for each component type and screening method (**Table 2-4**). As described above, the false positive detection rate for all samples was calculated to be 20% for the Gas Explorer and 6.5% for the FLIR. These rates were further divided by component type (**Table F-1** in Appendix F). The percent emitting and leaking were calculated as the number of corrected (with false positive detection rates) detections divided by the number of screened components.

Large valves were the component category with the highest 'emitting' and 'leaking' percentages. This was followed by regulators, small valves, other connectors, and flanged connectors. Pressure relief valves (PRVs) were not present at the wellheads at the depleted reservoir, but at the salt caverns were detected with the screening methods at similar rates as regulators. One open-ended line (OEL) was present at the salt caverns and was found to be leaking during one field campaign, resulting in a 33% leaking rate. Screening at additional salt cavern sites is needed to confirm the OEL values. OELs at the depleted reservoir were detected to be leaking and emitting at similar rates as small valves.

2.4.3 Component Emissions Quantification

A summary of methane emission rates by component type is presented in **Figure 2-10**. Large valves had highest emission rates, with a mean of 3.9 scf/hr and median of 0.40 scf/hr. This was followed by small valves (mean of 0.73 scf/hr, median of 0.20 scf/hr), and then flanged connectors (mean of 0.42 scf/hr, median of 0.34 scf/hr) and other connectors (mean of 0.45 scf/hr and median of 0.12 scf/hr) (**Figure 2-10**). PRVs are not included in the comparison due to the small sample size (n=2). Although large valves had higher mean and median emission rates than small valves, results of the KS test showed the valve subcategories were not significantly different (p=0.17). Similarly, other and flanged connectors were not significantly different (KS, p=0.73). These results indicate for the storage sites visited, it was not necessary to subdivide the connector and valve component categories when measuring emission rates. However, as discussed above, large valves had the highest percent of emitting components, and were found to be emitting more often than small valves. Therefore, when calculating population EFs, subdividing valves by size may be important.

It was not necessary to separate emissions by formation type/site for any component category for the three sites visited. Emissions from connectors at the depleted reservoir were not significantly different from connectors at the salt caverns (KS, p=0.80). Similarly, emissions from valves were not significantly different between the two formation types (KS, p=0.71). Results of the KS test were similar for subdivided component categories; there was no significant difference between formations for other connectors, flanged connectors, small valves, or large valves (p = 0.50, 0.77, 0.49, and 0.37 respectively). Sampling at additional sites, including aquifer storage sites, is recommended before concluding that site or formation type does not matter for component methane emission rates.

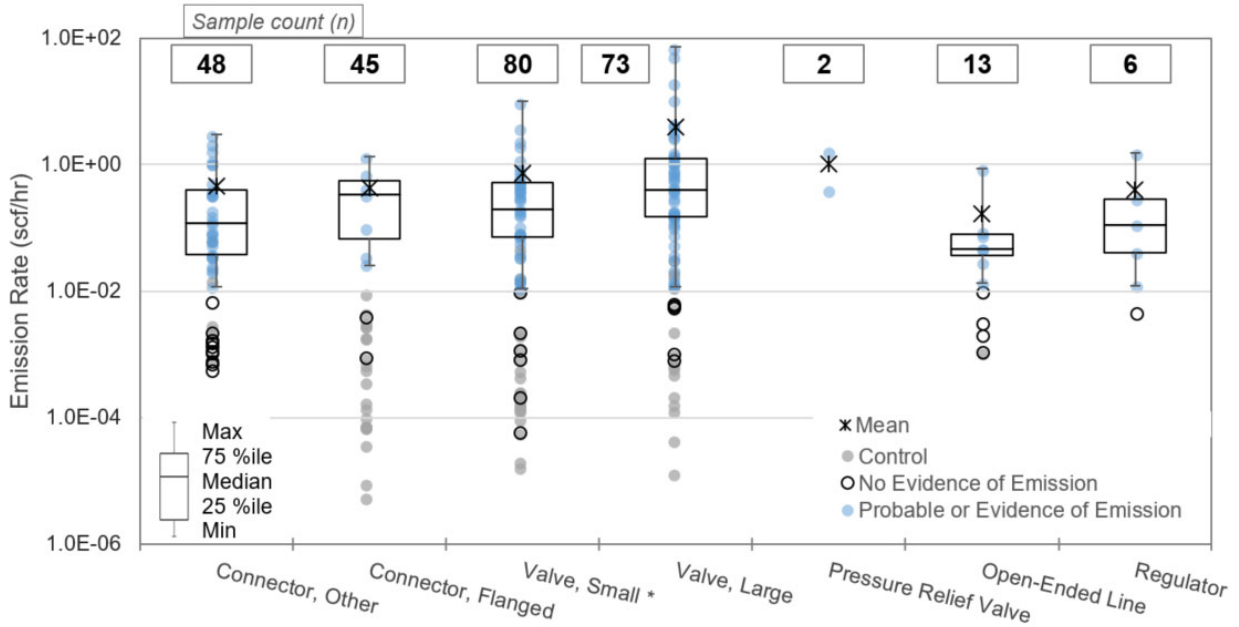

The total number of sampled components is given. Emission rates for detected samples are divided into the emission categories: no evidence of emission (< 0.01 scf/hr), and probable small emission or evidence of emission (≥0.01 scf/hr). Box and whisker plots of the probable or evidence of emission sample data are included in the figure. Box and whisker plots are not included for data sets with three or fewer data points.

Figure 2-10. *Emission Rates by Component Type; Both Formations, Field Campaigns 1 and 2*

2.4.4 Emission Factors

Compared to existing leaker EFs given in Subpart W, the leaker EFs calculated in this study are similar for 'other connectors' and valves and smaller for flanged connectors and open-ended lines (**Table 2-5**). As defined in Section 2.2.7, the leaker factor for a given category of components is the average rate of emissions detected with the FLIR. Although the leaker EF for large valves was over five times greater than that of small valves, there was no statistical difference between the emission rates of flanged and other connectors detected with the FLIR (KS p=0.49). Therefore, based on the results of this study, it was not necessary to calculate separate leaker EFs for the two connector subcategories. Similarly, there was no statistical difference between small and large valves (KS, p=0.073; Mann-Whitney, p=0.051). However, as the p-value was close to significant (<0.05) and the number of sites visited was small (n=3), it is recommended that additional measurements be taken before concluding there is no significant difference in leaker EFs by valve size.

Table 2-5. *Leaker and Population Emission Factors*

Component Type	Leaker EF (scf/hr/component)		Population EF (scf/hr/component)	
	This study	Subpart W [a]	This study	Subpart W [b]
Connector, all	0.88	n/a	0.0023	0.01
Connector, other	1.2	1.1	0.0029	n/a
Connector, flange	0.49	3.4	0.0013	n/a
Valve, all	3.6	4.1	0.10	0.1
Valve, small	0.96	n/a	0.016	n/a
Valve, large	5.65	n/a	0.46	n/a
Pressure relief valve	nd	3.7	0.10	0.17
Open-ended line	0.27	2.3	0.0053	0.03
Gauge	nd	n/a	0.027	n/a
Regulator	0.11	n/a	0.009	n/a

nd = not enough data, n/a = not available. [a] Values from Table W-4A, Storage Wellheads, Subpart W (USEPA, 2016). [b] Valu from Table W-4, Storage Wellheads, Subpart W (USEPA, 2011).

The population EFs calculated in this study were generally similar to corresponding factors in Subpart W, with values ranging from one sixth of the Subpart W EF (open-ended lines) to equivalence with the Subpart W EF (valves). The population EF for 'other connectors' was about two times larger than that of flanged connectors. As described above, there was no significant difference in methane emission rates between flanged and other connectors. 'Other connectors' were indicated to be 'emitting' with higher frequency than flanged connectors but were not consistently indicated to be 'leaking' more (**Table 2-4**). As such, the results of this study do not support the subdivision of flanged vs. other connectors for population EFs.

There was a substantial difference between the population EF for small and large valves, 0.016 and 0.46 scf/hr/component respectively. Although there was no significant difference in emission rate between the two valve subcategories (see previous section), the percent 'emitting' and 'leaking' were consistently higher for large valves (3.7 to 11.5 times higher depending on formation type, **Table 2-4**). Due to these factors, the subdivision of valves by size is supported by the data collected in this study.

The EFs developed in this study were calculated from emissions from a small number of distinct underground gas storage facilities (n=3) and may not be nationally representative of emissions from such operations. Three types of formations are used for underground gas storage: salt caverns, depleted reservoirs, and aquifers. This study included emissions from facilities using salt caverns and depleted reservoirs, but not aquifers. It is suggested that additional measurements be taken for aquifer formations to compare formation type.

2.4.5 Ground-Level Emission Fluxes

Measured methane soil flux rates at each sampling location are summarized in **Figure 2-11**. As shown, elevated methane fluxes, were observed at one salt cavern well and five depleted reservoir wells. These elevated results varied over several orders of magnitude among samples collected approximately 1 m apart from one another.

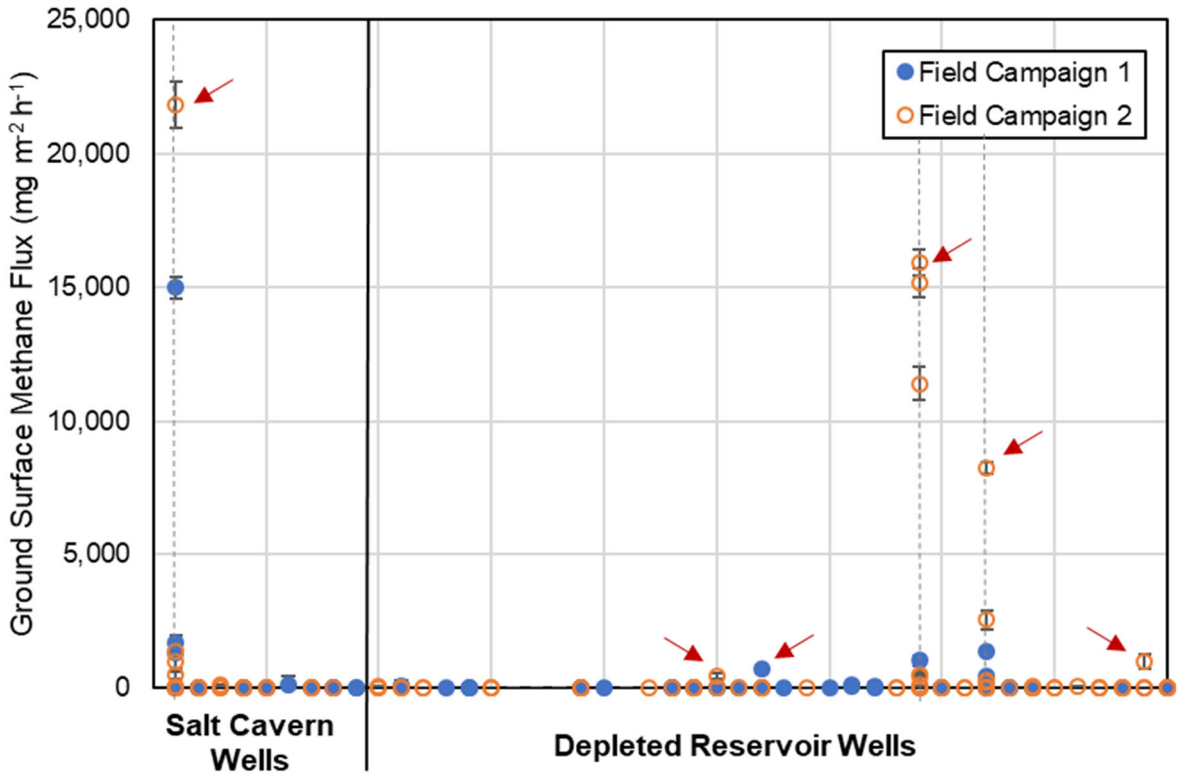

Dashed lines identify wells that were selected for the long-term longitudinal study (see Section 2.4.6) and high-resolution below-ground emissions monitoring (see Section 3). Arrows identify wells with elevated ground surface methane flux.

Figure 2-11. *Short-term ground-level methane emissions from subsurface sources*

As others have shown, the drivers of soil emissions from subsurface leaks are complex and lead to fluxes that vary both temporally and spatially. Gases in the soil tend to follow pathways of increased permeability, so the spatial distribution of methane emissions can be expected to be inconsistent (Cahill et al., 2017; Christophersen and Kjeldsen, 2001; Forde et al., 2019; Spokas et al., 2006). Gas moving through saturated zones tends to coalesce into large pockets, leading to pulsed flow (Dusseault et al., 2000). Also, passage through relatively low-permeability layers can require gas pressure to build up until it exceeds a threshold value, again leading to inconsistent or pulsed flow (Forde et al., 2019). These complex flow processes likely explain inconsistent correlations between fluxes and meteorological and well conditions, and they may explain the variability in methane flux observed at some locations.

Temporal Variability

An order of magnitude or more of variability was also observed 1) between seasonal pad-average methane fluxes, based on the short-term (15-minute) measurements taken at many wells, and also 2) among the time series of long-term flux measurements taken over 4 to 8 days at the three highest ground-emitting wells described above. Since stored gas volumes at the facilities were at their maxima in fall and at their minima in later winter/early spring, one may expect average

seepage fluxes to be higher in October/November than in March. Average fluxes were indeed higher in October/November at the Utah depleted reservoir facility (facility-average flux of 87 and 976 mg/m^2/h in March and October/November, respectively) and one Gulf Coast salt cavern facility (1127 vs 1385 mg/m^2/h) but not at the other (8 vs -1 mg/m^2/h). However, none of the differences were statistically significant (p values between 0.32 and 0.34).

Some of the temporal variability in methane fluxes could be caused by barometric pressure changes, as has been shown by others for methane fluxes from landfills (Czepiel et al., 2003). Decreasing barometric pressure tends to draw gas out of the soil, leading to increased fluxes, while increasing pressure has the opposite effect. This was observed during the 8-day test in November 2018 in Utah; however, no such relationship was exhibited at the same well in January 2018 or during the long-term tests at other wells. Similarly, the long-term flux measurements revealed no meaningful relationships between ground-level methane emissions with barometric pressure (rather than pressure changes), injection or withdrawal volumes, or well temperatures. Additional details of this analysis are discussed in Appendix D.

Spatial Variability

Lyman et al. (2017) showed that flux magnitude at natural gas production wells is inversely related to distance from the wellhead. Therefore, for most wells, soil fluxes were measured in close proximity to the wellhead. More recently, Forde et al. (2019) found that flux magnitude was not related to distance from the wellhead at wells in British Columbia, Canada. **Figure 2-12** compares the spatial distribution of methane flux at three wells sampled in this study. The spatial distributions of fluxes in the figures are not uniform, but they do show that the highest fluxes tend to occur closer to the wellhead.

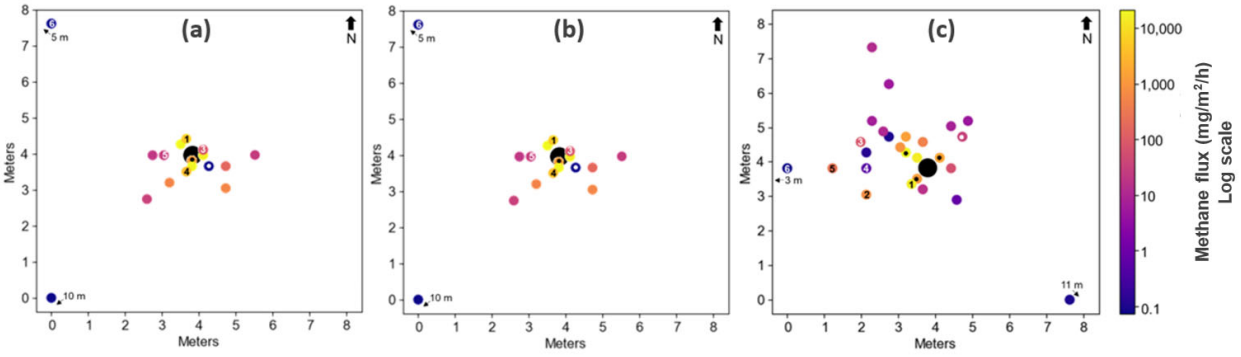

Spatial distribution of average methane fluxes around natural gas storage wellheads in Utah (a and b) and the Gulf Coast region (c). Each colored circle represents a flux measurement location. Circles with numbers are locations of long-terms measurements, and numbers correspond with flux data in Appendix D. Circles with black or white dots are locations where short-term fluxes were measured in Field Campaign 1. Other circles are locations where fluxes were measured in Field Campaign 2.

Figure 2-12. *Spatial Distribution of Average Methane Fluxes*

Total Combustible Soil Gas

At both Utah wells where soil gas probes were installed, total combustible soil gas concentrations tended to be highest at a depth of 0.75 m. This may indicate that the leaks that led to elevated soil gas concentrations were relatively shallow. Most of the soil probes at the Gulf Coast well at which soil gas probes were installed filled with water, blocking flow and making measurements impossible. The hydrocarbon composition of soil gas at all well pads was similar to the composition of natural gas, with methane comprising 95% of total hydrocarbons in the gas.

Comparison of Soil Fluxes with Other Well Pad Emission Sources

To provide a rough estimate of total soil emission rates for each well, the near-wellhead flux measurements were averaged for each well and the value was applied to a 3 m radius around the wellhead. Negative average fluxes were treated as zero for this calculation. This method makes the implicit assumptions that (1) fluxes are inversely related to distance from the wellhead (i.e., fluxes outside of the 3 m radius are negligible), and (2) the flux measurement locations are representative of the area within the 3 m radius. Comparison of this rough estimate of soil emissions against above-ground emissions (measured with the high-flow system) at each well and found that ground-level soil emissions represent a small portion of total per-well emissions. Total per-well emissions at the Utah gas storage facility averaged 2.9 (95% confidence range of 1.1-9.5) kg/day, while per-well soil emissions were only 0.1 (0.0-0.3) kg/day (3.9% of the total). The maximum soil emission rate at any well was 2.1 kg/day. **Figure 2-13** shows box and whisker plots of total above-ground and soil emissions for well pads at the Utah facility.

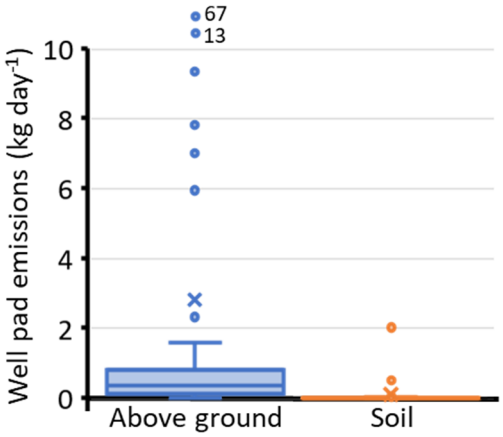

Figure 2-13. *Box and whisker plot showing total soil and above-ground emissions from Utah facility well pads.*

2.4.6 OP-FTIR Results

Methane emission rates were calculated using tracer correlations, based on downwind methane and tracer concentrations, and controlled tracer release rates. Tracer correlations were performed using three independent methods adapted from previous studies (USEPA, 2014; Galle et al., 2001; Monster et al., 2014; Schuetz et al., 2011; and Foster-Wittig, 2015): (i) time-series plume

integration, (ii) unconstrained slope, and (iii) mixing ratio methods. The plume integration method provides the most accurate estimate of emission rate given its effective consideration of an entire time series of measurements. However, to ensure the validity of these estimates several method quality indicators (MQIs, described below) were applied, based on the agreement of emission rates estimates among the three methods. When MQIs were satisfied, the result of the plume integration method was adopted as the final calculated value for methane emission rate.

Due to the nature of tracer correlation methods, several precautions must be taken to ensure that the recorded data is not inappropriately interpreted; most importantly, the methane and tracer plumes must be well mixed. Tracer correlation methods are not considered reliable for measurement periods during which downwind methane and tracer concentrations are poorly correlated or when there is substantial non-agreement among the three emission rate estimation methods described above. Such conditions suggest instability in either the methane or tracer plume, which may be caused by low wind speeds (causing pooling of the tracer, which is much heavier than methane), highly variable wind direction, variable methane upwind (background) methane concentrations during periods of downwind measurements, and other possible factors.

Foster-Wittig et al. (2015) propose that the correlation coefficient (R^2) between methane and tracer concentrations should be greater than 80% over a period of five or more consecutive measurement intervals. Additionally, Foster-Wittig et al. (2015) recommend that i) the relative difference in emission rates calculated by the plume integration and mixing ratio methods be less than 20% and ii) the relative difference in emission rates calculated by the plume integration and unconstrained slope methods be less than 55%.

Table 2-6 presents the calculated total methane emission rates for all measurement periods for which the MQIs were satisfied. The calculated methane emission rate for the salt cavern well measured on March 7 ranged from 20 to 63 scf/hr. It is noteworthy that at this same well, the USU sampling team had isolated and was measuring 54 scf/hr of emissions from a large valve on this well during part of the 13:10 to 13:40 OP-FTIR measurement period. The 43 scf/hr difference in total emission rates measured at different times at this well likely reflects this sampling activity rather than any significant difference in overall emissions between the two time periods. All other results on **Table 2-6** relate to single periods of measurements at other individual wells. As with the salt cavern well measured on March 7, these results also appear consistent with the overall level of above-ground component and flux chamber emissions observed at the corresponding well heads.

Table 2-6. *OPFTIR Tracer Analysis Results*

	Date	Start Time	End Time	n (5 min)	Tracer Emission Rate (g/s)	Avg. Measured Conc.		Calculated Methane Emission Rate (SCFH)			Method Quality Indicators		
						Methane (ppm)	Tracer (ppm)	Mixing Ratio Method	Plume Integration Method	Unconstrained Slope Method	R^2	RPD(1,2)	RPD(2,3)
Salt Cavern Wells	7-Mar	13:10	13:40	6	0.064	0.381	0.0243	**20**	**20**	**18**	0.889	0.3%	8%
		13:50	14:30	8	0.064	1.18	0.0237	**63**	**63**	**58**	0.945	0.4%	8%
	9-Mar	14:30	15:00	6	0.064	0.052	0.0474	**1.4**	**1.4**	**1.1**	0.808	0.4%	20%
Depleted Reservoir Wells	20-Mar	13:46	14:21	7	0.085	0.071	0.0442	**2.6**	**2.7**	**4.9**	0.911	2.6%	57%
	25-Mar	9:40	10:40	12	0.085	0.442	0.0655	**9.3**	**11**	**14**	0.832	17.8%	24%
	28-Mar	11:40	12:05	5	0.085	0.059	0.0342	**2.9**	**2.9**	**3.1**	0.882	0.3%	6%

ppm = part per million by volume at stadard temperature and pressure (e.g. ml/m^3)

In addition to highly variable wind conditions experienced during a majority of measurement periods, repeat measurements of upwind/background concentrations after numerous downwind measurement periods suggest highly variable background concentrations of methane. Consequently, only a small portion of all downwind OP-FTIR measurement periods satisfied the MQIs required for these data to be relied on for total emissions quantification. Possible sources of background interference remain unknown but could include periodic compressor blowdowns associated with the storage operations or daily atmospheric inversions which appeared to occur at the Utah, facility.

3.0 HIGH-RESOLUTION BELOW-GROUND EMISSIONS MONITORING

3.1 Objective

The three wells exhibiting the highest levels of ground-level emissions near the wellbore were selected for continuous, high-resolution, remote monitoring of soil conditions which may be indicative of thermogenic methane emissions and related atmospheric conditions. The goal of the high-resolution below-ground emissions monitoring study was to develop an advanced alert system that will identify changes in emission rates from gas storage wells. To achieve this goal, a network of in-ground temperature and moisture sensors was installed at three storage wells. The purpose of the installed monitoring systems was to measure—relative to background conditions—the magnitude, rate and significance of changes in soil temperature over time and space based on measurements of the heat released by microbial reactions, which intensify in the presence of elevated subsurface methane concentrations.

Methane released in the subsurface from a leaking wellbore should migrate towards the surface by diffusion and buoyancy effects. In unsaturated soils near the ground surface, naturally occurring methane-oxidizing bacteria can establish an aerobic biodegradation reaction zone in which heat is released as oxygen and methane are consumed in an exothermic reaction. Such heat resulting from below-ground emissions near a gas storage wellbore should be detectable—relative to the heat in soils at background locations where such emissions are not present—by a high-resolution thermal monitoring system, provided that the emissions are 1) large enough to generate enough heat to be detected near the ground surface; and 2) sustained over several days or weeks.

3.2 Methods

3.2.1 Monitoring System Equipment and Installation

Monitoring systems were installed at two wells at Clay Basin during the week of November 13, 2017 and at one well in the Gulf Coast Region during the week of March 5, 2018. The wells were chosen for high resolution monitoring based on exhibiting the highest short-term methane fluxes during Field Campaigns 1 and 2 (see Section 2). At the Utah wells, arrays of 27 and 29 sensors were installed at depths of approximately 20 to 60 inches. At the Gulf Coast region well, an array of 18 sensors was installed at depths of approximately 19 to 75 inches. The systems continuously measured in-situ soil temperature, moisture content and related above-ground ambient conditions, which were recorded as 5-min and 1-hour averages. Remote data collection became operational on November 18, 2017 at Clay Basin and on March 7, 2018 in the Gulf Coast region. Full details of the system equipment and installation procedures are provided in Appendix G.

Upon recommendation of the Utah facility operator, hydrovac excavation was used to safely excavate boreholes for in-ground sensors and trenches for underground conduits near the gas storage wellheads without posing risks to underground infrastructure. At each sensor placement location, soil cores were collected and analyzed for geotechnical parameters (grain size distribution, calculated porosity, bulk density, USCS classification) and for the presence of total

petroleum hydrocarbons (TPH) and total organic carbon (TOC) to confirm whether elevated microbial activity reflected in observed heat signatures could be a result of contamination from other activities not related to gas storage (e.g. previous gas production or well drilling). Corresponding analytical results are presented in Tables G-3 and G-4 in Appendix G.

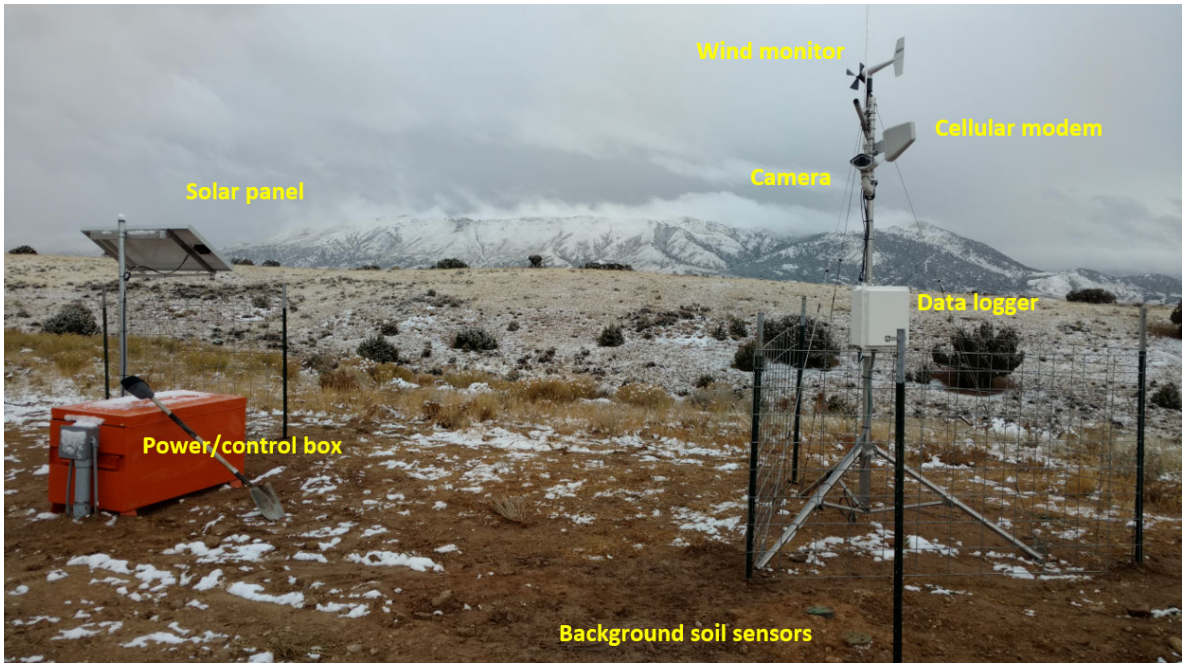

Figure 3-1. *Installed Meteorological Tripod Power/Control Box at a Utah Gas Storage Well*

To capture a range of depths, some of the sensors were clustered together, with three or four probes of various depths placed in separate boreholes about 0.3 m in horizontal distance apart (see Appendix G, Figure G-3). In order to support collection of soil gas samples, ¼-inch Nyaflow tubing with a filter tip was installed to rest above the sensor in each borehole. Each sensor was surrounded by native soil and then covered with a 6-inch thickness sand pack in which the filter tip rests. A layer of hydrated bentonite was emplaced atop the sand pack to an upper extent approximately 6 inches below ground. Each borehole was completed flush with the ground surface with a lidded valve box from which the sampling tube was accessible.

The installed below-ground sensors were connected to a solar-powered weather station (Model 1000, Campbell Scientific, Inc.) providing meteorological conditions as well as wireless communications, data logging, and a remote camera. Meteorological data collected was: barometric pressure (Model PTB110, Vaisala), relative humidity (Model EE181, CSI), temperature (Model EE181, CSI), precipitation (Model TR-5251, Texas Electronics), solar/net radiation (Model NR01-C, Hukeflux), wind direction (Model 05305, R.M. Young-AQ), and wind speed (Model 05305, R.M. Young-AQ). Layouts of the sensor configuration along with results of short-term methane soil flux chamber and TPH measurements are shown in **Figures G-3** to **G-9** of Appendix G.

3.2.2 Heat Signal Processing and Data Analysis

Conceptual Model Overview

Spatially and temporally variable soil temperature data from each monitoring network was processed and analyzed in an effort to discern a subsurface methanotrophic heat signature in a thermally "noisy" environment, where:

- The heat signature of interest is generated from the naturally occurring microbial oxidation (biodegradation) of methane that is present in the soils.
- Thermal noise is due to a number of factors, including short-term changes in weather, day-night cycles, longer-term seasonal changes, changes in soil moisture, and the heat radiation from the wellhead casing during gas withdrawal and injection operations.

Key assumptions and processes associated with these efforts and the underlying conceptual model are as follows.

d) A below-ground methane leak from a wellbore will migrate upwards towards the surface by diffusion and buoyancy effects and remain generally close to the wellbore. At some point in the unsaturated zone, a naturally occurring biodegradation reaction zone will be established with naturally occurring methane-oxidizing bacteria. These bacteria are ubiquitous and present in almost all soils. As the bacteria consume oxygen and methane, heat will be released.

e) The magnitude of heat delivered to near surface soils by methanotrophic processes depends on 1) the rate of methane that has been released and oxidized; 2) the depth of the release; and 3) thermal properties of the soil.

f) A methanotrophic heat signature can be observed if: 1) the subsurface leak is sustained over several days or weeks; and 2) localized heat signals generated by elevated biological activity are strong enough to be discernable from thermal background.

g) Compared to background locations, soils closer to the wellhead experience additional thermal noise (i.e., larger and more frequent temperature variations) related to wellhead operations, which can include rapid changes in gas injection and extraction rates. For example, when gas is withdrawn from storage, the well casing remains at near constant temperatures, as found in the underground reservoir; whereas during injection, well casing exhibit diurnal variations more closely aligned with ambient air temperatures.

h) After processing soil temperature data to remove thermal background noise, statistically significant increases in soil temperatures in a given area suggest elevated levels of methane in that area. A controlled below-ground release of methane was conducted to assess the efficacy of the monitoring system and signal processing algorithms to detect areas of elevated of methane in soils.

Transfer Function-Noise Modeling

Transfer function-noise (TFN) modeling is a well-established data-driven technique for estimating source-response relationships of linear systems using time series data (e.g., Box and Jenkins, 1970) and has been applied to many disciplines (e.g., Asmuth, et al, 2002). To assess whether methanotrophic heat signatures were discernable from background thermal noise, TFN modeling was applied to analyze the soil temperature data collected by the monitoring network at one well in Clay Basin, Utah, where the highest combustible soil gas concentrations were observed and where 4-day and 8-day soil flux tests were conducted in January and November 2018, respectively. The TFN analysis was implemented using the commercially available software MATLAB and its toolboxes (1) to estimate the contributions of different heat sources to the observed temperature variations, and (2) to remove these contributions from the observed temperature time series at each non-background sensor location.

Exploratory data analyses were performed to examine the characteristics and key dependencies of the temperature time series recorded by the sensor array. Large amounts of temporal variability in the model sources (i.e., thermal background noise for the sensor array) were observed to span a broad range of timescales, including from minutes/hours due to routinely dynamic well operating conditions), to hours/days with changes in the weather and atmospheric conditions, to months with the changing of seasons. Ultimately, the TFN analysis was performed in two parts to separately address the small-scale and large-scale background temperature variability, based on daily-averaged values for soil temperatures and meteorological parameters, as recorded by the monitoring network, and operations data provided by the facility operator. First, the TFN analysis considered the following model sources for their impacts on each background and non-background soil sensor, individually: (1) ambient atmospheric air temperature, and (2) temperature data recorded by a sensor in contact with the well casing, and (3) gas temperature inside the well. By this analysis, thermal background influences were evaluated independently for each sensor to account for the spatial variability of such influences, for example, as is related to the variable depths of the sensors and their distances from the well head. Second, for each the temperature residual calculated for background sensors was subtracted from the initial temperature residual from corresponding non-background locations, as applicable. The resulting residual temperature time series after removal of these contributions potentially reflect temperature changes due to methane seepage around the wellhead.

3.3 Results and Discussion

The high-resolution subsurface monitoring study has produced a variety of expected and unexpected contradictory results. These have raised new questions and introduced limitations and uncertainties regarding the analysis, interpretation and application of the soil temperature data measured at all monitored locations. Consequently, the findings, as detailed below, are inconclusive and warrant further evaluation.

The upper chart in **Figure 3-2** shows expected changes in background-adjusted temperature residual at sensors located at and immediately above a controlled release of methane conducted Nov. 2-8, 2018. The relatively constant residual temperature at sensor 9D, where methane was injected at a constant rate during this period, indicates that the temperature of the released gas

itself did not significantly change the soil temperature over the course of the controlled release. As expected, temperature residuals at shallower sensors, 9M and 9S, located above the release point, began to increase after approximately one day and continued increasing for more than a day after the release was terminated. As shown in the lower chart in **Figure 3-2**, these temperature changes corresponded directly to measured increases in combustible soil gas concentrations at the sensor locations as well as to increasing trends in methane and carbon dioxide fluxes measured at the ground surface. The observed carbon dioxide flux provides a strong indication of increased methane oxidation throughout this period in response to the controlled release. Methane degradation is most likely the predominant source of these observed increases in temperature residuals.

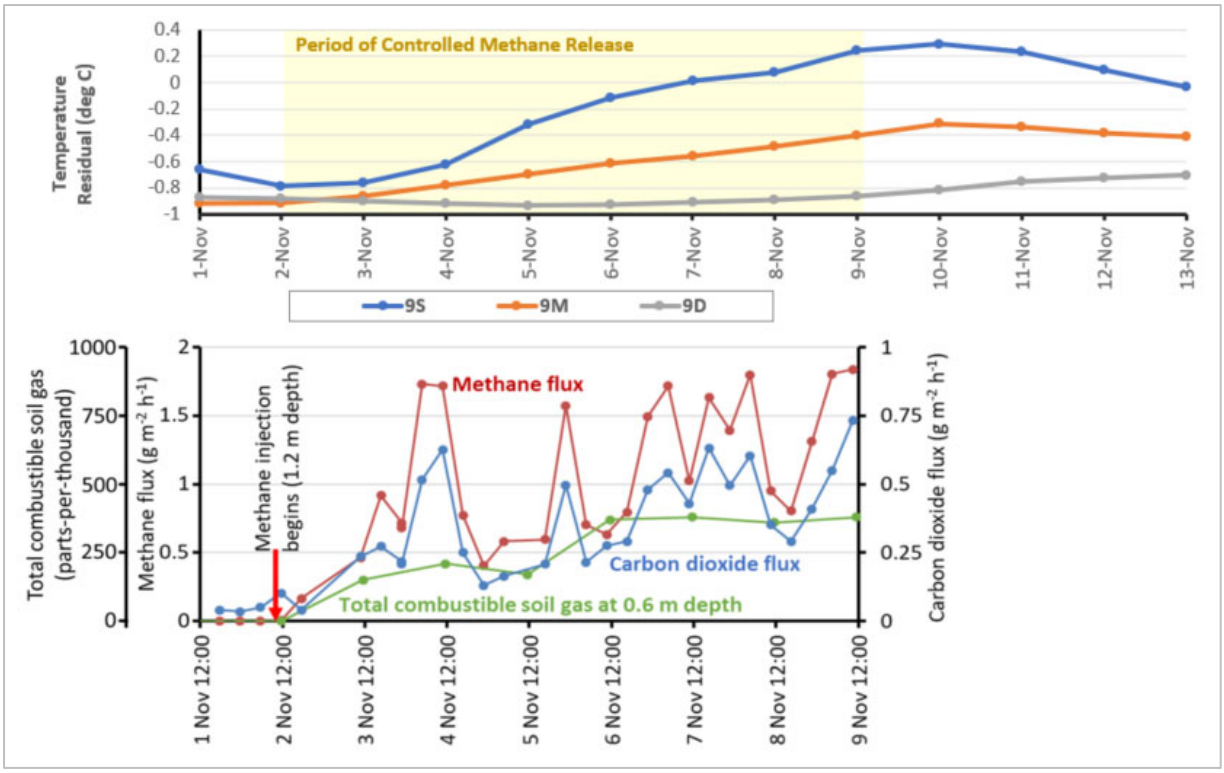

Figure 3-2. *Changing Soil Temperature Residuals Relative to Controlled Release of Methane*

Figure 3-3 shows monthly averages of the background-adjusted residual time series computed by TFN modeling for all non-background sensors in addition to daily averages of ambient air temperature and gas extraction and/or injection (negative values) at the well. These results exhibit several notable features of the residual temperature time series. First, the values are predominantly and unexpectedly *negative* on both monthly and daily timescales for all sensor locations. Nevertheless, the relative magnitudes (i.e., absolute values) of the negative residuals still appear to distinguish among locations with higher and lower methane presence. These also exhibit a consistent seasonal trend, which could be expected if the observed the residuals are associated with a leak that varies with pressures in the well or if there is greater biological activity associated with methane degradation within warmer soils in the summer than cooler soils in the winter.

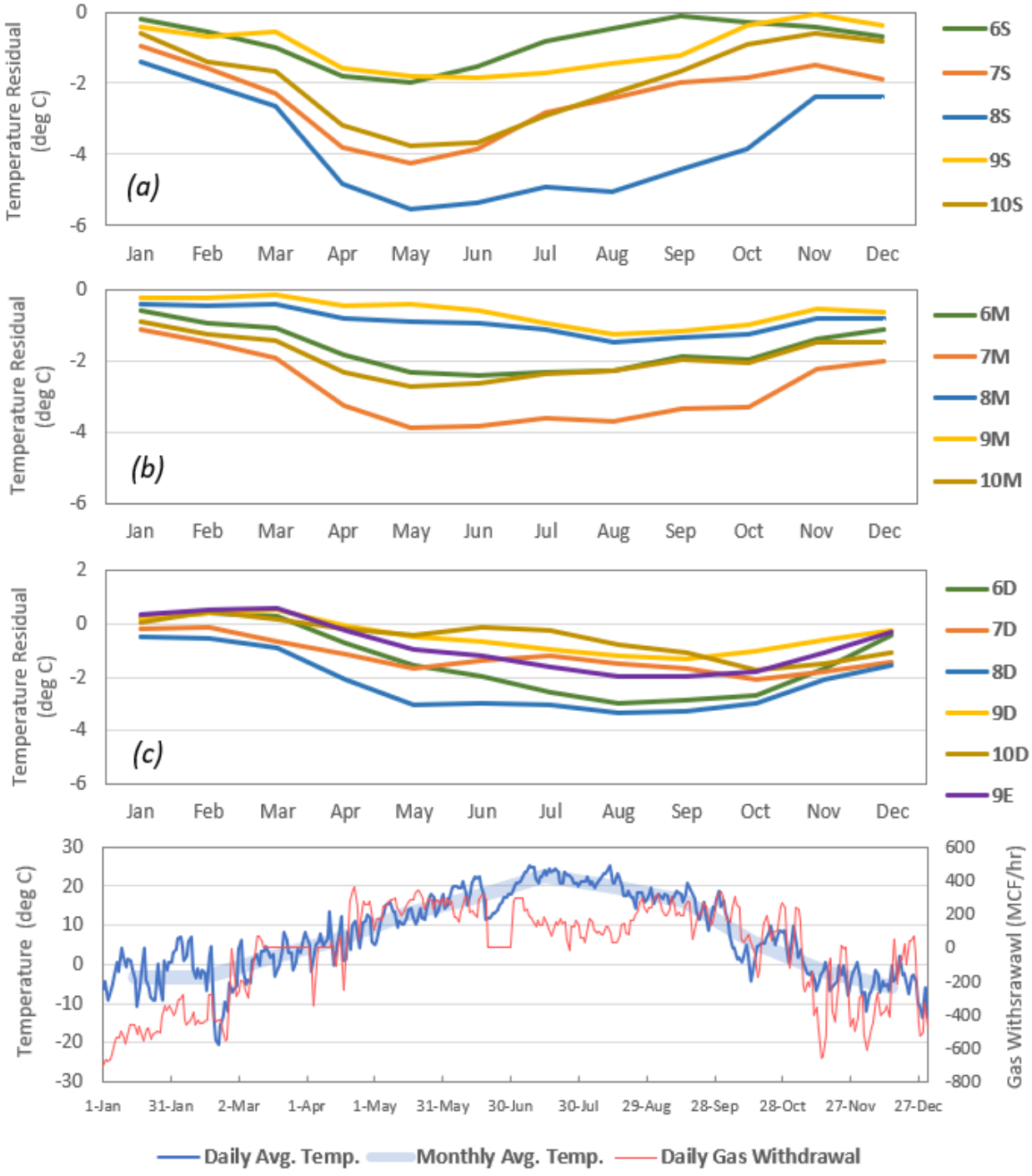

See Appendix G for sensor depths and additional details. (a) "S"-sensors, approx. 24 inches; (b) "M"-sensors; approx. 30 inches; (c) "D" and "E" sensors, approx. 48 and 64 inches, respectively.

Figure 3-3. *Monthly-Average Model Temperature Residuals and Daily Average Temperature and Gas Extraction Rate at a Utah Gas Storage Well*

Negative Non-Background Residuals

As discussed above and shown in **Figure 3-2**, elevated soil gas concentrations correspond to *increases* in the background-corrected temperature residuals observed during a controlled methane release. Consequently, average residuals are expected to be *positive* over any duration and any location where a sustained source of methane has generated increased heat due near-surface biological activity. Figure 3-2 also shows the value of residuals to be lower (i.e. more negative) with increasing depth, which is expected since the availability of oxygen—consumed together with methane—decreases with depth.

Therefore, one would not only expect methane-related residuals to be positive, but for their magnitudes to decrease with increasing depth. As shown in **Figure 3-3**, the observed residuals do not follow the expected behavior in terms of sign but do exhibit expected patterns in terms of the relative magnitude of absolute values. For example, indeed larger negative residuals are observed at locations near the well that have exhibited elevated ground level methane seepage and high subsurface soil gas concentrations. Additionally, the magnitude (absolute value) of these signals decreases with depth, consistent with expected behavior, such as depicted on **Figure 3-2**.

This finding is further illustrated in **Figure 3-4**, which shows possible negative correlations between average combustible soil gas concentrations and the background-corrected temperature residuals measured at the “M” and “D” sensors during the January and November 2018 soil flux tests. Whereas the cause for a negative correlation remains unknown, these results do appear to corroborate an observation that total combustible soil gas concentrations tended to be highest near a depth of 0.75 m (30 inches; see Appendix D). This may indicate that the source of elevated soil gas concentrations at these locations was relatively shallow and explain why there is a better fit between concentration measurements and temperature residuals at 30 inches (typical M-sensor depth) than at 48 inches (typical D-sensor depth). The plots for S-sensors suggest that residuals at those locations may be more associated with unfiltered surface temperature influences and not methane degradation.

Additional modeling and analysis of the collected data could yield additional insights. One potential explanation for the predominance of negative background-corrected residuals at all non-background locations is that the soil temperature response to ambient model-source fluctuations is substantially different at the background vs. non-background locations. Another possibility is that the relationships between temperature responses at each sensor location and various heat source fluctuations are highly non-linear, such that the modeling approach employed could not sufficiently resolve important differences among the influences of key short-term or long-term heat signals.

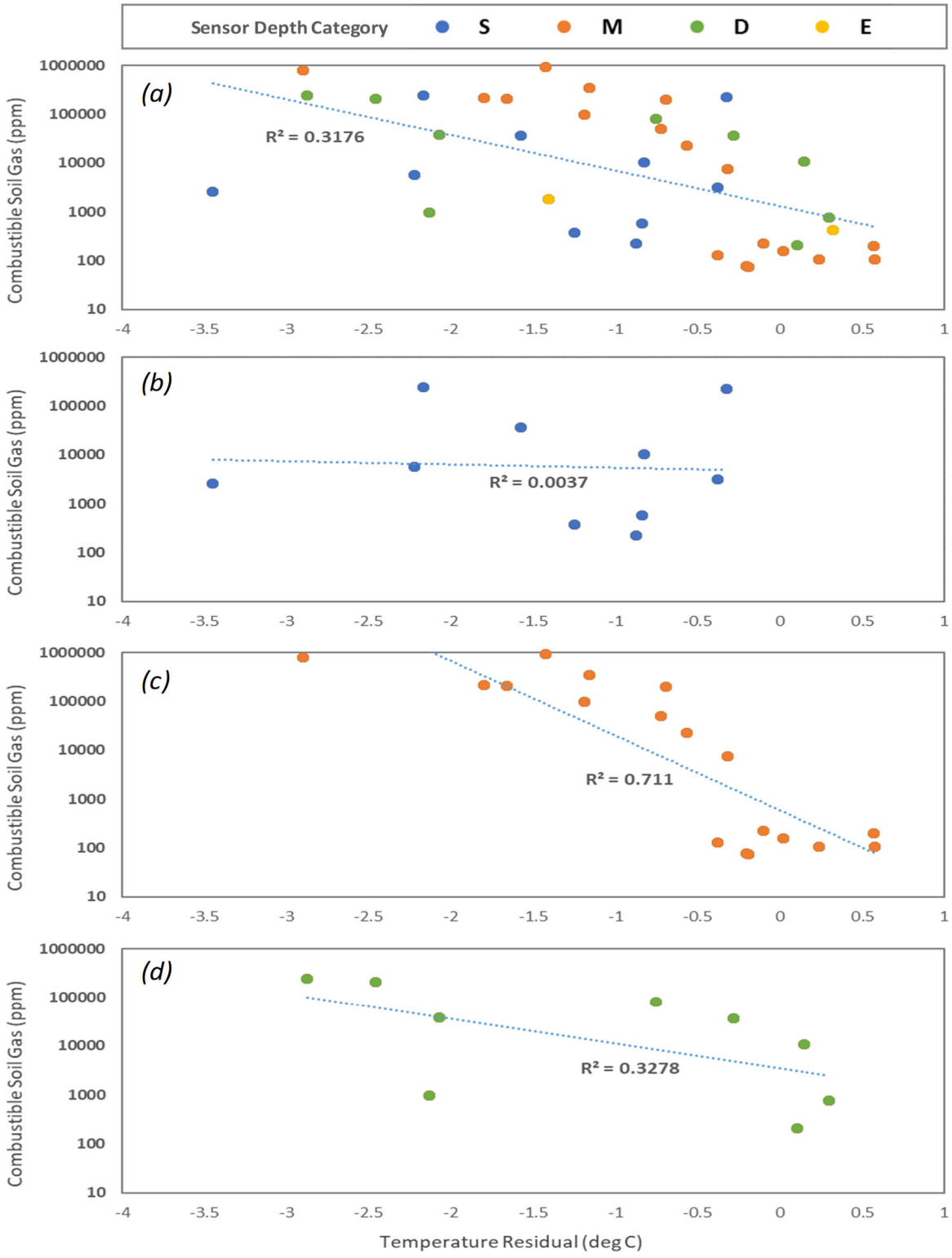

Figure 3-4. *Total Combustible Soil Gas Concentrations vs. Temperature Model Residual during 4-day (January 2018) and 8-day (November 2018) Ground-level Seepage Tests*

4.0 TECHNOLOGY TRANSFER

There was a high level of interest and participation on this project from industry and regulatory stakeholders concerned with methane emissions from gas storage wellheads and updates to Subpart W. Technical Advisory Steering Committees (TASC) consisting of participants from industry, regulatory agencies, non-governmental organizations, academia, and consulting were assembled to provide recommendations and feedback on project activities over the two-year program. A list of TASC participants is provided in **Table 4-1**.

Table 4-1. *List of TASC Participants*

Industry			
Anadarko	Dominion	GE	Pioneer
Apache	Enbridge	Gulf Coast Green Energy	QEP Resources
Chevron	Energy Transfer	Haliburton	Shell
Devon	FLIR	Kinder Morgan	Spectra
Regulatory Agencies			
BLM	KGS	PA DEP	UT DEW
CADOC	MDE	TRRC	WVDEP
COGCC	MI DEQ	USEPA	
DOE NETL	NDIC	USEPA Region 6	
IL DNR	NY DEC	UT DAQ	
Non-Governmental Organizations			
AGA	EDF	HARC	PHMSA
API	GTI	INGAA	
Academia & Consulting			
Colorado State University	Indaco Air Quality Services, Inc.	University of Colorado-Boulder	University of Utah
GHD	University of Cincinnati	University of Kentucky	

TASCs formed for this project represented two-way exchanges of information. This open communication provided an excellent opportunity for GSI to inform TASC participants of recent project findings, and for TASC participants to increase project efficiency by giving GSI real-time feedback on sampling protocols and data analysis. Feedback from participants was compiled and considered as GSI planned and implemented next steps throughout the project.

Knowledge gained from this program was also disseminated through technical presentations at conferences (as shown in **Table 4-2**) and development of public education brochures and fact sheets summarizing project highlights and findings. Papers for 1) emission factor development and 2) high-flow sampling methodology are in preparation for submission to peer-reviewed journals.

Table 4-2. *Technology Transfer Events*

Event Title	Date	Organization	Description
API Technical Meeting	February-2017	American Petroleum Institute	Ann Smith presented project scope and objectives to industry representatives and solicited participation in the TASC
Environmentally Friendly Drilling (EFD) Sponsors Meeting	April-2017	Houston Advanced Research Center	Richard Bowers presented project accomplishments and challenges.
AUVSI XPONENTIAL 2017	May-2017	Association for Unmanned Vehicle Systems International	Richard Bowers presented information on sampling technologies used in field programs and how automation could improve the accuracy of data collected.
TCEQ Trade Fair	May-2017	Texas Commission on Environmental Quality	GSI representatives discussed value of the project with TCEQ Commissioners.
SPE Annual Technical Conference and Exhibition	October-2017; September 2018	Society of Petroleum Engineers	Richard Bowers disseminated brochures and fact sheets highlighting project findings.
O&G Environmental Conference	November-2017	Environmental Training Institute	GSI representatives disseminated brochures and fact sheets highlighting project findings.
CH4 Connections Conference	December-2017	Gas Technology Institute	GSI representatives disseminated brochures and fact sheets highlighting project findings.
Gas Storage Outlook Conference	January-2018	S&P Global Platts	Ann Smith and Richard Bowers disseminated brochures and fact sheets highlighting project findings.
CH4 Connections Conference	September 2018	Gas Technology Institute	Ann Smith presented results from this and the compressors methane emissions study to industry, regulatory and academia stakeholders.
EPA GHGRP Stakeholder workshop	October2018	U.S. EPA	Richard Bowers and Ann Smith presented methods and findings regarding preliminary emission factor calculations.

5.0 REFERENCES

Asmuth, J., and M. Knotters. 2004. “Characterising Groundwater Dynamics Based on a System Identification Approach.” Journal of Hydrology 296: 118–134. https://doi.org/10.1016/j.jhydrol.2004.03.015.

Box, G. E. P., and G. M. Jenkins. 1970. “Time Series Analysis Forecasting and Control”. San Francisco: Holden Day.

Czepiel, P., Shorter, J., Mosher, B., Allwine, E., McManus, J., Harriss, R., Kolb, C., Lamb, B., 2003. The influence of atmospheric pressure on landfill methane emissions. Waste Manage. (Oxford) 23, 593-598.

Foster-Wittig, T. “Mobile Sensors: Assessment of Fugitive Methane Emissions from Near and Far-Field Sources by Abstract Mobile Sensors: Assessment of Fugitive Methane Emissions from Near and Far-Field Sources” PhD dissertation, Duke University, 2015.

Foster-Wittig, T. A., Thoma, E. D., Green, R. B., Hater, G. R., Swan, N. D., & Chanton, J. P. Development of a mobile tracer correlation method for assessment of air emissions from landfills and other area sources. Atmospheric Environment, 102, 323–330. https://doi.org/10.1016/j.atmosenv.2014.12.008, 2015.

Galle, B. O., Samuelsson, J., Svensson, B. H., & Borjesson, G. Measurements of methane emissions from landfills using a time correlation tracer method based on FTIR absorption spectroscopy. Environmental Science and Technology, 35(1), 21–25. https://doi.org/10.1021/es0011008, 2001.

Lamb, B., McManus, J. B., Shorter, J. H., Kolb, C. E., Mosher, B., Harriss, R. C., Allwine, E., Blaha, D., Howard, T., Guenther, A., Lott, R. A., Siverson, R., Westberg, H., and Zimmerman, P. Development of Atmospheric Tracer Methods to Measure Methane Emissions from Natural Gas Facilities and Urban Areas, Environ. Sci. Technol., 29, 1468–1479, 1995.

Lyman, S., Measurement of Methane and Nonmethane Hydrocarbon Soil Flux Near Oil and Gas Wells in Utah, Performance Report summited to Utah Bureau of Land Management, Cooperative Agreement No. L13AC00292, 2016.

Monster, J. G., Samuelsson, J., Kjeldsen, P., Rella, C. W., & Scheutz, C. Quantifying methane emission from fugitive sources by combining tracer release and downwind measurements - A sensitivity analysis based on multiple field surveys. Waste Management, 34(8), 1416–1428. https://doi.org/10.1016/j.wasman.2014.03.025, 2014.

Niska Gas Storage, 2010, Gas Storage Industry Primer, September 2016, http://www.niskapartners.com/wp-content/uploads/2010/04/GasStorageIndustryPrimer.pdf.

Petron, G., G. Frost, B. Miller, A. Hirsch, S. Montzka, et al.: Hydrocarbon emissions characterization in the Colorado Front Range: A pilot study, Journal of Geophysical Research D:Atmospheres, 117, D04304, 2012.

Stolp, B.J., A.L. Burr, K.K. Johnson: Methane gas concentration in soils and ground water, Carbon and Emery Counties, Utah, 1995-2003, U.S. Geological Survey, Salt Lake City, Utah, Scientific Investigations Report 2006-5227, 2006.

Subramanian, R., Williams, L. L., Vaughn, T. L., Zimmerle, D. J., Roscioli, J. R., Herndon, S. C., Yacovitch, T. I., Floerchinger, C., Tkacik, D.S., Mitchell, A. L., Sullivan, M. R., Dallmann, T. R., and Robinson, A. L. Methane Emissions from Natural Gas Compressor Stations in the Transmission and Storage Sector: Measurements and Comparisons with the EPA Greenhouse Gas Reporting Program Protocol. Environmental Science & Technology 49 (5), 3252-3261. DOI: 10.1021/es5060258, 2015.

USEPA, AP 42, Fifth Edition, Volume I, Chapter 14.4: Enteric Fermentation -- Greenhouse Gases, 1998. Retrieved from https://www3.epa.gov/ttn/chief/ap42/ch14/final/c14s04.pdf

USEPA, Mandatory Greenhouse Gas Reporting Subpart W - Petroleum and Natural Gas Systems. 2011; Vol. 40 CFR Part 98 Subpart W.

USEPA. 2014. Other Test Method 33a, 1–91. Retrieved from https://www3.epa.gov/ttn/emc/prelim/otm33a.pdf

USEPA, Mandatory Greenhouse Gas Reporting Subpart W - Petroleum and Natural Gas Systems. 2016; Vol. 40 CFR Part 98.

Zimmerle, D. J., Williams, L. L., Vaughn, T. L., Quinn, C., Subramanian, R., Duggan, G. P., Willson, B., Opsomer, J. D., Marchese, A. J., Martinez, D. M., and Robinson, A. L. Methane Emissions from the Natural Gas Transmission and Storage System in the United States. Environmental Science & Technology 49 (15), 9374-9383. DOI: 10.1021/acs.est.5b01669, 2015.

APPENDIX A

Fugitive Emissions Screening Procedures

APPENDIX A

FUGITIVE EMISSIONS SCREENING PROCEDURES

1.0 TECHNOLOGY BACKGROUND

As a component of field investigation activities, a FLIR™ GF320 infrared imaging camera was used as a screening tool to visually locate (but not quantify or speciate) losses and leaks from components on natural gas wellheads. Optical gas imaging instruments were used in accordance with 40 CFR Part 60, Subpart A, §60.18 of the Alternative Work Practice for Monitoring Equipment Leaks. Field personnel operating the FLIR™ GF320 received training and certification for proper operation of the camera for optical gas imaging prior to use.

Infrared cameras convert thermal signatures to optical images. The GF320 camera is lightweight with features designed to detect gas emissions in field applications, resulting in efficient screening of large areas. The GF320 is capable of detecting methane emissions with temperatures up to 350 °C and within ±1 °C accuracy. The spectral response is in the range of 3.2-3.4 µm with a resolution of 320x240. Total pixel count is 76,800. Minimum acceptable accuracy is ±1°C for temperature ranges of 0 °C to 100 °C or ± 2% of reading for temperature range >100 °C. The minimum detected leak rate for methane in FLIR lab testing is 0.8 grams per hour (g/hr). In the field, the FLIR is usually able to detect natural gas emissions in the range of 1 standard cubic foot per hour (scf/hr) or larger from 3 meters away (Ravikumar et al., 2018).

2.0 FIELD METHODS

When imaging an object during field activities that was of a temperature similar to the surroundings, such contrast was not evident. In order to compensate for this, a background material of differing thermal properties was placed behind the object to create contrast. The camera was also moved to different angles to find a background with sufficient thermal contrast. Shifting through the various color palettes also afforded better images.

At the beginning of daily field activity, the FLIR camera was powered up, commencing an automatic startup sequence. This sequence included cooling of the internal spectral detector and other electronic system checks. After the automatic startup sequence was concluded, a Non-Uniformity Correction (NUC) check was performed to assure that the camera was functioning properly prior to conducting gas imaging activities.

3.0 FLIR GF320 SPEC SHEET

Specifications

Model	GF300 / GF320
Detector Type	FLIR Indium Antimonide (InSb)
Spectral Range	3.2 – 3.4 µm
Resolution	320 x 240 pixels
Detector Pitch	30 µm
NETD/Thermal Sensitivity	<15 mK @ +30°C (+86°F)
Sensor Cooling	Stirling Microcooler (FLIR MC-3)
Electronics / Imaging	
Image Modes	IR Image, visual image, high sensitivity mode (HSM)
Frame Rate (Full Window)	60 Hz
Dynamic Range	14-bit
Video Recording / Streaming	Real-time non-radiometric recording: MPEG4/H.264 (up to 60 min./clip) to memory card Real-time non-radiometric streaming: RTP/MPEG4
Visual Video	MPEG4 (25 min./clip) to memory card
Visual Image	3.2 MP from integrated visible camera
GPS	Location data stored with every image
Camera Control	Remote camera control via USB
Measurement	
Standard Temperature Range	–20°C to +350°C (–4°F to +662°F)
Accuracy*	±1°C (±1.8°F) for temperature range (0°C, to +100°C, +32°F to +212°F) or ±2% of reading for temperature range (>+100°C, >+212°F)
Optics	
Camera f/number	f/1.5
Available Fixed Lenses	14.5° (38 mm), 24° (23 mm)
Focus	Automatic (one touch) or manual (electric or on the lens)
Image Presentation	
On-Camera Display	Built-in widescreen, 4.3 in. LCD, 800 x 480 pixels
Automatic Gain Control	Continuous/manual, linear, histogram
Image Analysis*	10 spotmeters, 5 boxes with max./min./average, profile, delta temperatures, emissivity & measurement corrections
Color palettes	Iron, Gray, Rainbow, Arctic, Lava, Rainbow HC
Zoom	1-8x continuous, digital zoom
General	
Operating Temperature Range	–20°C to +50°C (–4°F to +122°F)
Storage Temperature Range	–30°C to +60°C (–22°F to +140°F)
Encapsulation	IP 54 (IEC 60529)
Bump / Vibration	25 g (IEC 60068-2-27) / 2 g (IEC 60068-2-6)
Power	AC adapter 90-260 VAC, 50/60 Hz or 12 V from a vehicle
Battery System	Rechargeable Li-ion battery
Weight w/ Battery & Lens	1.94 kg (4.27 lbs)
Size (L x W x H) w/ Lens	305 x 169 x 161 mm
Mounting	Standard, 1/4"-20

* GF320 model only

FLIR Systems, Inc.
9 Townsend West
Nashua, NH 03063
USA
PH: +1 866.477.3687

PORTLAND
Corporate Headquarters
FLIR Systems, Inc.
27700 SW Parkway Ave.
Wilsonville, OR 97070
USA
PH: +1 866.477.3687

EUROPE
FLIR Systems
Luxemburgstraat 2
2321 Meer
Belgium
PH: +32 (0) 3665 5100

www.flir.com/ogi
NASDAQ: FLIR

CANADA
FLIR Systems, Ltd.
920 Sheldon Court
Burlington, ON L7L 5L6
Canada
PH: +1 800.613.0507

CHINA
FLIR Systems Co., Ltd
Rm 1613-16, Tower II
Grand Central Plaza
138 Shatin Rural
Committee Road Shatin
New Territories
Hong Kong
PH: +852 2792 8955

LATIN AMERICA
FLIR Systems Brasil
Av. Antonio Bardella, 320
Sorocaba, SP 18052-852
Brasil
PH: +55 15 3238 7080

www.flir.com

FLIR The World's Sixth Sense™

APPENDIX B

Component Classification and Counting Procedures

APPENDIX B

COMPONENT CLASSIFICATION AND COUNTING PROCEDURES

1.0 INTRODUCTION

Component classification and counts were completed at a depleted reservoir facility in Clay Basin, UT and two salt cavern facilities in the Gulf Coast region. Facilities were visited twice, and the methodology was refined between the field programs. As a result, an organized and reliable methodology was developed for classifying and counting components at natural gas underground storage wellheads. The purpose of this appendix is to describe the refined component classification and counting protocol used by GSI Environmental Inc. (GSI) during the Field Campaign 2 of this study. In general, this protocol explains the methods used to classify components into major component categories and disaggregate components into various subcategories.

2.0 COMPONENT COUNT PROTOCOL

Component types were separated into the following main categories: connectors (flanged and other), valves, pressure relief valves (PRV), open ended lines (OEL), meters, gauges, and regulators. The categories of connectors, valves, PRVs, and OELs are consistent with U.S. Environmental Protection Agency's (USEPA) Mandatory Greenhouse Gas Reporting Program (GHGRP) Subpart W (Tables W-4A) (U.S EPA 2016). Meters, gauges, and regulators were added to the counting protocol due to i) the relatively large number of these components at the sites (gauges and regulators), or ii) the presence of the category in different sections of Subpart W (meters).

When applicable, classified components were further subdivided based on physical and/or operational characteristics. A summary of major component categories and subcategories is presented in Table B-1.

Table B-1. *Component categories used in classification and count protocol*

Major Component Categories	Major Component Subcategories	Component Specifics
Connector	Other or flanged; Size of other connector (d=0.5", 0.5" < d < 6", d ≥ 6); Size of flanged connector (d < 1', 1' ≤ d < 3', d ≥ 3')	• Within pneumatic loop? • Function (e.g. pressure, temperature, emergency shutdown [ESD], etc.) • Other (visibility limitations)
Valve	Size (small, large); type (ball, gate, needle); and operating mechanism (manual, pneumatic, electronic)	
Pressure Relief Valve	n/a	
Meter	n/a	

Gauge	n/a	
Regulator	n/a	
Open-Ended Line	n/a	

Additional component specifics were documented to support further subcategorizations and/or data analyses, as discussed below:

- Components within a pneumatic device loop (Figure B-1), such as small valves, regulators, and connectors were counted individually and documented as being associated with a pneumatic loop.
- Components located within a pneumatic loop that were operated on system air (instead of natural gas) were not included in the population counts.
- The primary function of each component was documented. Major component functions include: flow, pressure, and temperature control and/or measurement; emergency relief or shutdown.

Figure B-1 *Examples of pneumatic loops: a) and b) pneumatic loop shed and closeup of interior at underground reservoir facility, c) small pneumatic loop box on wellhead at underground reservoir facility, d) pneumatic loop at salt cavern facility, e) and f) pneumatic loop shed and closeup of interior at salt cavern facility.*

3.0 COMPONENT SPECIFIC DETAILS

Detailed descriptions of various component types and classification and subcategorization procedures are discussed in the following sections.

3.1 Connector, Other

Examples of other connectors and counts are shown in Figure B-2. These components connect piping or tubing together, connect piping/tubing to other components, or connect piping/tubing to equipment. This category includes all non-flanged connections, such as threaded (e.g., Figure B-2c) and compression (e.g., Figure B-2a) fittings.

- Other connectors were subdivided based on the diameter of tube/pipe that was being connected: d = 0.5”, 0.5” < d < 6”, and d ≥ 6”. Connectors on tubing less than 0.5” were seen infrequently and not counted.
- Threaded or compression connections that connected tubing/piping to a component (regulators, gauges, valves) were counted as individual connectors, and not part of the connected component. In other words, emissions from these connections were classified as connectors, not emitting regulators, gauges, valves, etc.
- Connectors (threaded, compression) located within a pneumatic loop were counted individually. (e.g., Figure B-2c).
- Connectors (threaded, compression) that were part of a larger component and not used to connect tubing/piping or other components were not counted as separate connections. For example, a grease fitting on a large valve was not included in the connector count. Emissions from these fittings were included as part the larger component.

3.2 Connector, Flanged

Examples of flanged connectors and counts are shown on Figure B-2b. These components connect lengths of pipe together, connect other large components to pipes, or cap pieces of equipment with a ring of bolts.

- Flanged connectors were subdivided based on the diameter of the flange: d < 1’, 1’ ≤ d < 3’, d ≥ 3’.
- Flanges that were part of a larger component (e.g. valves) were counted separately. For example, a large valve that has three separate flanges (see Figure B-3g) would contribute three flanges to the total flanged connector count.

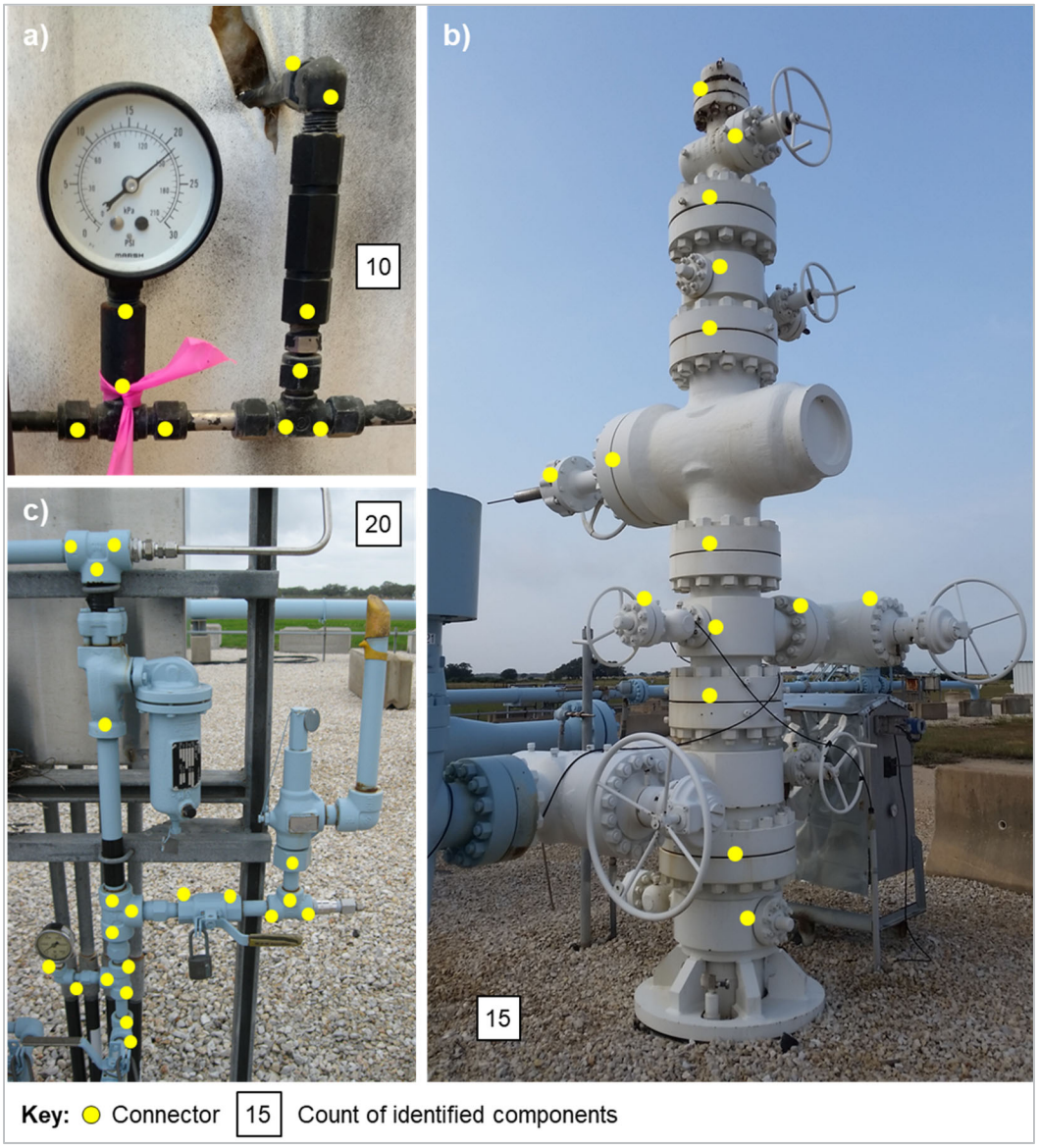

Figure B-2. *Connectors and example component counts at gas storage wellheads*

3.3 Valves

Examples of valves and counts are shown in Figures B-3 and B-4. The function of a valve is to control flow and/or pressure through the line. The field sites had valves that could be operated manually, pneumatically, or a combination of these two mechanisms. Manual valves were categorized as those that require a person to physically turn a handle or wheel to open or close the valve (e.g., Figures B-3c and B-4a). Pneumatic valves were actuated (opened/closed, throttled) and controlled by pneumatic (e.g. instrument/fuel gas) means (e.g., Figure B-3a).

Manual Valves

- Manual valves were subdivided based on size and type. Valves that could be turned with one hand were classified as small, valves that could not easily be turned with one hand were classified as large.
- Small manual valves were identified as ball, needle, or gate valves (Figure B-4); large manual valves were identified as ball or gate valves (Figure B-3).
- Small manual valves located within pneumatic device loops were classified as individual valves and counted towards the total valve population. However, these valves were noted as being associated with a pneumatic device.

Figure B-3. *Examples of Large Valves on Underground Natural Gas Storage Wellheads*

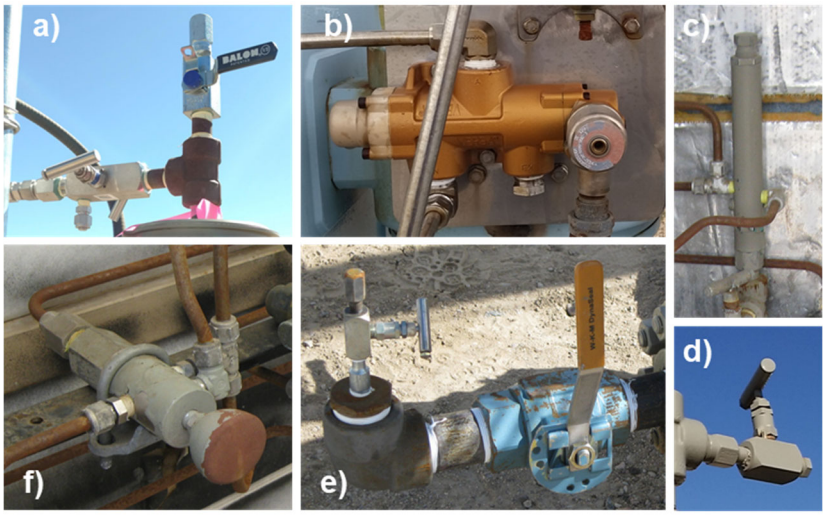

Figure B-4 *Examples of Small Valves on Underground Natural Gas Storage Wellheads*

Pneumatic Valves

- In pneumatic valves, the size of the flow passage is controlled by a signal from the pneumatic controller.
- Pneumatic valves were identified by an instrument or fuel gas supply line, examples are shown in Figure B-3d and f.
- At the sites visited, the valve-portion of the pneumatic loop was not designed to vent; therefore, any emissions coming from a pneumatic valve were classified as a leak.

Pressure Relief Valves

Examples of PRVs and component counts are shown on Figure B-5. The function of a PRV is to protect equipment from being subjected to pressures the equipment is not designed to handle. The PRV is designed to open when a certain pressure is exceeded, relieving the unsafe pressure. Many PRVs encountered in this study had a pipe or stack attached to their outlet side to route any emissions to a higher elevation (see Figure B-5). All components on pipes/stacks after PRVs are at atmospheric pressure and any emissions that appear to come from them are because of a malfunction (or activation) in the upstream PRV, therefore:

- Components on pipes/stacks following PRVs were not counted.
- Open pipes/stacks following PRVs were **not** categorized as open-ended lines (OEL).

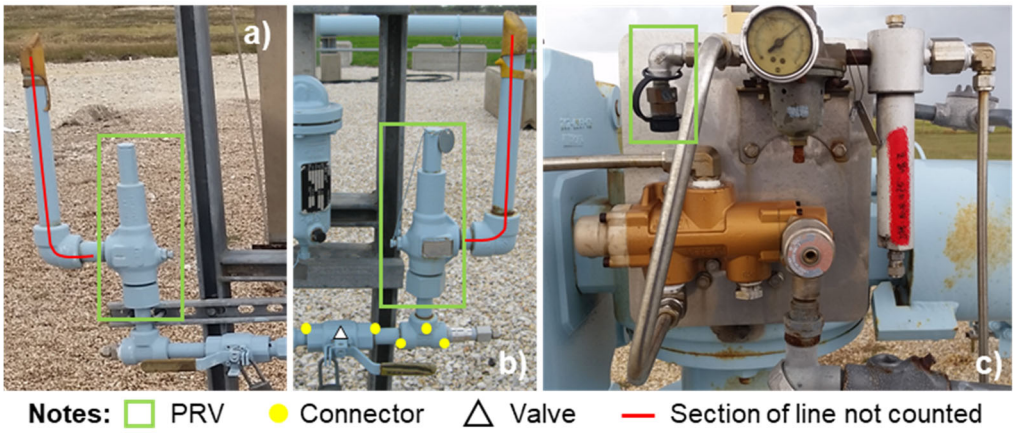

Figure B-5. *Examples of PRVs on Underground Natural Gas Storage Wellheads*

3.4 Gauges

Examples of gauges are shown on Figure B-6. The purpose of a gauge is to instantaneously measure an operational parameter (e.g., pressure, temperature). Gauges do not provide information on the rate or usage of a parameter. At underground storage wellheads, gauges can be analog (dial) (Figure B-6a) or electronic (Figure B-6b), and usually measure pressure or temperature.

- For a gauge to be classified as leaking, the emissions had to come from the gauge itself (e.g., cracked glass, top of gauge), not the connectors that attached the gauge to pipes or equipment.
- Gauges were divided into categories based on type of measurement: pressure, temperature, level (i.e., site glass).
- Many pneumatic devices have gauges on the fuel gas line. These gauges were included in the site-wide count, but also identified as part of a pneumatic device.

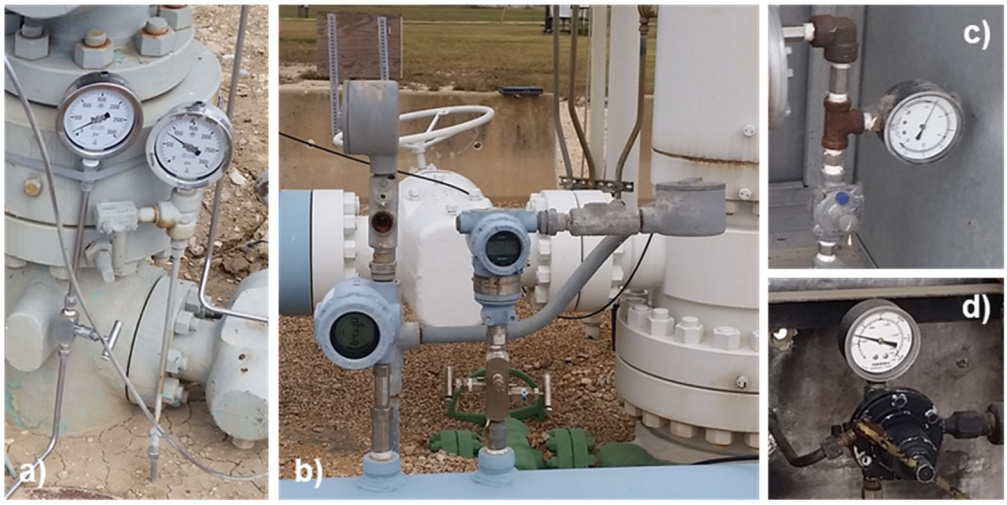

Figure B-6. *Examples of Gauges on Underground Natural Gas Storage Wellheads*

3.5 Regulators

Examples of regulators are shown on Figure B-7. For this study, regulators were defined as devices that reduce the inlet pressure of gas to smaller output pressure. At underground natural gas storage wellheads regulators were commonly found in pneumatic loops. These regulators reduce the fuel gas pressure to the required pneumatic loop input.

- Many different types of pressure regulators were encountered during this study, some of which were designed to vent while others were not. If there was uncertainty on whether emissions from a regulator should be classified as a leak or vent, site operators were asked to confirm.
- Regulators were only classified as leaking or venting if the emission was confirmed to be sourced from the regulator (e.g. damaged seals, rusted/cracked housing, vent ports, etc.). Leaks from threaded or compression connections attaching tubing/pipe to the regulators did not qualify as a leak from a regulator.
- Many pneumatic loops have multiple regulators in series on their fuel/instrument gas lines. These regulators were counted individually and included in the site-wide count, but also identified as part of a pneumatic device.

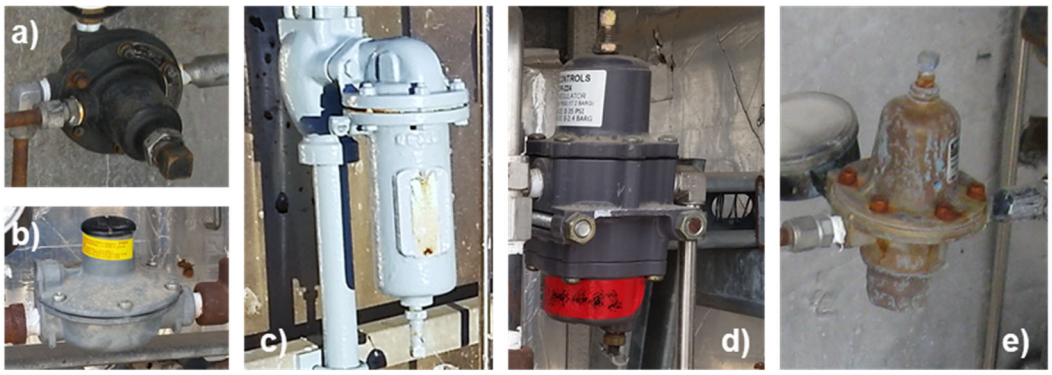

Figure B-7. *Examples of Regulators on Underground Natural Gas Storage Wellheads*

3.6 Meters

Examples of meters are shown on Figure B-8. In this protocol, meters are defined as instruments that measure the rate or usage of an operational parameter, such as cumulative gas flow. Most meters in this study were identified by digital read-outs of parameters being measured.

- Small connections (threaded, compression) and valves connected to meters were counted individually, and therefore included in the site-wide count.
- Meters seen at underground storage wellheads in this study could easily be misidentified as gauges, and vice versa. To ensure the component is identified correctly check the parameter being measured, flow/throughput indicates the component is a meter while temperature or pressure indicates the component is a gauge. Devices that measured multiple parameters were classified as meters if one of the parameters was flow.

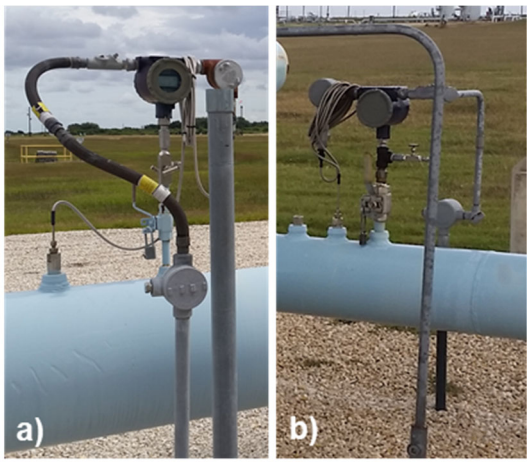

Figure B-8. *Examples of Meters on Underground Natural Gas Storage Wellheads*

4.0 REFERENCES

U.S. EPA, 2016. Mandatory Greenhouse Gas Reporting Subpart W – Petroleum and Natural Gas Systems, 40 C.F.R. §98.232.

APPENDIX C

High Flow Sampling Procedures

APPENDIX C

HIGH VOLUME SAMPLING PROCEDURES

1.0 TECHNOLOGY BACKGROUND

High flow samplers have been used in the oil and gas industry to detect natural gas leaks for decades, have been used in a number of scientific studies (Allen et al., 2013; Johnson et al., 2015) and are approved by USEPA for leak quantification (CFR, 2016). However, only one commercial high flow sampler exists, the backpack-mounted Bacharach HI FLOW, and it suffers from several biases. The Bacharach sampler uses detectors that do not distinguish between methane and other organics, and that do not detect all organic compounds with the same sensitivity, leading to uncertainty in measurements, especially for sources for which non-methane organics make up a high percentage of total emissions. Because of the size of its pump, the Bacharach sampler is limited to leaks smaller than about 1,000 standard cubic feet per hour (SCFH). Most importantly, the sampler uses two detectors, and its software does not switch from the low-range to the high-range detector reliably, leading to a low bias in measurements (Howard et al., 2015; Ravikumar et al., 2018). Bacharach has stopped manufacturing the HI FLOW, and the instrument is difficult to obtain from equipment rental companies.

Alternatives to high flow sampling exist for measuring emissions from oil and gas infrastructure. Traditional bag sampling techniques (EPA, 1995) are more complicated, take longer to set up, and only work for low flows. Bag-filling techniques (CFR, 2016; Subramanian et al., 2015) suffer from poor accuracy, especially at low and high flows. Methods that directly measure actual emission flow rates from exhaust streams (Hendler et al., 2009) can provide as much or more accuracy than high flow sampling methods but are only applicable for equipment with an exhaust pipe to which a flow measurement tube can be attached. For most fittings, valves, meters, or other small components of gas infrastructure, high flow sampling provides the simplest and most versatile method to quantify emission rates.

2.0 SYSTEM DESCRIPTION

2.1 System Overview

A custom high-flow sampling system was developed to quantify methane leaks from gas infrastructure. This system is similar to that developed by Johnson et al. (2015). The following sections describe this system and report on its performance. A diagram of the high flow sampling system is shown in Figure C-1, and photographs of the system are shown in Figure C-2. The system operates by:

1. Pulling sample gas from a leaking component into a sampling duct.
2. Precisely measuring the total flow rate of sample gas through the sampling duct.
3. Analyzing the sample gas to determine the methane concentration.

4. Correcting sample gas concentrations for the methane concentrations in ambient air near the leaking component.

The methane emission rate is calculated as:

$$E = C \times F \qquad \textit{(Equation C-1)}$$

where E is the methane emission rate, C is the concentration of methane in the sample gas (corrected for the concentration in ambient air), and F is the flow rate of sample gas. In practice, E is calculated in metric units, so E has units of g s^{-1}, C has units of g m^{-3}, and F has units of m^3 s^{-1}. The ideal gas law was then used to convert E to the commonly used units of SCFH at standard temperature of 60° F.

The system was mounted in a generator-powered trailer and included 40 m of sample ducting, which allowed for a large area to be sampled without moving the trailer. The entire flow path was intrinsically safe or conductive and grounded to the trailer, which was grounded to the earth.

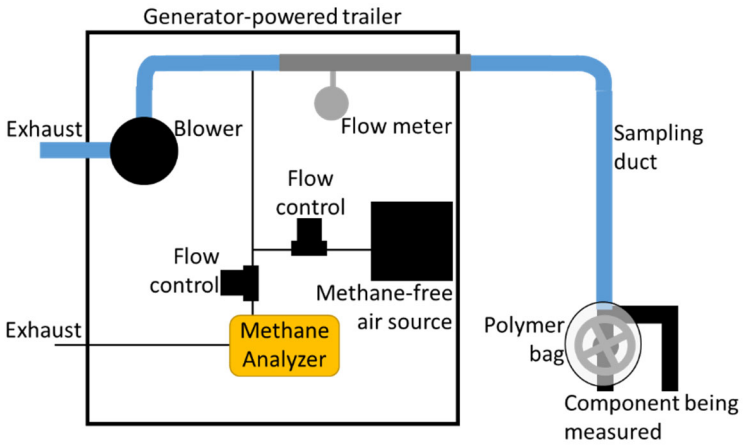

Figure C-1. *Diagram of high flow sampling system.*

Figure C-2 *Photographs of the high flow sampling system in operation: a) entire system, b) interior of the trailer, and c) bagging a valve for sampling.*

3.0 DETAILED SYSTEM DESCRIPTION

3.1 Locating Leaks

Leak locations were detected with a FLIR GF320 optical gas imaging camera and/or a Bascom Turner Gas Rover (see Appendix A for details on FLIR screening). The Bascom Turner Gas Rover is a handheld instrument to measure methane concentrations. It is able to detect methane in air at 10 ppm or greater. The Gas Rover is generally able to detect smaller emission sources than the FLIR camera, but the camera is better able to pinpoint the exact source of emissions.

After locating a leak, it was flagged, given an identification number, and then the leak rate was quantified with the high flow sampling system.

3.2 Isolating Leaks for Measurement

The high flow system's sampling duct was constructed of 13 cm diameter conductive ducting in 8-m lengths. Aluminum foil tape was used to seal the duct connections. In most cases, an antistatic polymer bag was wrapped around the component and the duct inlet. This isolated the sample from surrounding air and ensured that all of the leaking gas was entrained into the sampling duct. Metal clips and aluminum foil tape were used to aid in this process. In some cases, leaking components could be inserted into the end of the sampling duct, allowing for all leaking gas to be entrained without bagging. In all cases, after connecting the duct to the leaking component, a Bascom Turner Gas Rover was used to measure methane all around the leaking component, sample duct, and bag to ensure that all leaking gas was entrained in the duct.

3.3 Sample Flow System

An explosion-proof vacuum blower pulled a high volume of gas (between 0.5 and 2.5 cubic meters per minute [$m^3\ min^{-1}$]) from the sampled component, through the sample duct, and through a flow measurement tube. A manual flow damper was used to adjust the flow if needed. A Fox Thermal Instruments Model FT1 mass flow meter was used to measure flow. The flow meter was housed in a 3 m long, 11 cm diameter stainless steel tube with a stainless-steel flow conditioner at the upstream end. The flow meter was positioned 1.7 m from the upstream end of the tube.

One shortcoming of all mass flow measurements is that the measured flow depends on the composition of the gas sampled. This was compensated for by correcting flows for the methane concentration in the sample gas. However, non-methane organic compounds in emitted gas were not measured and could have resulted in a flow bias, especially for components with high emission rates of gas with high concentrations of non-methane organics, such as liquid storage tanks (Hendler et al., 2009).

3.4 Methane Measurement

A Los Gatos Research (LGR) Ultraportable Greenhouse Gas Analyzer was used to measure methane concentrations in sample gas. Sample lines leading to and from the analyzer were composed either of PFA tubing or Tygon 2475 high-purity tubing. The analyzer detects methane concentrations of up to 10% in air. It detects up to 1000 ppm with a low-concentration laser and

greater than 1000 ppm with a separate high-concentration laser. The results were recorded from both lasers for all samples. When the methane concentration in sample gas exceeded 10%, the analyzer flow was diluted with methane-free air to keep within the analyzer's range. Methane-free air was generated with a custom-built air scrubber system, and the system was tested daily to ensure air produced by the system contained less than 0.2 ppm methane. The flow into the analyzer was measured, as well as the flow rate of methane-free dilution air, with Alicat mass flow controllers. The calibration of the mass flow controllers was checked with a NIST-traceable flow standard prior to each measurement campaign.

3.5 Correction for Background Methane

The methane concentration in sample gas was equal to the ambient methane concentration in the air being pulled into the high flow sampling duct plus any methane added from the leaking component. To correct for ambient methane, the ambient methane concentration was measured through a PTFE filter and a 0.5 cm line composed of Tygon 2475 high-purity tubing. The inlet of this line was positioned as close to the sample duct inlet as possible. A LGR Multiport Inlet Unit allowed the methane analyzer to switch between analyzing sample gas and analyzing air from the background line. Usually, the system was programmed to measure sample gas for three minutes and then background air for two minutes. Data for the first minute was discarded after each valve switch. The background methane concentration was subtracted from the sample gas concentration prior to calculating emission rates.

3.6 Sampling Intervals

All measurement data was sampled once every 5 seconds and stored data as 20 second averages. In most cases, emissions from each measured component were quantified for 8-12 minutes. If the emission rate was variable, or as an occasional test of emission stability, the measurement time was extended. A 10-minute sampling time resulted in about ten separate 20-second emission rate measurements.

3.7 Measurement System Calibrations

The calibration of the methane analyzer was checked daily at four or five points along its measurement range, including points within the range of both methane lasers. The analyzer was also periodically checked at 15-20 points to ensure its response was linear across its range. The scrubber system mentioned above was used to generate methane-free air, and NIST-traceable compressed gas standards or an ultra-high purity methane cylinder was diluted to generate methane at specific concentrations. Alicat mass flow controllers were used to control and measure flows in the calibration system. The calibration of all mass flow controllers was checked with a NIST-traceable flow standard prior to each measurement campaign.

A mass flow controller was used to add methane from an ultra-high purity methane cylinder to the upstream end of the high flow sampling duct daily to verify the performance of the high flow measurement system. Methane was added at two different flow rates between 0.1 and 30 liters per minute (L min^{-1}). As a blank test, the emission rate was measured daily while the high flow duct was not sampling any emission source.

The Fox FT1 mass flow meter was calibrated at the factory annually, and its flow was checked prior to each measurement campaign with a Pacer DA420 anemometer. Wind speed output of the Pacer anemometer was converted to mass flow by multiplying the speed by the orifice size and correcting for temperature and ambient pressure.

3.8 Meteorological Measurements

Basic meteorology was measured during all measurement periods from a retractable 6 m pole attached to the measurement trailer. A New Mountain NM150WX was used to measure temperature, relative humidity, barometric pressure, GPS location, and GPS heading. A Campbell CS300 was used to measure solar radiation. A Gill WindSonic was used to measure wind speed and direction, and wind direction was automatically corrected based on the GPS heading. All meteorological measurements were checked against NIST-traceable standards annually.

3.9 Data Collection, Processing, and Storage

All measurement data was collected with a Campbell Scientific CR1000 data logger. Sample names, times, and all other notes were recorded electronically throughout each measurement day. At the end of each day, all collected data and notes were uploaded to an automatically archived, cloud-based server. All collected data and generated final results were processed in Microsoft Excel. Every 30 days all data was backed up in three locations, including a cloud-based server, a local hard drive, and a separate local hard drive that was disconnected from the internet except during archival operations.

3.10 Safety

All external components of the high flow system were grounded to the trailer (all components were conductive), and the trailer was attached to an earth ground. All components that came into contact with sample gas were antistatic and/or explosion proof, including all pumps, flow controllers, and flow meters. The interior of the trailer was not rated for environments that may be rich in flammable gases, so the trailer was kept 10 m or more from potential sources of flammable gas, and the generators that powered the trailer were kept 20 m or more from flammable gas sources. Additionally, a natural gas monitor was mounted in the trailer to provide a warning if combustible gas concentrations in the trailer built up to dangerous concentrations.

4.0 DETECTION LIMITS

4.1 Method Detection Limit

The method detection limit of the high flow system was calculated as (a) three times the standard deviation of a set of 20-second emission measurements when the instrument was not measuring any emission source (i.e., a blank) (EPA, 2016), and (b) three times the standard deviation of a set of 20-second emission measurements when the system was sampling a very low emission rate generated with a mass flow controller (1.1×10^{-3} SCFH). Method detection limits calculated using (a) and (b) were 2.3×10^{-4} and 1.0×10^{-4} SCFH, respectively.

Figure C-3 shows emission rate data from (a) and (b), which were collected outside the laboratory in Vernal, Utah, distant from oil and gas industrial facilities, but in the vicinity of urban and agricultural sources of methane. Gaps in the emission rate data shown in Figure C-3 are from periods when the ambient (background) methane concentration was measured. It is expected, but be cannot confirmed, that the variability in blank values observable in Figure C-3 was due to variation in ambient methane concentrations. The blank variability shown in Figure C-3 corresponds to a variability in methane concentration of ± 35 parts per billion (ppb).

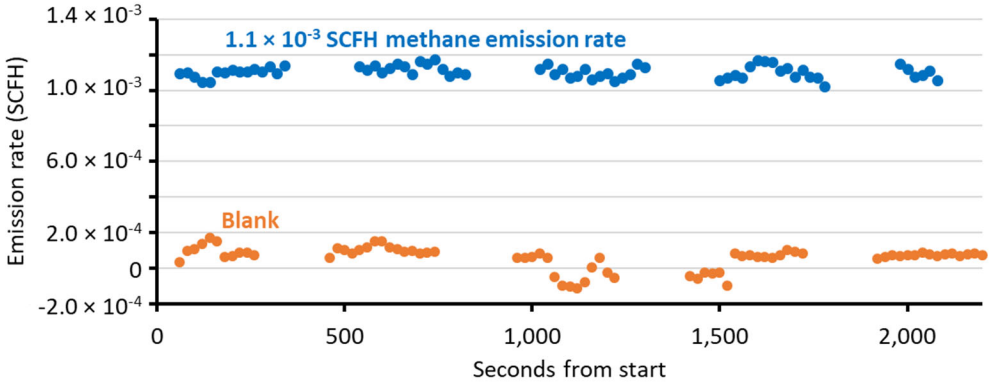

Figure C-3 *Methane emission measurement data from a detection limit test, including blank measurements and measurements of a 1.1 × 10-3 SCFH emission rate produced with a mass flow controller.*

4.2 Practical Detection Limit in Field Conditions

Industrial gas facilities have many methane emission sources and variable ambient methane levels. Because the high flow measurement system does not measure background methane and methane in sample gas simultaneously, short-term variations in ambient methane are not adequately corrected for in emission measurements, leading to a decrease in measurement precision (but not accuracy) at industrial facilities. To assess the practical detection limit (a measure of precision) in field conditions, emission measurement blanks were collected (~10 min each) at natural gas storage wells (n = 28). These data were used to calculate practical detection limits for gas storage wells as described above. These values are shown in Table C-1.

Table C-1. *Statistical information for blank emission measurements collected outside the laboratory and at natural gas storage wells, in units of SCFH. Values shown were calculated from 20 s data.*

SCFH	Lab Blank	Gas Storage Wells	Gas Storage Wells (no outliers)
Average	4.8 × 10-5	2.1 × 10-3	3.6 × 10-4
Median	7.0 × 10-5	1.0 × 10-4	6.7 × 10-5
Std. Deviation	7.8 × 10-5	1.1 × 10-2	1.4 × 10-3
Detection Limit	2.3 × 10-4	3.4 × 10-2	4.1 × 10-3
95% Conf. Interval	1.6 × 10-5	6.7 × 10-4	8.1 × 10-5

In addition to having higher detection limits (a measure of precision), emission measurement blanks collected at gas storage wells had higher average values than the laboratory blank (Table C-1). In other words, the sample duct had higher methane concentrations than the background measurement line. It was found that sample methane concentrations remained higher than ambient methane for at least 30 minutes after sampling strongly leaking components, indicating that residual methane remained in the sample flow path. It is not clear whether this residual methane was in the sample duct, the sample line from the duct to the analyzer, or the switching unit. Assuming the residual methane in the sample line is released at a steady rate, it likely had only a small impact on calculated detection limits.

A few of the blank samples (n = 6) were statistical outliers, determined as 10-minute average blanks that were higher or lower than 1.5 times the interquartile range. These outliers were either the result of high methane in the sample line prior to the blank measurement or highly variable background methane. With these outliers removed, the practical detection limit was lowered by about an order of magnitude (Table C-1).

5.0 CALIBRATION RESULTS

Table C-3 provides a summary of the results of calibration checks performed on field measurement days.

Table C-3. *Summary of field calibration results. Zero indicates the analyzer response when methane-free air was sampled. The analyzer's low laser was used for methane concentrations less than 1000 ppm, and the high laser was used for concentrations greater than 1000 ppm.*

	Zero (ppm)	Low Laser (% Recovery)	High Laser (% Recovery)	High Flow System (% Recovery)
Average	0.10	101.0	99.7	104.1
Count	49	67	86	95
95% Conf. Interval	0.04	0.8	1.0	1.2

6.0 MEASUREMENT RANGE

The method detection limit of 2.3×10^{-4} SCFH is, by definition, the lower end of the measurement range for the high flow sampling system. The maximum flow rate of the sample duct was about 2,500 L min^{-1} and was limited by the flow producible by the blower. Thus, the maximum methane emission rate the system could measure was 2,500 L min^{-1} methane, or 5,727 SCFH. A larger blower, or two blowers in series, could perhaps double the flow rate, leading to a maximum of 11,454 SCFH, eight orders of magnitude higher than the method detection limit. The highest emission rate measured was a large valve, which had a methane emission rate of 72.8 SCFH.

7.0 REFERENCES

Allen, D.T., Torres, V.M., Thomas, J., Sullivan, D.W., Harrison, M., Hendler, A., Herndon, S.C., Kolb, C.E., Fraser, M.P., Hill, A.D., 2013. Measurements of methane emissions at natural gas production sites in the United States. Proc. Natl. Acad. Sci. U. S. A. 110, 17768-17773.

CFR, 2016. CFR Title 40, Part 98, Subpart W, Section 98.234, https://www.gpo.gov/fdsys/pkg/CFR-2011-title40-vol21/pdf/CFR-2011-title40-vol21-sec98-234.pdf.

EPA, U.S., 1995. Protocol for equipment leak emission estimates. United States Environmental Protection Agency, Research Triangle Park, NC, https://www3.epa.gov/ttnchie1/efdocs/equiplks.pdf.

EPA, U.S., 2016. Definition and Procedure for the Determination of the Method Detection Limit, Revision 2. United States Environmental Protection Agency, Washington, D.C., https://www.epa.gov/sites/production/files/2016-12/documents/mdl-procedure_rev2_12-13-2016.pdf.

Hendler, A., Nunn, J., Lundeen, J., 2009. VOC emissions from oil and condensate storage tanks: Final report prepared for Texas Environmental Research Consortium. Texas Environmental Research Consortium, http://www.mcilvainecompany.com/Decision_Tree/subscriber/articles/Emissions_From_Oil_and_Condensate_Storage_Tanks_Final_Report.pdf.

Howard, T., Ferrara, T.W., Townsend-Small, A., 2015. Sensor transition failure in the high flow sampler: implications for methane emission inventories of natural gas infrastructure. J. Air Waste Manage. Assoc. 65, 856-862.

Johnson, D.R., Covington, A.N., Clark, N.N., 2015. Methane emissions from leak and loss audits of natural gas compressor stations and storage facilities. Environ. Sci. Technol. 49, 8132-8138.

MKS, 2017. Flow Measurement & Control, https://www.mksinst.com/docs/UR/FLOWfaq.aspx.

Ravikumar, A.P., Wang, J., McGuire, M., Bell, C.S., Zimmerle, D., Brandt, A.R., 2018. Good versus Good Enough? Empirical tests of methane leak detection sensitivity of a commercial infrared camera. Environ. Sci. Technol.

Subramanian, R., Williams, L.L., Vaughn, T.L., Zimmerle, D., Roscioli, J.R., Herndon, S.C., Yacovitch, T.I., Floerchinger, C., Tkacik, D.S., Mitchell, A.L., 2015. Methane emissions from natural gas compressor stations in the transmission and storage sector: Measurements and comparisons with the EPA greenhouse gas reporting program protocol. Environ. Sci. Technol. 49, 3252-3261.

APPENDIX D

Evaluation of Ground-Level Emission Fluxes

APPENDIX D

EVALUATION OF GROUND-LEVEL EMISSION FLUXES

1.0 METHODS

1.1 Soil Fluxes of Methane and Carbon Dioxide

The flux chamber was the same as that used by Lyman et al. (2017). It consisted of a 40 cm diameter half sphere polycarbonate chamber attached to a stainless steel ring that was pounded into the soil to create a seal. The chamber had a mixing fan at the top and a 1.2 cm hole on one side for air to pass through. A vacuum pump pulled air from within the chamber (on the opposite side from the hole) and from immediately outside the chamber through 0.6 cm PFA tubing at 10 L min^{-1}, and brought the air into an enclosed trailer for analysis. We used an LGR Ultraportable Greenhouse Gas Analyzer with an LGR valve switching unit to sequentially measure concentrations of methane and carbon dioxide in chamber and outside air. The valve switched between inside and outside air every 2 minutes, so one flux measurement was collected every 4 minutes. We used the last 60 seconds of each 2-minute measurement to calculate fluxes. We calculated fluxes as

$$F = (\Delta C \times Q) / S$$

Where F is the soil-air flux, ΔC is the difference in concentrations of the compound of interest inside versus outside the chamber, Q is the flow rate, and S is the surface area covered by the chamber.

At some flux measurement locations, we also measured fluxes of 54 non-methane hydrocarbons. We collected whole air samples in 6-liter (L) silonite-coated stainless steel canisters from the inside and outside chamber lines over a period of 30 minutes. In the laboratory, we pressurized canisters to 1035 millibar (mbar) (our average laboratory pressure is 860 mbar) and analyzed them within 40 days via gas chromatography (GC)/flame ionization detection (FID)/mass spectrometry (MS). We used an Entech 7200 to separate hydrocarbons from sample air and introduce them to the GC. Compounds with two and three carbons passed through a 60 m 100% polydimethylsiloxane column, a 30 m alumina/Na_2SO_4 PLOT column, and into the FID for analysis. All other compounds passed through 60 m and 30 m 100% polydimethylsiloxane columns and into the MS for analysis.

1.2 Sampling Locations, Frequency, and Duration

At the two natural gas storage facilities in the Gulf Coast region, we measured soil fluxes over 15-minute periods (two or three 4-minute flux measurements) at every well at each facility. At the Utah facility, we measured fluxes over 15-minute periods at 90% of the more than 40 wells at the facility. For all the 15-minute measurements, we measured at three locations near the wellhead at each well. We attempted to space the measurement locations equally around and within 1 m

of the wellhead, but the locations of equipment on well pads occasionally prevented this. In these cases, we placed flux chambers as close to the wellhead as possible, and as close to equally spaced as possible. We collected 15-minute measurements at all three facilities in March 2017 and again in October/November 2017. At the Utah facility, 40% of the wells at which we sampled were the same in both campaigns.

At two wells in Utah and one in the Gulf Coast region, we collected between 9 and 16 additional 15-minute flux measurements in October/November 2017. We installed probes to measure total combustible soil gas at each of these three wells (see next section), and we returned to these wells to collect flux measurements over longer periods. We measured soil flux at six chamber locations over four days at the two Utah wells in January 2018, over four days at the Gulf Coast well in March 2018, and again over eight days at one of the Utah wells in November 2018. Throughout this text, we refer to the Utah well at which we sampled in January and November 2018 as Utah Well #1, and we refer to the Utah well at which we only sampled in January as Utah Well #2.

For the 4-day and 8-day flux measurements, we used a manifold with solenoid valves to select among six flux chambers that were placed around each well, and we switched among the chambers hourly. We discarded the first 30 minutes of each hour-long measurement period to allow for equilibration of gas concentrations within the chamber.

1.3 Meteorological Measurements

We measured temperature and relative humidity (New Mountain NM150WX), wind speed and direction (Gill WindSonic), barometric pressure (New Mountain NM150WX), and total incoming solar radiation (Campbell CS300) at each facility at 6 m above ground level while collecting soil flux measurements and recorded these with a Campbell Scientific CR1000 data logger. All meteorological instruments were checked against NIST-traceable standards at least annually.

1.4 Total Combustible Soil Gas Measurements

We used a Bascom Turner Gas Rover to measure total combustible soil gas concentrations from subsurface probes that consisted of 0.6 cm tubing buried in 10 cm diameter holes that were augered to depths of 1.70, 1.20, 0.75, or 0.60 m. Some of the probes were clustered together, with three or four probes of various depths about 0.3 m in horizontal distance apart, in each cluster. The bottom 15 cm of each hole was backfilled with native soil. The next 15 cm was packed with sand, and the remainder of each hole, to a depth of 15 cm from the surface, was filled with hydrated bentonite. The 15 cm from the surface to the bentonite was capped, and we removed the cap to access the sampling tube. We allowed the soil gas analyzer to sample for 30 seconds (flow rate of ~1 L min^{-1}) before recording its output. Soil gas sampling probes were only installed at the three well pads where we collected flux measurements over 96 hours.

1.5 Quality Assurance

The LGR analyzer was equipped with two lasers for methane. We used the low-concentration laser for 0-2000 ppm methane (and the entire measurement range for carbon dioxide), and the

high-concentration laser for >2000 ppm methane. On each sampling day, we introduced air scrubbed of methane, carbon dioxide, and water vapor to the analyzer as a zero check, and we added calibration gas from certified compressed gas standards to the scrubbed air to check the instrument's calibration at several concentrations. We performed checks of the mass flow controllers used to regulate scrubbed air and calibration gas flows at least twice annually, and flows were always within 5% of expected values. In scrubbed air, methane was 51 ± 18 ppb (mean ± 95% confidence interval), and carbon dioxide was 0.2 ± 0.1 ppm. Recoveries for non-zero calibration values were 102 ± 1%, 101 ± 1%, and 103 ± 1% for the low methane laser, high methane laser, and carbon dioxide, respectively. The detection limits for methane and carbon dioxide fluxes were 0.06 and 18.9 milligrams per square meter per hour (mg m^{-2} h^{-1}), respectively.

The five-point calibration curves for each batch of whole-air canister samples analyzed had coefficient of determination (r^2) values of 0.998 ± 0.000. Samples analyzed in duplicate for each batch analyzed were 6 ± 3% different. Analytical blanks averaged 0.18 ± 0.02 ppb, and individual compounds in each sample were blank-corrected. Recovery of calibration standards analyzed in each batch was 99.7 ± 0.3%.

We checked the total combustible soil gas analyzer at two points daily with a certified compressed methane standard, and recovery was 102 ± 2%.

At some locations, facility operators asked us not to operate flux chamber mixing fans, since the fan motors were not intrinsically safe. On two separate sampling days, we turned a mixing fan on and then off again over 8-minute intervals while measuring soil flux. We did not observe any significant differences in methane or carbon dioxide flux between the fan-on and fan-off periods.

2.0 RESULTS AND DISCUSSION

2.1 Spatial Variability

For most wells, we only collected samples in close proximity to the wellhead, since Lyman et al. (2017) showed that flux magnitude at natural gas wells is inversely related to distance from the wellhead. More recently, Forde et al. (2019) found that flux magnitude was not related to distance from the wellhead at wells in British Columbia, Canada. Figures D-1 through D-3 show the spatial distribution of methane flux at three wells sampled in this study. The spatial distributions of fluxes in the figures are not uniform, but they do show that the highest fluxes tend to occur closer to the wellhead.

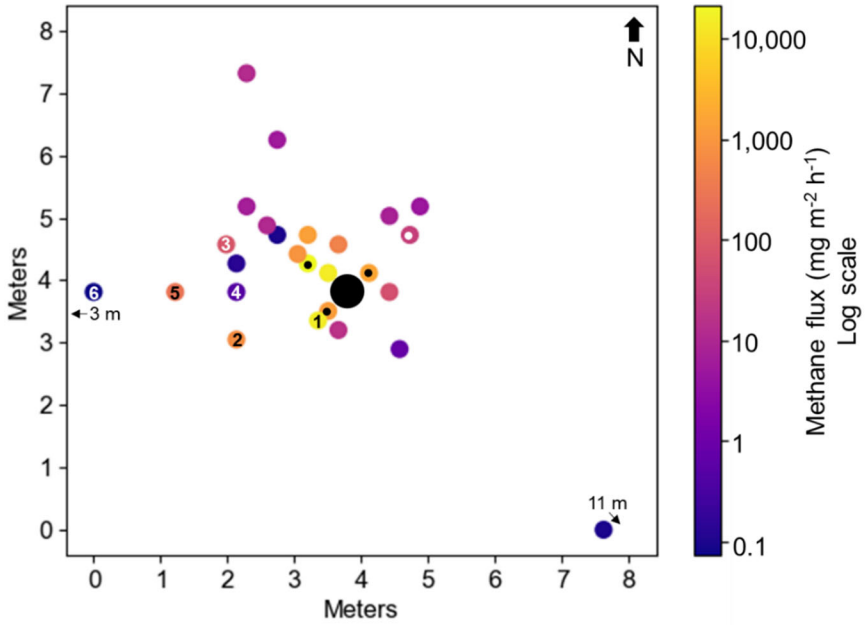

Figure D-1 *Spatial distribution of average methane fluxes around a natural gas storage wellhead in the Gulf Coast region. Each colored circle represents a flux measurement location. Circles with black or white dots are locations where short-term fluxes were measured in March 2017. Circles with numbers are locations of 4-day flux measurements in March 2018, and numbers correspond with flux data in subsequent figures. Other circles are locations where fluxes were measured in October/November 2017.*

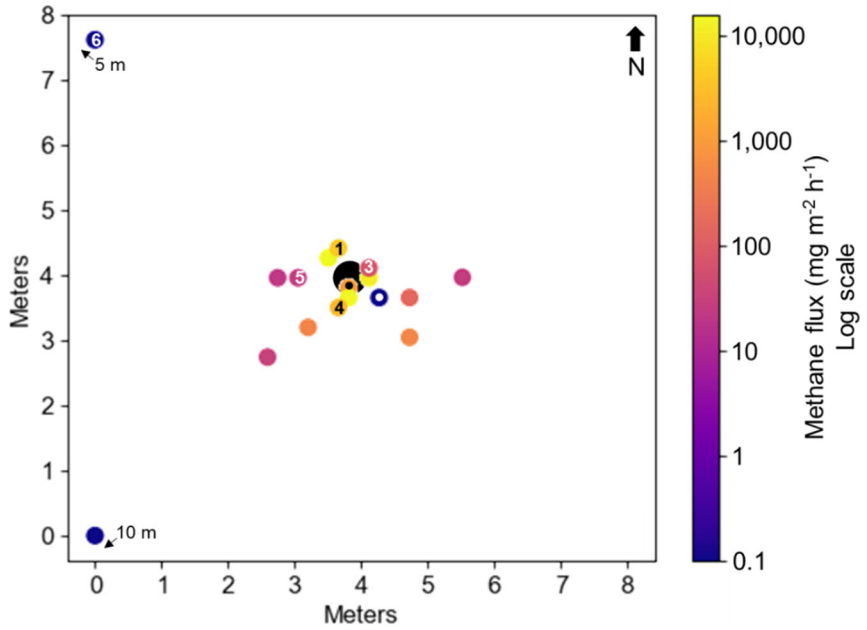

Figure D-2 *Spatial distribution of average methane fluxes around a natural gas storage wellhead in Utah (Well #1). Each colored circle represents a flux measurement location. Circles with black or white dots are locations where fluxes were measured in March 2017. Circles with numbers are locations of long-term flux measurements (average of 4 days in January 2018 and 8 days in*

November 2018), and numbers correspond with flux data in subsequent figures. Other circles are locations where fluxes were measured in October/November 2017.

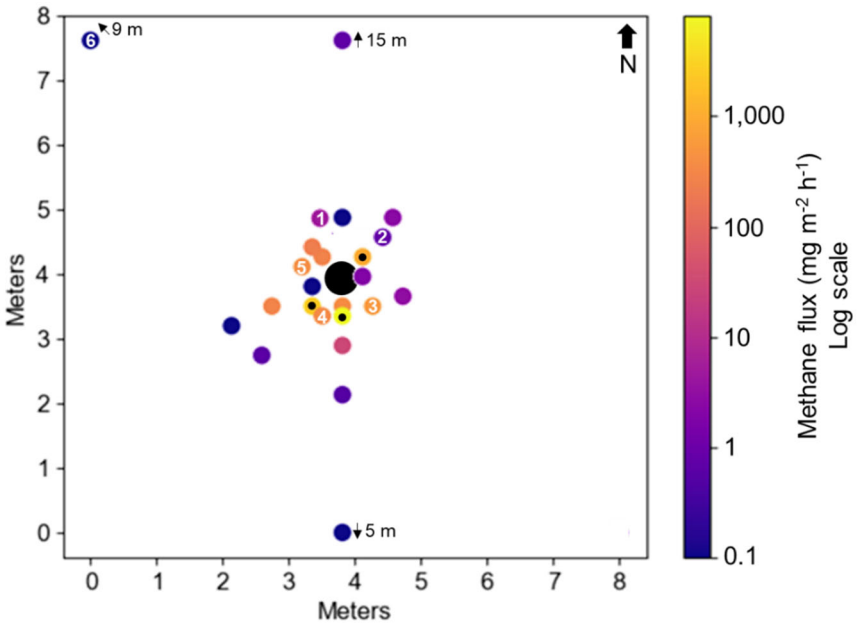

Figure D-3 *Spatial distribution of average methane fluxes around a natural gas storage wellhead in Utah (Well #2). Each colored circle represents a flux measurement location. Circles with black or white dots are locations where fluxes were measured in March 2017. Circles with numbers are locations of 4-day flux measurements, and numbers correspond with flux data in subsequent figures. Other circles are locations where fluxes were measured in October/November 2017.*

2.2 Seasonal Variability

Pad-average methane fluxes varied by an order of magnitude or more between March and October/November 2017 (Figure D-4). Since stored gas volumes at the facilities we visited were at their maxima in fall and at their minima in later winter/early spring, we expected that fluxes would be higher in October/November than in March. Average fluxes were higher in October/November at the Utah facility (facility-average flux of 87 and 976 mg m^{-2} h^{-1} in March and October/November respectively) and one of the Gulf Coast facilities (1127 vs 1385 mg m^{-2} h^{-1}) but not at the other Gulf Coast facility (8 vs -1 mg m^{-2} h^{-1}), and none of the differences were statistically significant (p values between 0.32 and 0.34). For the Utah facility, we only used fluxes from wells that were sampled in both campaigns in this analysis.

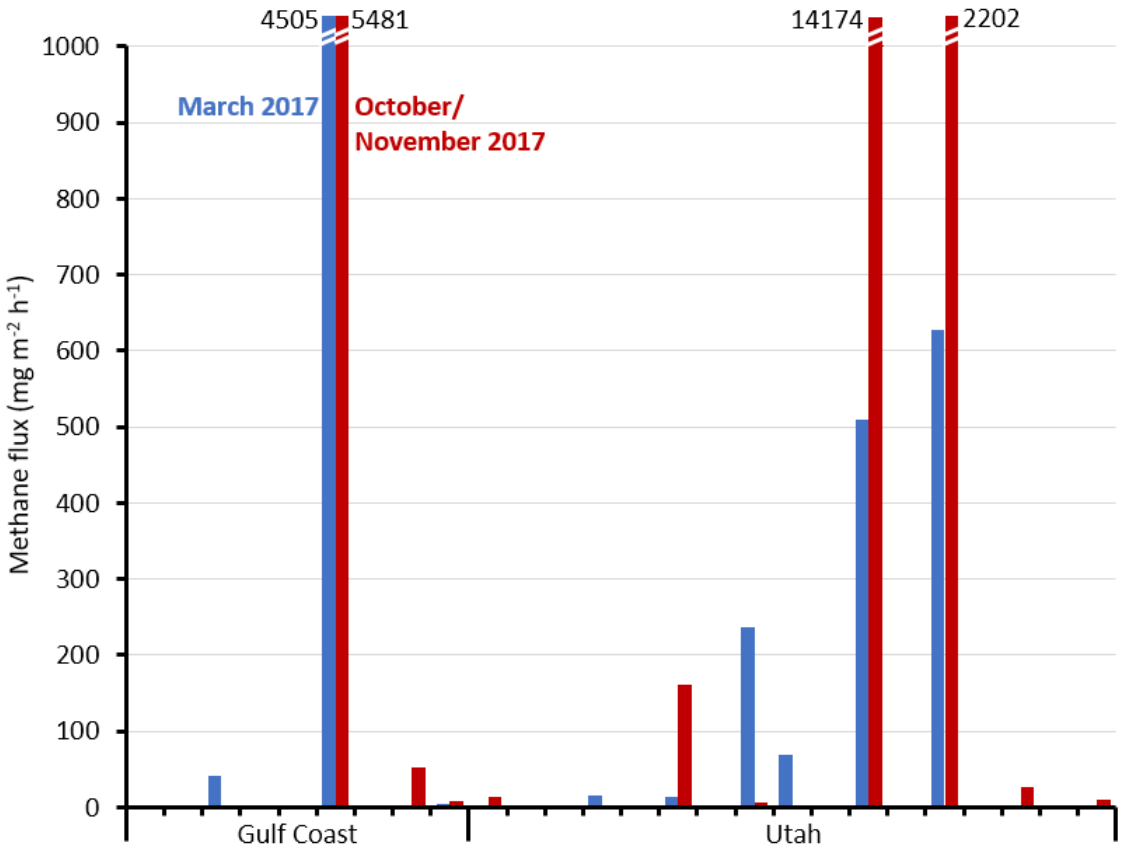

Figure D-4 *Average methane flux at wells visited in March and October/November 2017. Each blue and red pair of bars represents one well. Some bars are too small to be visible.*

2.4 Short-term Variability

Figures D-5 through D-7 show a time series of methane fluxes for the wells at which fluxes were measured over several days. These figures show that flux variability over several orders of magnitude occurred at some of the same chamber locations from day to day, and sometimes (e.g., Chamber 5 in Figure D-7) over 30-min measurement periods.

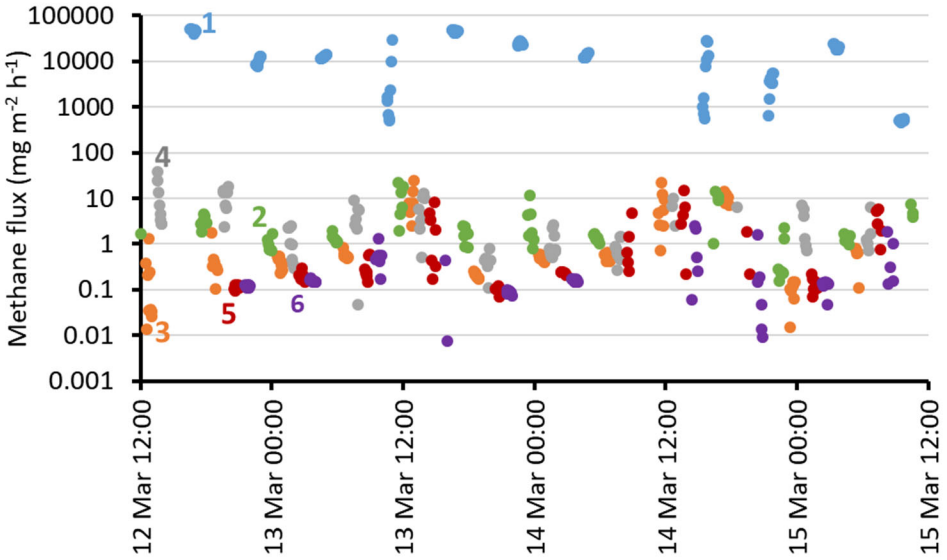

Figure D-5 *Methane fluxes in March 2018 at a gas storage well in the Gulf Coast region. Numbers correspond with chamber locations in Figure D-1.*

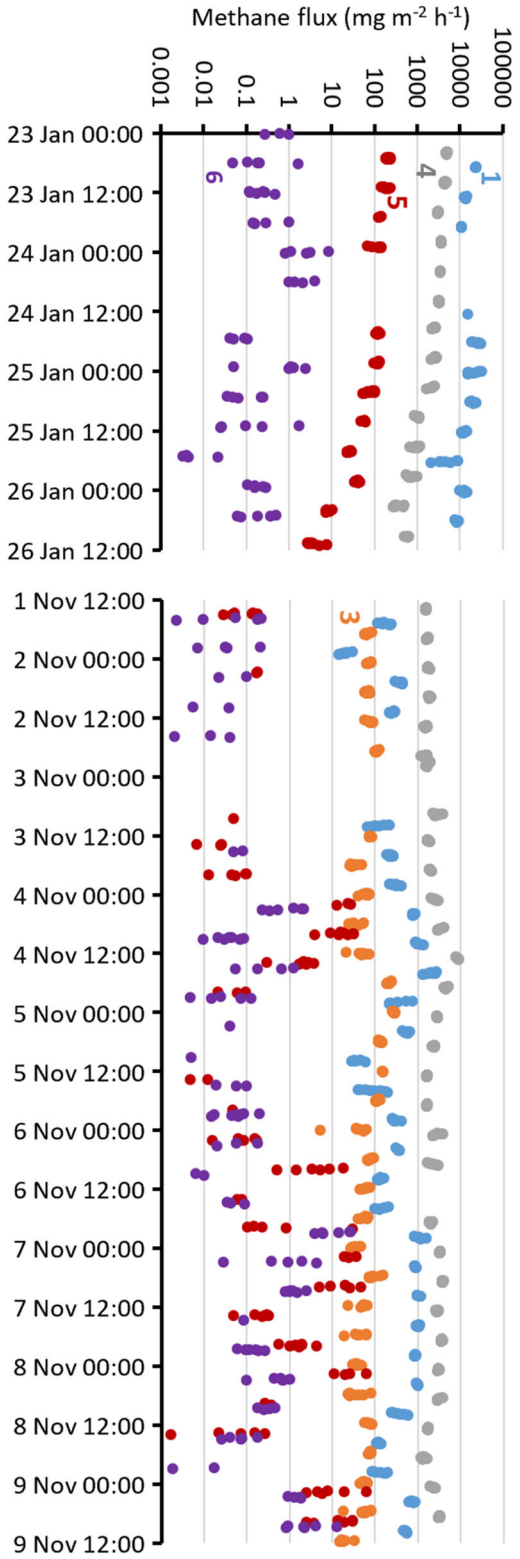

Figure D-6 *Methane fluxes in January and November 2018 at a gas storage well in Utah (Utah Well #1). Numbers correspond with chamber locations in Figure D-2.*

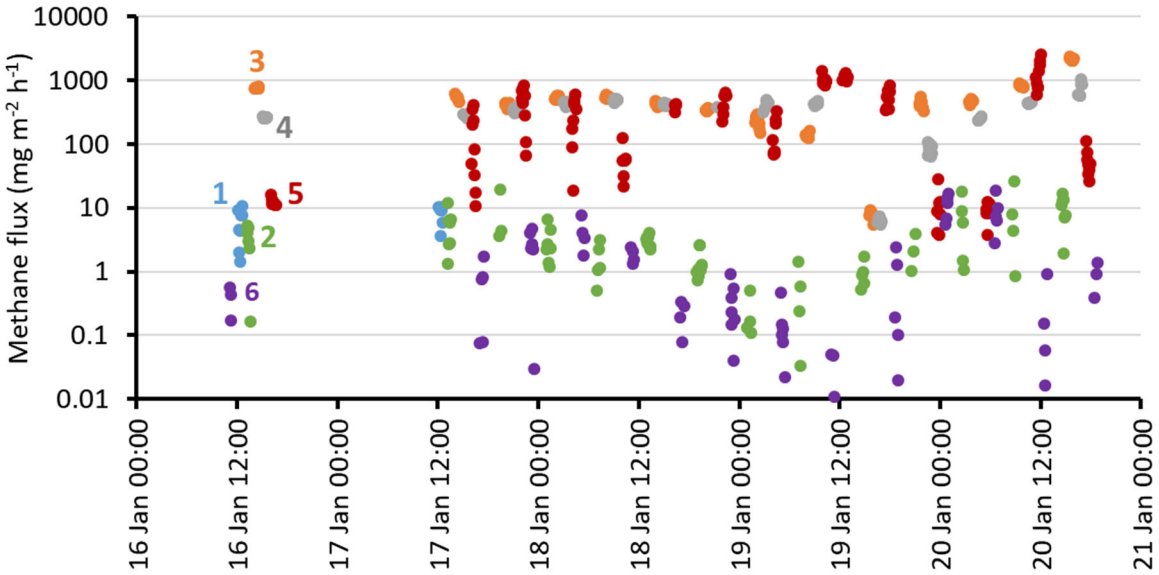

Figure D-7 *Methane fluxes in January 2018 at a gas storage well in Utah (Utah Well #2). Numbers correspond with chamber locations in Figure D-3.*

Some of the variability in methane fluxes shown in Figures D-5 through D-7 could be caused by barometric pressure changes, as has been shown by others for methane fluxes from landfills (Czepiel et al., 2003). Decreasing barometric pressure tends to draw gas out of the soil, leading to increased fluxes, while increasing pressure has the opposite effect. Figure D-8 shows that this relationship held for Utah Well #1 in November 2018. No other correlations between methane fluxes and meteorological conditions were observed at Utah Well #1 or any of the other wells. Barometric pressure effects on fluxes were not observable at the other wells at which long-term sampling occurred, including Utah Well #1 in January 2018.

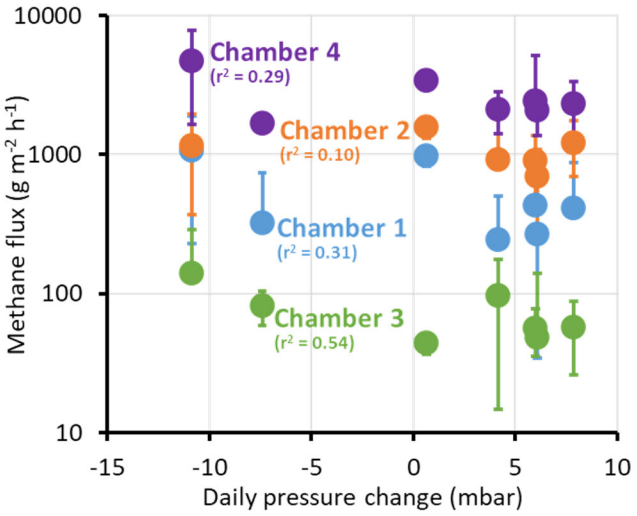

Figure D-8 *Daily average methane fluxes at Utah Well #1 in November 2018 versus daily change in barometric pressure. Chamber locations are given in Figure D-2. Only chamber locations with fluxes consistently above 10 mg m^{-2} h^{-1} are shown. Whiskers show 95% confidence intervals.*

Figure D-9 shows that decreasing well bore pressure was associated with increases in methane flux at Utah Well #2 in January 2018. We expected that increasing pressure would lead to higher fluxes, but the opposite held in this case. We did not observe consistent relationships between well bore pressure changes and fluxes at other wells, and we did not observe consistent relationships between well bore pressure (rather than pressure changes) at any wells. We did not observe any meaningful relationships of fluxes with injection or withdrawal volumes or well temperatures.

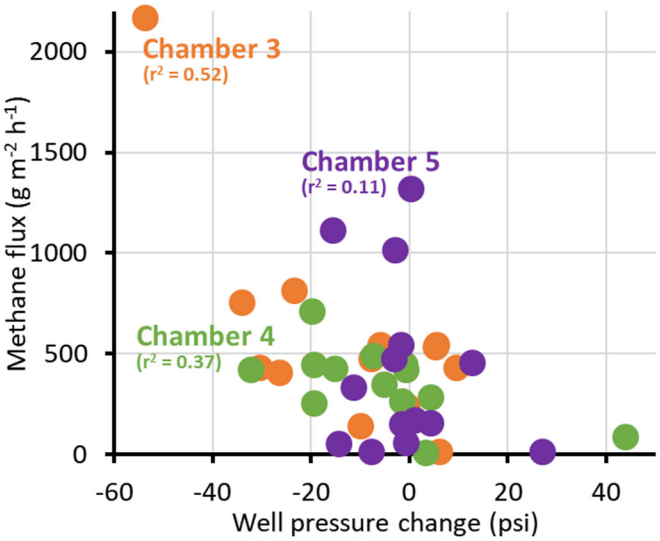

Figure D-9 *Hourly average methane fluxes at Utah Well #2 in January 2018, versus hourly change in well bore pressure. Chamber locations are given in Figure D-3. Only chamber locations with fluxes consistently above 10 mg m^{-2} h^{-1} are shown.*

As others have shown, the drivers of soil emissions from subsurface leaks are complex and lead to fluxes that vary both temporally and spatially. Gases in the soil tend to follow pathways of increased permeability, so the spatial distribution of methane emissions can be expected to be inconsistent (Cahill et al., 2017; Christophersen and Kjeldsen, 2001; Forde et al., 2019; Spokas et al., 2006). Gas moving through saturated zones tends to coalesce into large pockets, leading to pulsed flow (Dusseault et al., 2000). Also, passage through relatively low-permeability layers can require gas pressure to build up until it exceeds a threshold value, again leading to inconsistent or pulsed flow (Forde et al., 2019). These complex flow processes likely explain the inconsistent correlations between fluxes and meteorological and well conditions, and they may explain the high temporal variability in methane flux observed at some chamber locations. Figure D-10 shows fluxes from chamber 5 at Utah Well #2 at higher temporal resolution than in Figure D-7, so the rapid changes in flux can be seen more clearly.

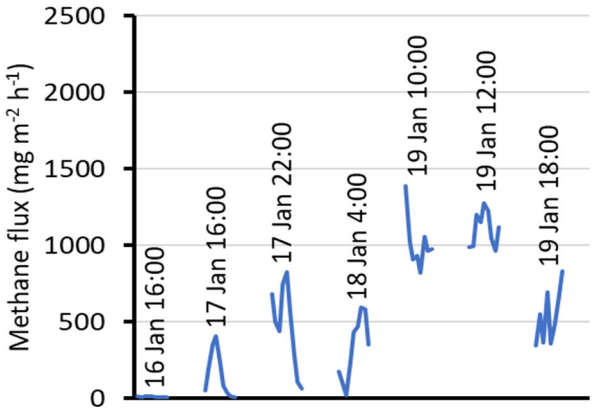

Figure D-10 *Methane fluxes measured at chamber 5 at Utah Well #2 in January 2018. The same data are shown in Figure D-7, but with less temporal resolution. Each blue line shows a time series of 4-min flux measurements over a period of 30 min.*

Another driver of variability in methane fluxes is bacterial consumption of methane in the soil (Lyman et al., 2017; Schout et al., 2019). Bacteria consume methane and respire carbon dioxide, and the rate of bacterial methane consumption changes with soil conditions. In our measurements, methane and carbon dioxide fluxes tended to be positively correlated (r^2 = 0.41 ± 0.14 for all chamber locations where fluxes were measured for at least four days; 80% of correlations were positive), indicating that carbon dioxide and methane fluxes had a common source.

We calculated total carbon flux as the carbon component of methane and carbon dioxide flux. We found that the percent of the total carbon flux that was due to methane was positively correlated with the total carbon flux (r^2 = 0.32 ± 0.14 for all chamber locations where fluxes were measured for at least four days; all correlations were positive). In other words, higher total carbon fluxes tended to contain relatively more methane and less carbon dioxide, which could indicate that the ability of bacteria to consume methane plateaus at high methane concentrations in the soil.

To better understand short-term temporal variability in fluxes, we injected methane into one of the soil gas probes at Utah Well #2. The results of that experiment are shown in Figure D-11. We continuously injected 100% methane at a rate of 100 milliliters per minute (mL min^{-1}) into a soil gas probes at a depth of 1.2 m. Probes at depths of 1.6, 0.8, and 0.6 m were within 0.3 m of the probe into which we injected methane, and we measured total combustible soil gas from these probes. We also measured soil fluxes within 0.3 m of the probe into which methane was injected.

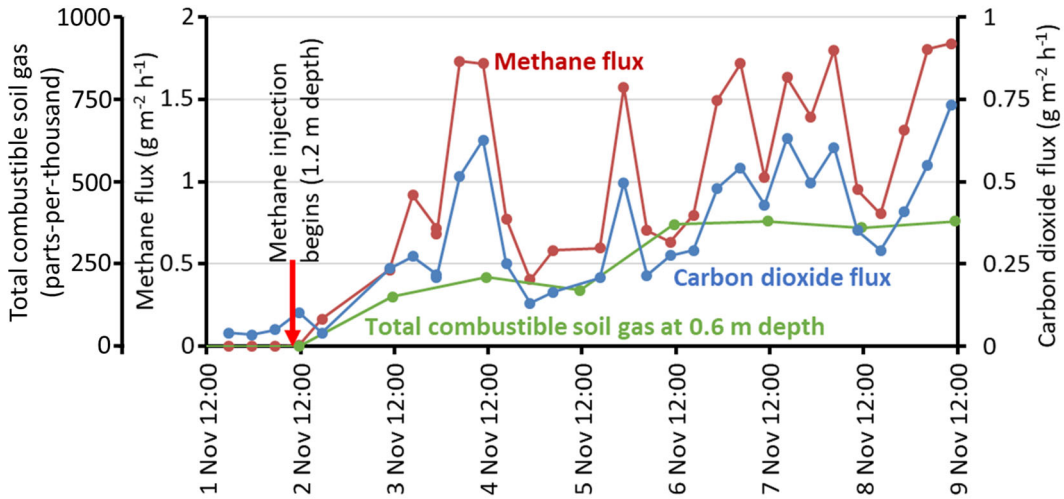

Figure D-11 *Methane and carbon dioxide flux and total combustible soil gas concentrations at a location at Utah Well #1 where we injected methane into the subsurface at a rate of 100 mL min-1.*

Figure D-11 shows that total combustible soil gas concentrations, methane fluxes, and carbon dioxide fluxes all increased after the methane injection began. Total combustible soil gas increased for about 48 hours, leveled off, and then increased again for about 24 hours before again leveling off. Methane and carbon dioxide fluxes followed this same general trend, but with much more short-term variability.

Methane and carbon dioxide fluxes measured near the injection location were highly correlated (r^2 = 0.95). Daily average methane and carbon dioxide flux was also correlated with daily measurements of total combustible soil gas concentrations (r^2 = 0.80 and 0.81, respectively). Soil gas and fluxes from this location were not well correlated with barometric pressure changes (r^2 = 0.11).

At other locations, methane soil flux and total combustible soil gas concentrations were not temporally correlated (r^2 range of 0.00 to 0.16). The flux chamber that was placed near the injection probe was in the center of four soil gas probe locations, and it is possible that the disturbed soil around the chamber created a preferential pathway that was responsible for the strong correlation between soil gas concentrations and soil fluxes in this case.

2.5 Spatial Variability in Total Combustible Soil Gas Concentrations

At both Utah wells where soil gas probes were installed, total combustible soil gas concentrations tended to be highest at a depth of 0.75 m (Figures D-12 and D-13). This may indicate that the leaks that led to elevated soil gas concentrations were relatively shallow. Most of the soil probes at the Gulf Coast well at which soil gas probes were installed filled with water, blocking flow and making measurements impossible.

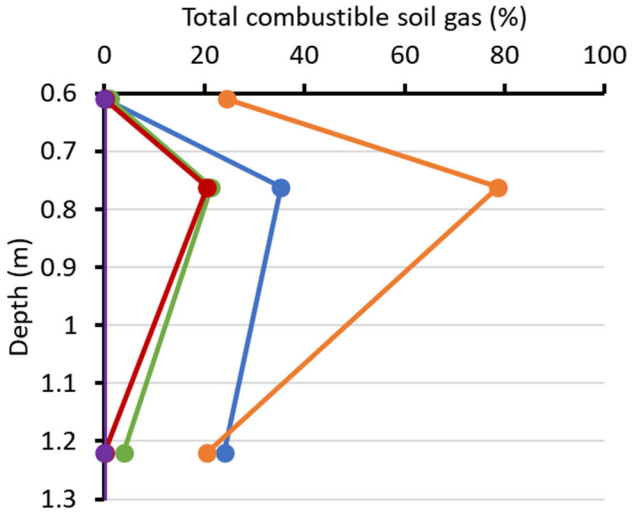

Figure D-12 *Total combustible soil gas concentrations versus measurement depth (average over eight days in November 2018) at Utah Well #1.*

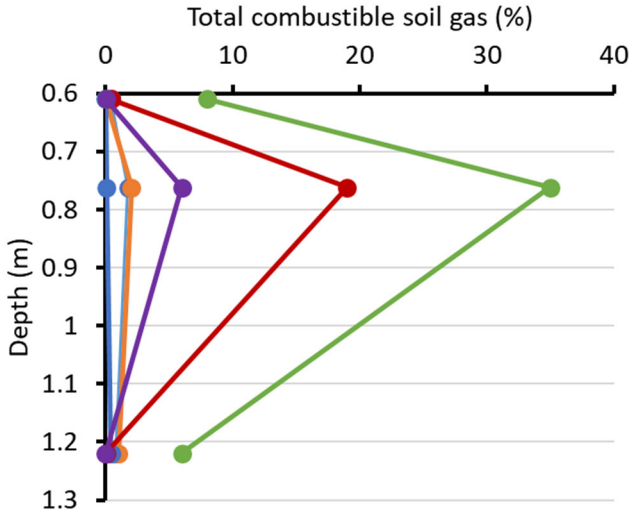

Figure D-13 *Total combustible soil gas concentrations versus measurement depth (measured in January 2018) at Utah Well #2.*

Figures D-14 and D-15 show the spatial distribution of total combustible soil gas concentrations at the two wells at which soil gas probes were installed in Utah. The figures show concentrations at 0.75 m depth since more probes existed at this depth. Spatial information shown in Figures D-14 and D-15 is the same as in Figures D-2 and D-3, respectively.

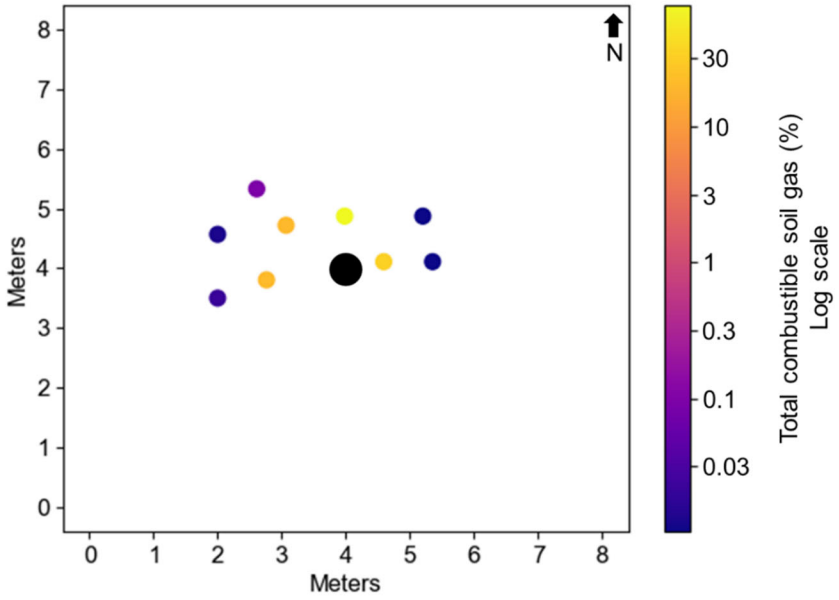

Figure D-14 *Spatial distribution of total combustible soil gas concentrations at a depth of 0.75 m (average over eight days in November 2018) at Utah Well #1.*

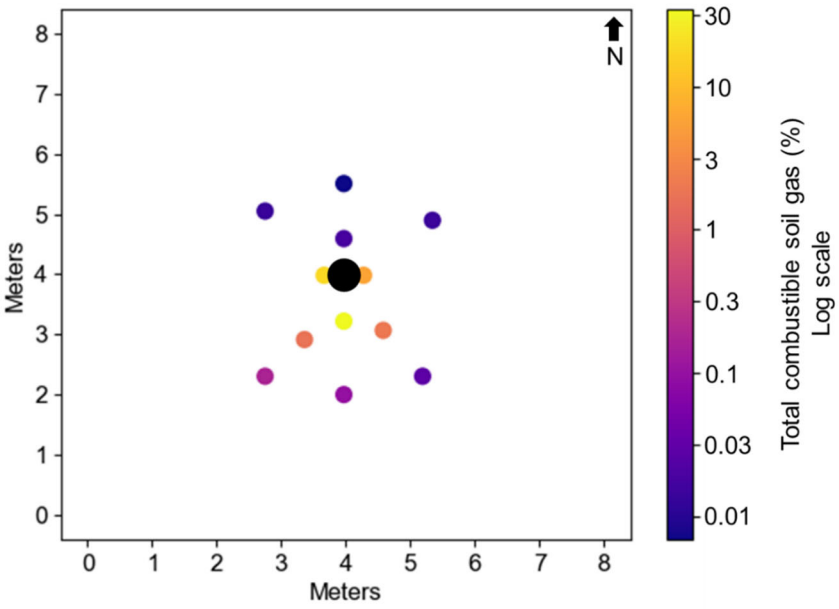

Figure D-15 *Spatial distribution of total combustible soil gas concentrations at a depth of 0.75 m (measured in January 2018) at Utah Well #2.*

2.6 Hydrocarbon Composition of Soil Gas and Fluxes

The hydrocarbon composition of soil gas at well pads was similar to the composition of natural gas (Figure D-16), with methane comprising 95% of total hydrocarbons in the gas. The hydrocarbon flux composition was more methane-dominated (Figure D-17), with methane comprising 98% of the total hydrocarbon flux.

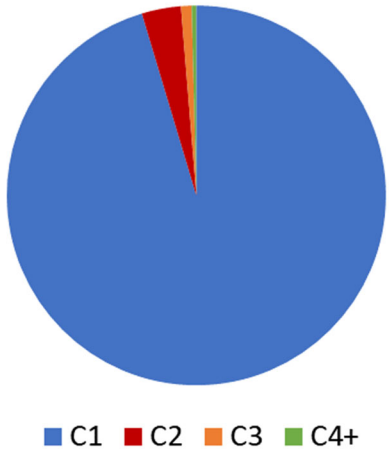

Figure D-16 *Hydrocarbon composition of soil gas collected at four natural gas storage wells in Utah and the Gulf Coast region.*

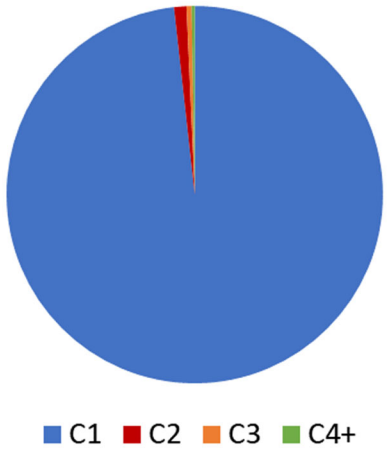

Figure D-17 *Hydrocarbon composition of soil fluxes measured at four natural gas storage wells in Utah and the Gulf Coast region.*

2.7 Comparison of Soil Fluxes with Other Well Pad Emission Sources

To provide a rough estimate of total soil emission rates for each well, we averaged the near-wellhead flux measurements for each well and applied the average flux value to a 3 m radius around the wellhead. Negative average fluxes were treated as zero for this calculation. This method makes the implicit assumptions that (1) fluxes are inversely related to distance from the

wellhead (i.e., fluxes outside of the 3 m radius are negligible), and (2) the flux measurement locations are representative of the area within the 3 m radius.

We compared this rough estimate of soil emissions against above-ground emissions (measured with the high-flow measurement system) at each well and found that emissions from soils were a small portion of total per-well emissions. Total per-well emissions at the Utah gas storage facility averaged 2.9 (95% confidence range of 1.1-9.5) kilograms per day (kg day^{-1}), while per-well soil emissions were only 0.1 (0.0- 0.3) kg day^{-1} (3.9% of the total). The maximum soil emission rate at any well was 2.1 kg day^{-1}. Figure D-18 shows box and whisker plots of total above-ground and soil emissions for well pads at the Utah facility.

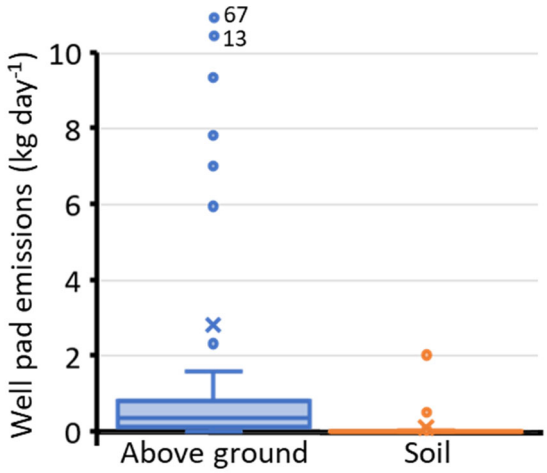

Figure D-18 *Box and whisker plot showing total soil and above-ground emissions from well pads at the Utah gas storage facility. The box shows the first and third quartiles. The middle line in the box shows the median, and the whiskers show minima and maxima. X shows the mean, and circles show outliers (>1.5 times the interquartile range).*

3.0 REFERENCES

Cahill, A.G., Steelman, C.M., Forde, O., Kuloyo, O., Ruff, S.E., Mayer, B., Mayer, K.U., Strous, M., Ryan, M.C., Cherry, J.A., 2017. Mobility and persistence of methane in groundwater in a controlled-release field experiment. Nature Geosci. 10, 289.

Christophersen, M., Kjeldsen, P., 2001. Lateral gas transport in soil adjacent to an old landfill: factors governing gas migration. Waste Manag. Res. 19, 579-594.

Czepiel, P., Shorter, J., Mosher, B., Allwine, E., McManus, J., Harriss, R., Kolb, C., Lamb, B., 2003. The influence of atmospheric pressure on landfill methane emissions. Waste Manage. (Oxford) 23, 593-598.

Dusseault, M.B., Gray, M.N., Nawrocki, P.A., 2000. Why oilwells leak: cement behavior and long-term consequences, International Oil and Gas Conference and Exhibition in China. Society of Petroleum Engineers.

Forde, O., Mayer, K., Hunkeler, D., 2019. Identification, spatial extent and distribution of fugitive gas migration on the well pad scale. Sci. Total Environ. 652, 356-366.

Lyman, S.N., Watkins, C., Jones, C.P., Mansfield, M.L., McKinley, M., Kenney, D., Evans, J., 2017. Hydrocarbon and Carbon Dioxide Fluxes from Natural Gas Well Pad Soils and Surrounding Soils in Eastern Utah. Environ. Sci. Technol. 51, 11625-11633.

Schout, G., Griffioen, J., Hassanizadeh, S.M., de Lichtbuer, G.C., Hartog, N., 2019. Occurrence and fate of methane leakage from cut and buried abandoned gas wells in the Netherlands. Sci. Total Environ. 659, 773-782.

Spokas, K., Bogner, J., Chanton, J., Morcet, M., Aran, C., Graff, C., Moreau-Le Golvan, Y., Hebe, I., 2006. Methane mass balance at three landfill sites: What is the efficiency of capture by gas collection systems? Waste Manage. (Oxford) 26, 516-525.

APPENDIX E

OP-FTIR Measurement Procedures

APPENDIX E

OP-FTIR MEASUREMENT PROCEDURES

1.0 TECHNOLOGY BACKGROUND

The RAM2000™ open-path Fourier transform infrared (OP-FTIR) spectrometer was operated with a corner-cubed prismatic retroreflector, oriented to accept prevailing winds through an open-air optical path. With this technology, a beam of light spanning a range of wavelengths in the mid-infrared portion of the electromagnetic spectrum is propagated from the transmitter portion of the OP-FTIR instrument. Methane, ethane and other chemicals present in the air cross the beam path, interfere with modulated infrared energy from a silicon carbide glower source, become energetically excited by the resonant frequency of the source, and cause the beam to divest of relative energy.

The retroreflector bends the source energy back to a mercury/cadmium/telluride detector in the OP-FTIR optics chamber, where a Michelson interferometer achieves further modulation by splitting the returning beam of radiation into two paths and recombining those in a way to generate an interference from the phase difference. The phase difference, and thus the interference, is dependent on the wavelengths present in the beam. In one of the paths, the radiation is reflected off a moving mirror, resulting in an intensity variation which is measured as a function of the path difference between the two mirrors. The resultant output of this process is called an interferogram. A spectrum (in optical frequency units) is obtained by performing a Fourier transform upon a broadband interferogram expressed as a sum of cosine waves.

2.0 DATA PROCESSING

Interferograms were created at a chosen rate of 32 signal-averaged scans per one sample frame. Resultant absorbance spectra were compared to reference spectra using multi-component regression algorithms. Concentrations were path-averaged and path-integrated.

Compounds were identified and quantified via a computer-based spectral search involving sequential, compound-specific analyses and comparison to the system's internal reference spectra library. The most widely employed technique for analyzing FTIR spectral data is the multi-component classical least squares technique. Any gaseous compound which absorbs the IR region is a potential candidate for monitoring using this technology.

The minimum detect levels (MDL) were algorithmically calculated values that defined the minimum methane concentration, within six sigma statistical confidence. Upon completion of a time-lapsed sampling session, all frames (samples) were averaged per analyte (methane/ethane/carbon monoxide) by the software. A mean MDL for each analyte was calculated based upon the full sampling session. According to the manufacturer, the range of detection limits for a 100-meter separation between the sensor and retroreflector was from 0.10 to 15 ppb for most infrared active chemicals.

Concentrations of analytes were reported only if the time-weighted mean concentration was found to be in excess of two times the software calculated mean MDL. The maximum detected concentration, observed at any given time during sampling history, was only reported if the maximum was found to be at least two times the software-calculated-mean MDL. As a result of these ultra conservative steps, the concentration values for methane (mean or max), were only reported if the results were beyond a 12 sigma statistical confidence range above the MDL. As a result, the possibility of having a false positive concentration was null.

3.0 OP-FTIR AND RETROREFLECTOR SET UP

The upwind and downwind locations were determined in relation to the physical properties of the compressors and gas gathering lines. The optical beam path between the OP-FTIR spectrometer and the retroreflector was oriented perpendicular to prevailing wind direction as much as possible.

Downwind setup locations for the OP-FTIR and retroreflector were restricted to areas that were free of traffic flow and were oriented such that the infrared beam was unobstructed by facility equipment or buildings. Each retroreflector array consisted of thirty-seven 2.5-inch hollow reflector cubes consisting of three mutually perpendicular mirrors that bend infrared light back to its exact point of origin and, as such, reduced the divergence of the beam on its return path back to the detector. The spectrometer was adjusted so that the siting scope (located between the spectrometer and telescope) displayed crosshairs at the upper left corner of the retroreflector mirror. A range finder or measuring wheel was used to measure the distance from the spectrometer to the retroreflector. The instruments required a round trip beam path for the measurement so it was necessary to multiply the distance by a factor of two.

Since the OP-FTIR system contained a liquid nitrogen cooling unit, liquid nitrogen was added to the spectrometer prior to measurement. Once the spectrometer system was engaged and the nitrogen cooling began, the OP-FTIR detector was allowed to cool for 20 minutes. Hotter ambient temperatures required a longer cooling time.

4.0 BACKGROUND (UPWIND) SAMPLING

Background or upwind samples were collected and evaluated to determine the possibility of upwind emitting sources contributing to emission levels at the study site. Upwind sampling sites were chosen as close to the sample area as possible and were free of wind obstacles to the extent possible. At least one hour of upwind measurement was gathered at each location.

5.0 METHODS TO SUPPORT EMISSION FLUX CALCULATIONS

A controlled stream of gas-phase sulfur hexafluoride (SF_6) was released during OP-FTIR measurement periods. The OP-FTIR spectrometer detected and quantified the SF_6 plume along with methane and ethane (target compounds) to distinguish between thermogenic and biogenic methane sources. Since the SF_6 emission rate was known, the emission rate of other compounds were scaled based on the ratio of their concentrations to the measured SF_6 concentration.

Cylinders containing 99% pure SF_6 were utilized in conjunction with a 0-10 L min^{-1} mass flow controller to control the release of SF_6 from the cylinder. After the mass flow controller, the SF_6

traveled through a 50-m length of inert tubing to a tripod and was released from the end of the tubing at the tripod.

All meteorological measurements were collected at 6 m above ground level concurrent with, and using the sample instrumentation as, measurements collected for the high flow sampling program (see Appendix C). All measurements were recorded with a Campbell Scientific CR1000 data logger.

Flow rates of the SF_6 mass flow controller used to release the tracer were checked at least monthly against a BIOS dry gas meter, and the dry gas meter was calibrated at least annually against a NIST-traceable standard.

APPENDIX F

False Negative and False Positive Above-Ground Emission Screening Rates

APPENDIX F

FALSE NEGATIVE AND FALSE POSITIVE ABOVE-GROUND EMISSION SCREENING RATES

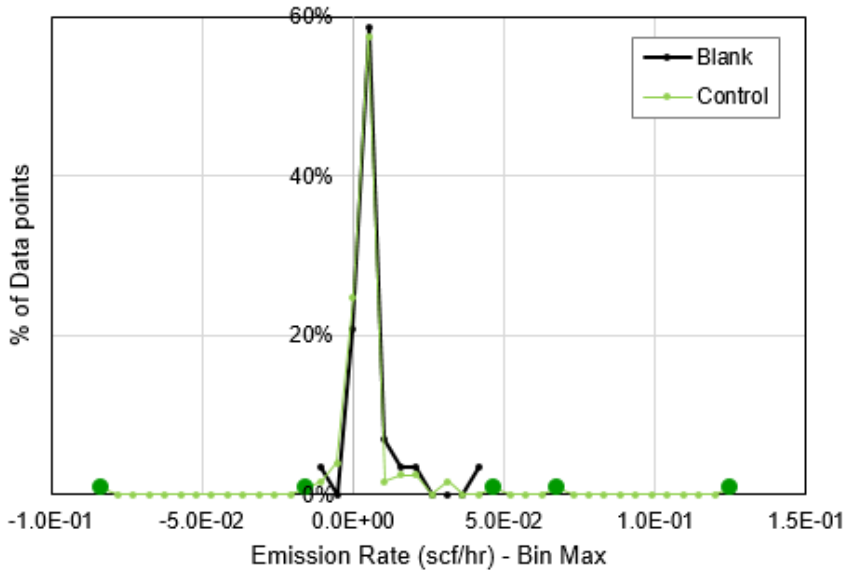

Figure F-1 *Relative frequency histogram of blank and control methane emission rate data. Control samples outside the range of blank samples are highlighted with large, dark green circles*

Table F-1. *False Positive Detection Rate by Component Type and Screening Method*

Component Type	% False Positive Detections	
	Gas Explorer	FLIR
Connector, all	43	6.3
Connector, other	38	10
Connector, flange	80	0
Valve, all	28	4.8
Valve, small	37	3.7
Valve, large	20	5.7
PRV	0	0
OEL	40	33
Gauge	25	0
Regulator	33	0

APPENDIX G

High Resolution Below-Ground Emissions Monitoring

APPENDIX G

HIGH RESOLUTION BELOW-GROUND EMISSIONS MONITORING

1.0 EQUIPMENT INSTALLATION

1.1 Overview

Remote monitoring systems were installed to continuously measure in-situ soil temperature, moisture content and related above-ground ambient conditions, which were recorded as 5-minute and 1-hour averages. GSI provided all hardware for the installed systems, which was leased to DOE-NETL for the duration of monitoring at each of three natural gas storage well locations. All instrumentation and related electronic/electric hardware was procured new, tested/calibrated, and installed by the vendor Meteorological Solutions, Inc. (MSI).

The monitoring systems were installed at two wells at Clay Basin during the week of November 13, 2017 and at one well in the Gulf Coast Region during the week of March 5, 2018. The wells were chosen for high resolution monitoring based on having the highest short-term methane flux as measured during Field Campaigns 1 and 2 (see Section 2 for details).

1.2 Hydrovac Excavation

Upon recommendation of the gas storage site operator, hydrovac excavation was used to safely dig boreholes for in-ground sensors and trenches for underground conduits near the gas storage wellheads. This method uses a high-pressure water stream and vacuum to remove liquefied soil cuttings without posing risks to underground infrastructure. Boreholes were excavated to specified dimensions (approximately 6 inches wide and up to 6 feet deep) to a depth approximately 6 inches above the sensor installation depth to allow room for soil core and grab samples to be collected.

1.3 Soil Sampling

A subset of soil cores was collected with a slide hammer and plastic core sleeves and were analyzed for geotechnical parameters (grain size distribution, calculated porosity, bulk density, USCS classification). Soil grab samples were collected at the base of each borehole using a hand auger and analyzed for the presence of total petroleum hydrocarbons (TPH) and total organic carbon (TOC) to confirm whether elevated microbial activity reflected in future observed heat signatures could be due to contamination from other activities not related to gas storage (e.g. previous gas production or well drilling).

1.4 Sensor Installation

Soil volumetric water content and temperature soil water content reflectometers (Model CS655, Campbell Scientific, Inc.) These can measure volumetric water content ranging from 0 to 100% with a precision of <0.5%, and soil temperature ranging from -50 to 70 °C with a precision of

±0.02 °C. At Clay Basin wells, arrays of 27 and 29 sensors were installed at depths of approximately 20 to 60 inches. At the Gulf Coast region well, an array of 18 sensors was installed at depths of approximately 19 to 75 inches. Sensor installation at Clay Basin is shown in Figure G-1. Layouts of the configuration of sensors at the three wells are shown in Figures G-1 to G-3. Placement of the sensors along with short-term methane soil flux measurements (Section 2) and soil TPH concentrations (from soil sampling, Section 3.2.3) are shown in Figures G-4 to G-6.

Figure G-1. *In-ground Sensor and Sample Tubing Installation in Progress*

Figure G-2. *Completed Meteorological Tripod Power/Control Box at Clay Basin Well*

To capture a range of depths, some of the sensors were clustered together, with three or four probes of various depths placed in separate boreholes about 0.3 m in horizontal distance apart in each cluster (Figure G-3). Due to the depth of the boreholes, the instruments were installed vertically into the base of the boreholes using a PVC pole to push the metal rods extending from the sensor into the base of the borehole. If a full push into the soil was not feasible due to soil stiffness or gravel content, the borehole was backfilled with soil from the borehole wall and compacted around the rods of the soil sensor to provide a solid foundation composed of in situ soil. Tables G-1 and G-2 list the measured install dimensions of each borehole. In order to support future collection of soil gas samples, ¼-inch Nyaflow tubing with a filter tip was installed to rest above the sensor in each borehole. Each sensor was surrounded by native soil and then covered with a 6-inch thickness sand pack in which the filter tip rests. A layer of hydrated bentonite was emplaced atop the sand pack to an upper extent approximately 6 inches below ground. Each borehole was completed flush with the ground surface with a lidded valve box from which the sampling tube was accessible.

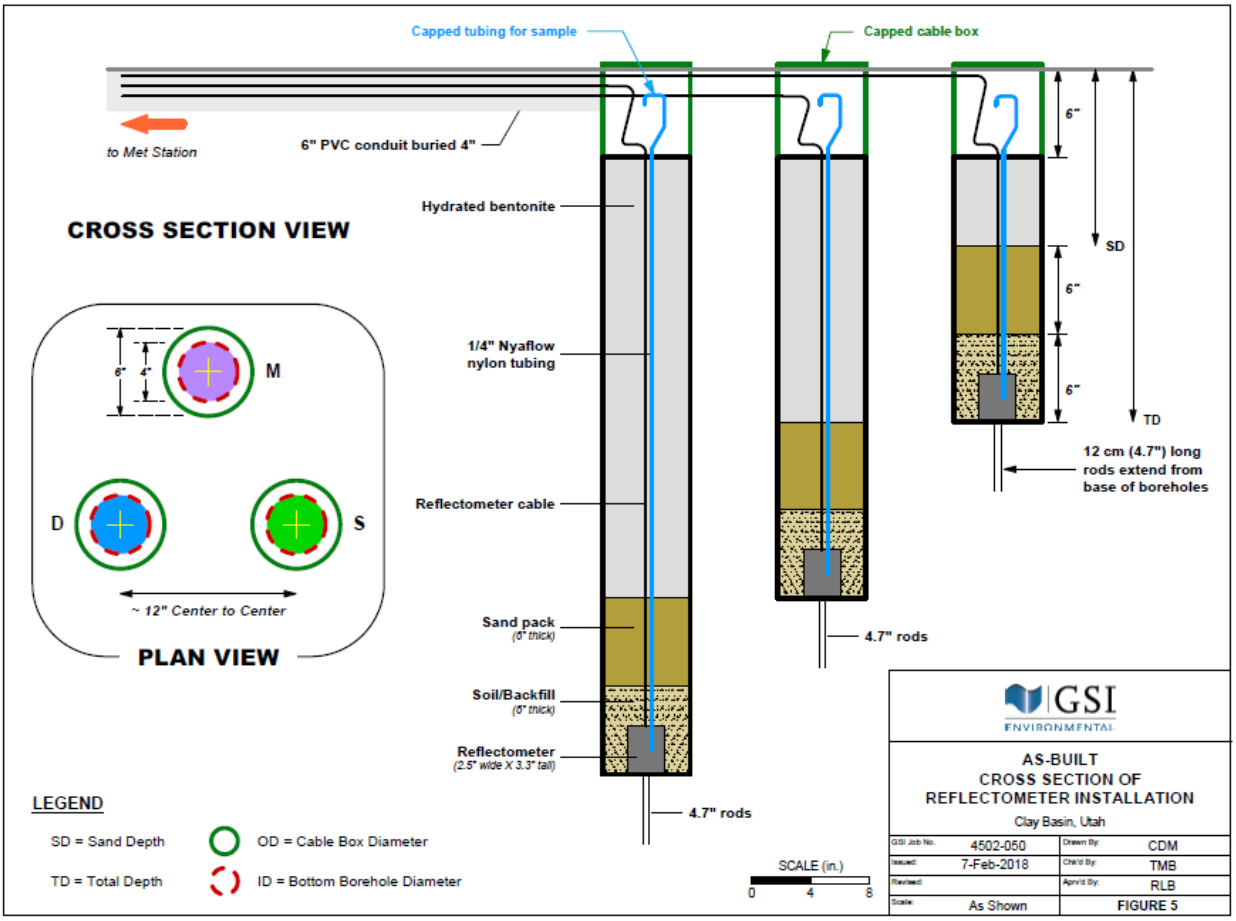

Figure G-3. *As-built Cross Section of Reflectometer Installation*

1.5 Instrumentation

The installed below-ground reflectometers were connected to a solar-powered weather station (Model 1000, Campbell Scientific, Inc.) providing meteorological conditions as well as wireless communications, data logging, and a remote camera. Meteorological data collected was: barometric pressure (Model PTB110, Vaisala), relative humidity (Model EE181, CSI), temperature (Model EE181, CSI), precipitation (Model TR-5251, Texas Electronics), solar/net radiation (Model NR01-C, Hukeflux), wind direction (Model 05305, R.M. Young-AQ), and wind speed (Model 05305, R.M. Young-AQ). The systems continuously measured in-situ soil temperature, moisture content and related above-ground ambient conditions, which were recorded as 5-minute and 1-hour averages. Remote data collection became operational on November 18, 2017 at Clay Basin and on March 7, 2018 in the Gulf Coast region.

All cabling and electrical connections were protected from the elements and situated either underground or greater than 30 feet from the gas storage wellhead. Cables for in-ground sensors and meteorological instruments were routed at least 4 inches below ground through PVC conduits to the data logger (Model 1000, Campbell Scientific Inc.) in a watertight box at the edge of the well pad. Proper functioning of all system components and data logging was confirmed prior to departure from the field.

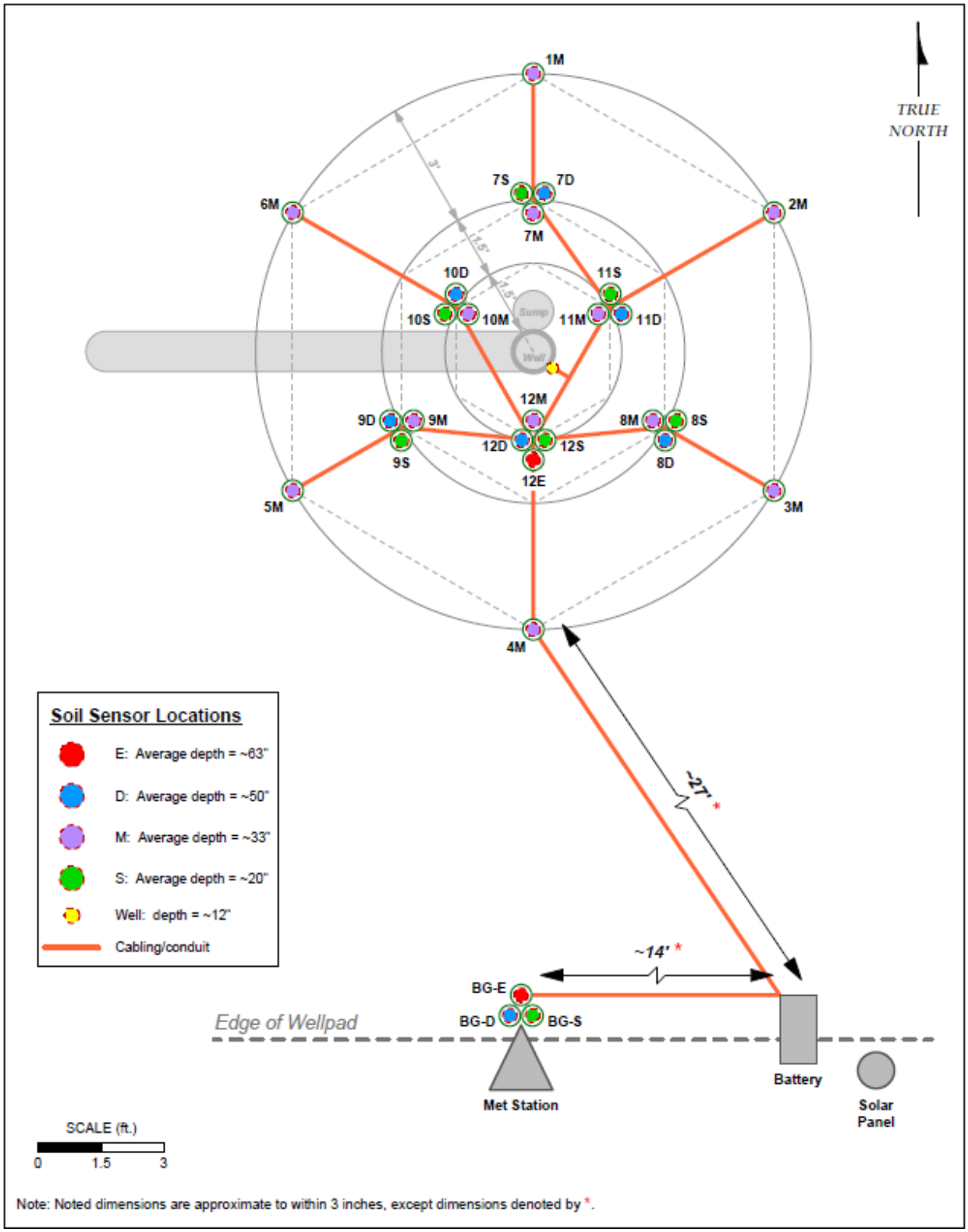

***Figure G-4**. Monitoring System Layout at Clay Basin, Utah, Well 52*

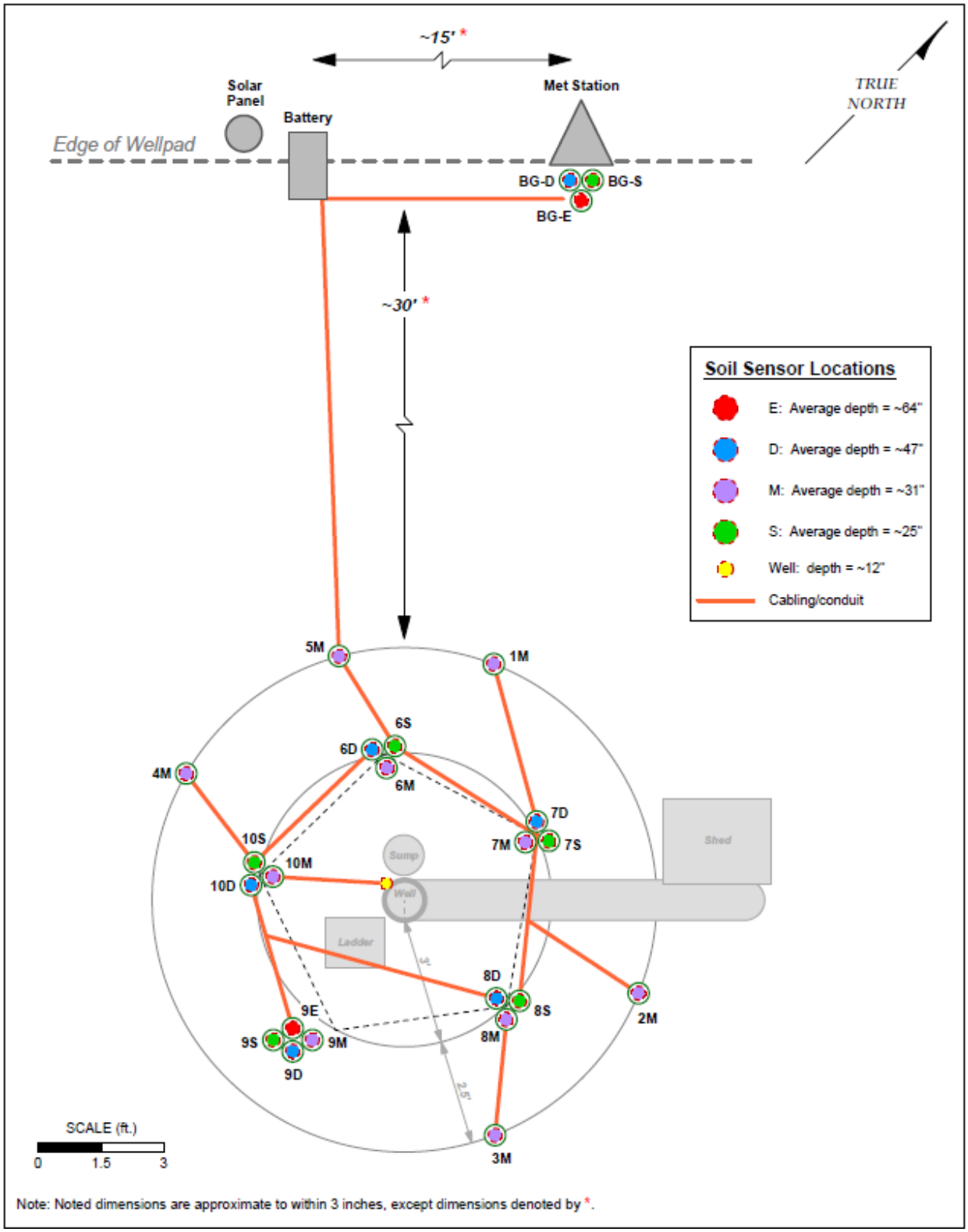

Figure G-5. *Monitoring System Layout at Clay Basin, Utah, Well 49*

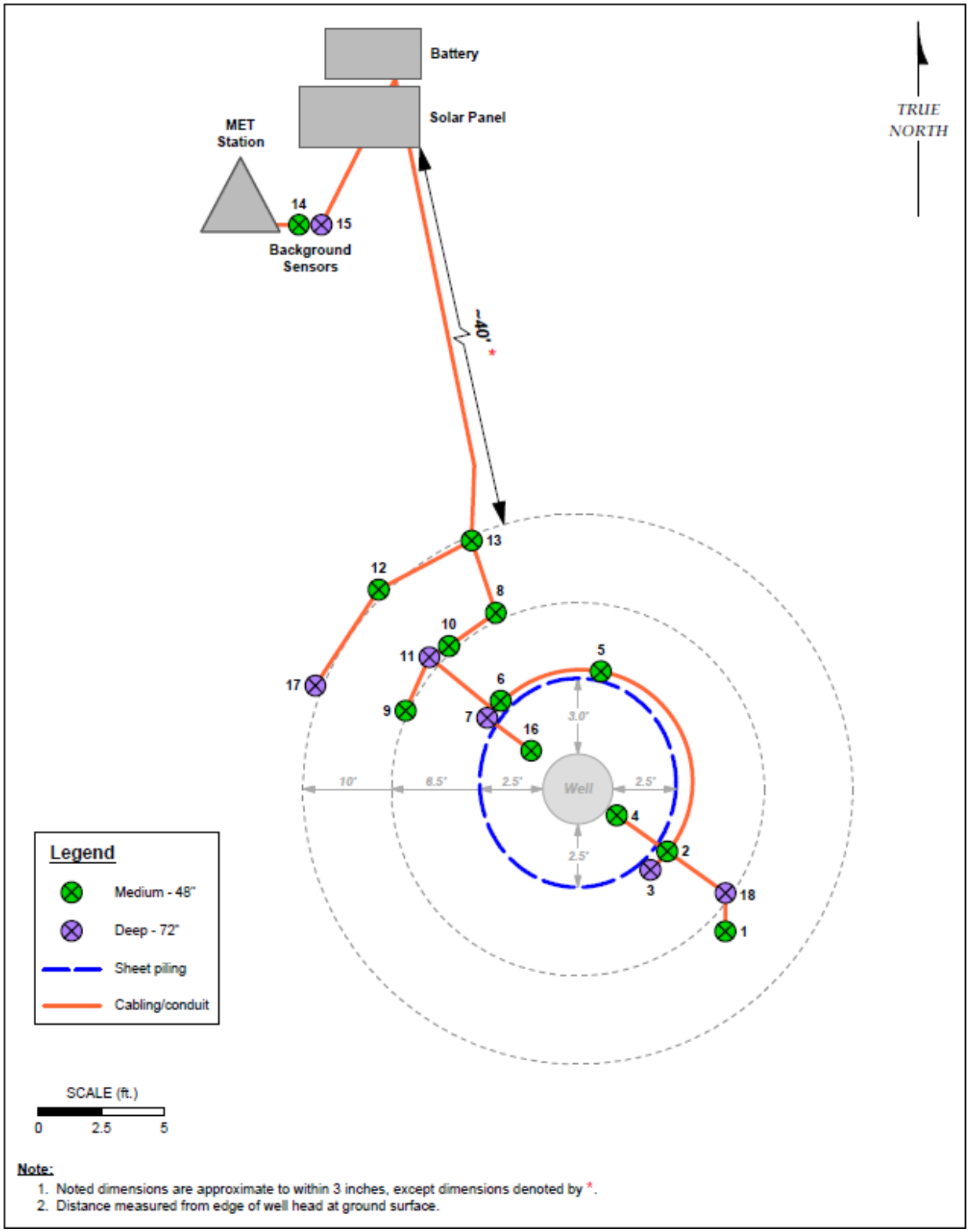

Figure G-6. *Monitoring System Layout at Gulf Coast Region Salt Cavern Well*

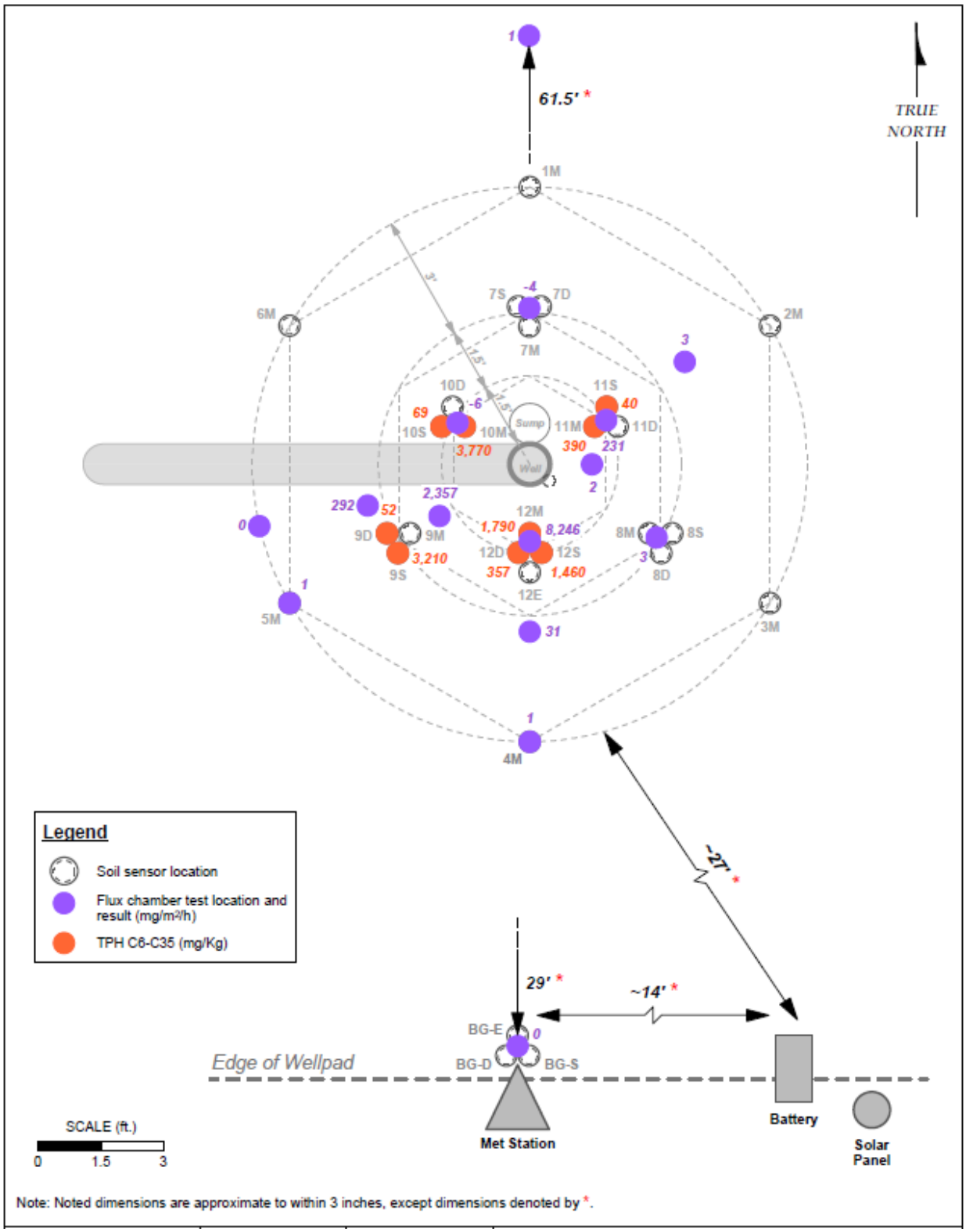

Figure G-7. *Initial Flux Chamber and Soil Sampling Results at Clay Basin, Utah, Well 52*

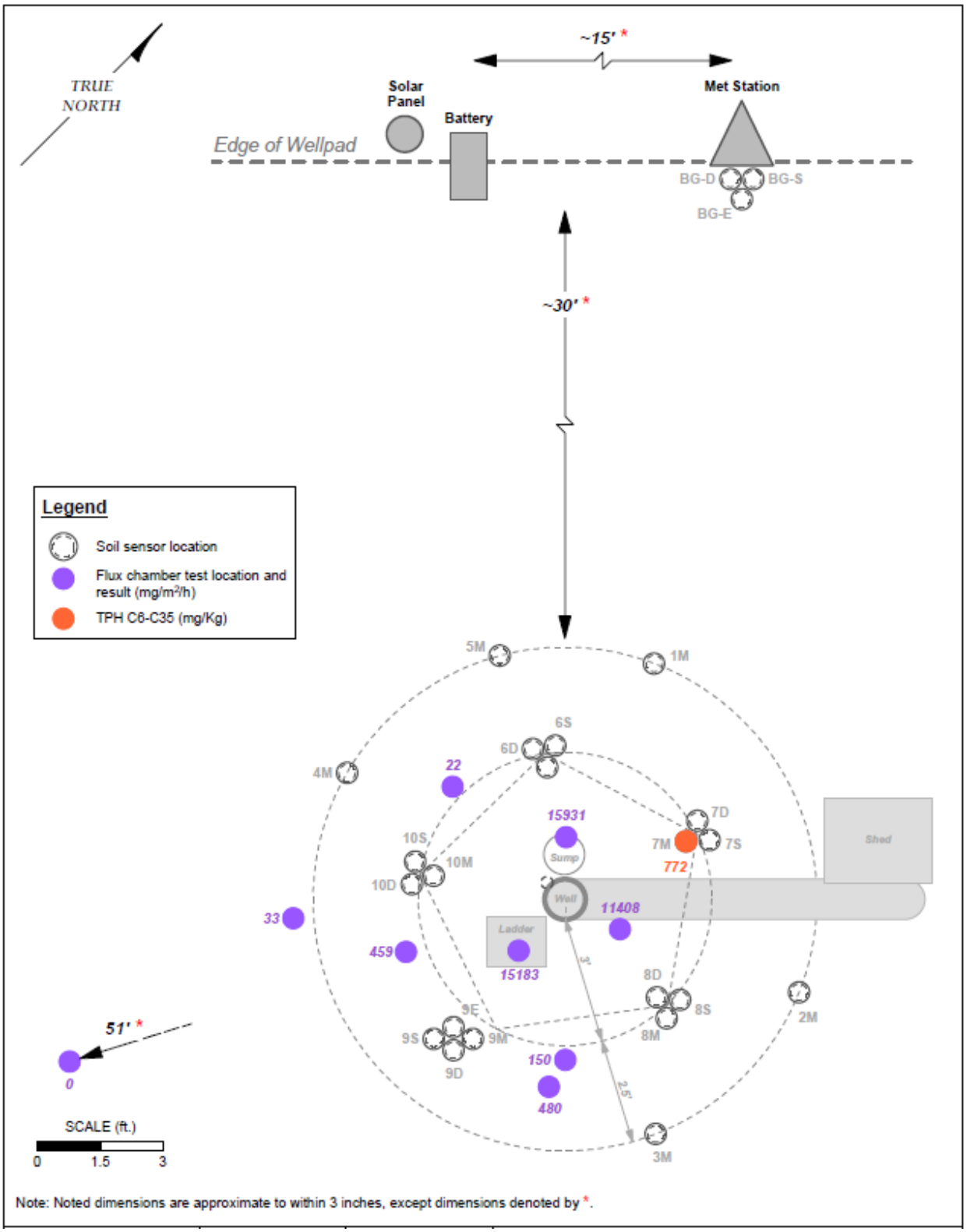

Figure G-8. *Initial Flux Chamber and Soil Sampling Results at Clay Basin, Utah, Well 49*

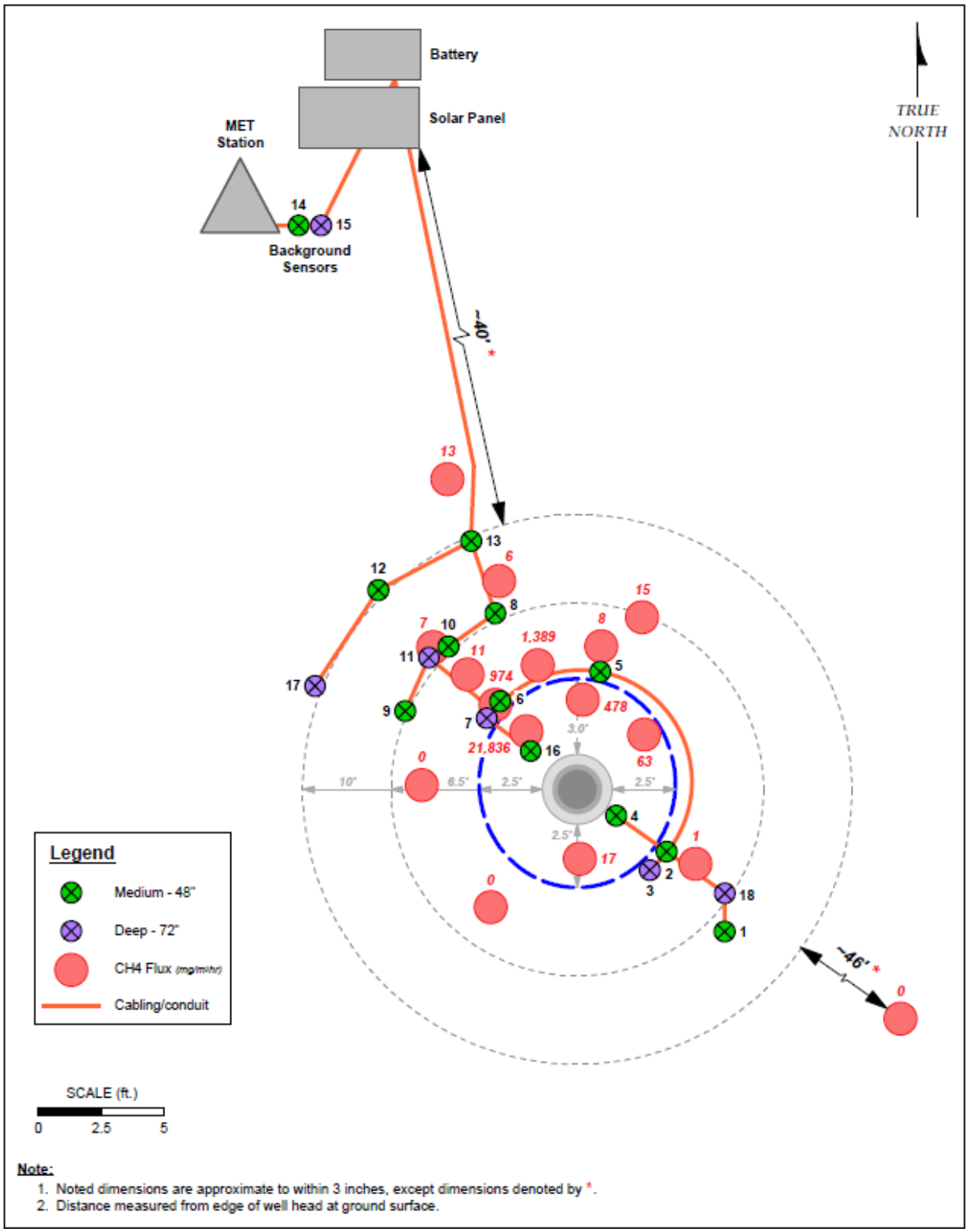

Figure G-9. *Initial Flux Chamber and Soil Sampling Results at Gulf Coast Region Salt Cavern Well*

Table G-1. *Soil Senor Borehole Dimensions, Utah Depleted Reservoir Wells*

Sensor ID	Sample depth (inches)	Sensor depth (inches)	Depth to top of sand pack (inches)	Top borehole width (inches)	Bottom borehole width (inches)
Well 49-S					
49-Well	6	18	---	---	---
49-BG-S	24	20	17	10	4
49-BG-D	50	44	41	8	4
49-BG-E	65	63	59	8	4
49-1M	36	33	27	10	4
49-2M	35	32	22	11	4
49-3M	40	35	30	12	4
49-4M	36	30	26	10	4
49-5M	30	22	19	10	4
49-6S	27	21	17	10	4
49-6M	37	33	26	10	4
49-6D	47	44	38	12	4
49-7S	29	24	21	10	4
49-7M	36	34	28	10	4
49-7D	47	48	39	10	4
49-8S	28	23	21	10	4
49-8M	33	27	19	10	4
49-8D	61	56	51	12	8
49-9S	30	26	20	12	4
49-9M	34	28	26	10	6
49-9D	53	49	44	10	4
49-9E	70	65	60	10	4
49-10S	36	35	28	10	4
49-10M	38	38	26	10	4
49-10D	40	41	36	10	4
Well 52-S					
52-Well	6	---	---	---	---
52-BG-S	24	---	---	---	---
52-BG-D	66	---	49	---	---
52-BG-E	84	---	72	---	---
52-1M	41	35	---	10	4
52-2M	37	34	27.5	10	4
52-3M	43	39	36	10	4
52-4M	37	31	27	8	4
52-5M	42	38	---	5	4
52-6M	---	34	30	10	4

Sensor ID	Sample depth (inches)	Sensor depth (inches)	Depth to top of sand pack (inches)	Top borehole width (inches)	Bottom borehole width (inches)
52-7S	---	18	14	10	7
52-7M	32	29	24	9	4
52-7D	53	47	---	10	4
52-8S	24	---	---	---	---
52-8M	34	31	---	8	4
52-8D	54	44	42	9	4
52-9S	26	20	17.5	9	4
52-9M	37	33	26	10	4
52-9D	46	43	---	10	4
52-10S	24	18	15	8	4
52-10M	40	37	33	8	4
52-10D	56	---	45	---	---
52-11S	31	24	20	9	4
52-11M	31	28	24	9	4
52-11D	59	53	48	10	4.5
52-12S	---	18	16	8	4
52-12M	---	32	28	8	4
52-12D	---	58	51	8	4
52-12E	---	66	60	8	5

Table G-2. *Soil Sensor Borehole Dimensions, Gulf Coast Region Salt Cavern Well*

Sensor ID	Sample depth (inches)	Sensor depth (inches)	Depth to top of sand pack (inches)	Top borehole width (inches)
1	54	49	43	10
2	53	43	40	10
3	76	72	70	10
4	n/a	18	14	10
5	52	48	44	10
6	58	51	47	10
7	67	69	60	10
8	47	48	40	10
9	50	53	48	10
10	54	48	42	10
11	78	74	69	10
12	76	50	41	10

Sensor ID	Sample depth (inches)	Sensor depth (inches)	Depth to top of sand pack (inches)	Top borehole width (inches)
13	53	48	44	10
14	48	52	48	10
15	74	80	69	10
16	46	40	40	10
17	76	73	66	10
18	75	76	69	10

2.0 SOIL SAMPLING RESULTS

Table G-3. *Soil Sampling Summary for Utah Depleted Reservoir Wells*

Sensor ID	USCS Designation	Porosity	Bulk Density	TOC (mg/Kg)	TPH (mg/Kg)			
					>C12-C28	>C28-C35	C6-C12	C6-C35
Well 49-S								
49-BG-S	Lean clay with sand (CL)	0.46	103.5	11,900	<50	<50	<50	<50
49-BG-D	Lean clay with gravel (CL)	0.39	115.5	11,600	<50	<50	<50	<50
49-BG-E	Gravelly lean clay (CL)	0.42	122.4	7,470	<50	<50	<50	<50
49-1M	*No core collected*	---	---	2,840	<50	<50	<50	<50
49-2M	*No core collected*	---	---	2,940	<50	<50	<50	<50
49-3M	Lean clay (CL)	0.42	117.3	7,360	<50	<50	<50	<50
49-4M	*No core collected*	---	---	2,970	<50	<50	<50	<50
49-5M	*No core collected*	---	---	9,270	<50	<50	<50	<50
49-6S	*No core collected*	---	---	11,800	<50	<50	<50	<50
49-6M	*No core collected*	---	---	2,520	<50	<50	<50	<50
49-6D	*No core collected*	---	---	7,960	<50	<50	<50	<50
49-7S	Insufficient sample for testing	0.44	118.0	10,300	<50	<50	<50	<50
49-7M	*No core collected*	---	---	16,200	**610**	<50	**162**	**772**
49-7D	Lean clay with sand (CL)	0.44	112.3	9,160	<50	<50	<50	<50
49-8S	*No core collected*	---	---	14,200	<50	<50	<50	<50
49-8M	*No core collected*	---	---	9,540	<50	<50	<50	<50
49-8D	*No core collected*	---	---	2,790	<50	<50	<50	<50
49-9S	Sandy lean clay (CL)	0.40	132.8	13,900	<50	<50	<50	<50
49-9M	Gravelly lean clay with sand (CL)	0.46	112.8	12,900	<50	<50	<50	<50
49-9D	Clayey gravel (GC)	0.37	128.2	10,100	<50	<50	<50	<50
49-9E	Clayey gravel with sand (GC)	0.41	121.4	14,600	<50	<50	<50	<50
49-10S	*No core collected*	---	---	2,340	<50	<50	<50	<50
49-10M	*No core collected*	---	---	11,700	<50	<50	<50	<50
49-10D	*No core collected*	---	---	9,810	<50	<50	<50	<50

Sensor ID	USCS Designation	Porosity	Bulk Density	TOC (mg/Kg)	TPH (mg/Kg)			
					>C12-C28	>C28-C35	C6-C12	C6-C35
Well 52-S								
52-BG-S	Insufficient sample for testing	0.40	108.2	9,970	<50	<50	<50	<50
52-BG-D	Silty, clayey sand with gravel (SC-SM)	0.41	111.0	7,000	<50	<50	<50	<50
52-BG-E	Clayey gravel with sand (GC)	0.44	107.1	7,140	<50	<50	<50	<50
52-1M	Gravel with Silt and Sand	0.31	125.6	10,300	<50	<50	<50	<50
52-2M	*No core collected*	---	---	8,910	<50	<50	<50	<50
52-3M	Silty, clayey sand (SC-SM)	0.38	128.2	7,280	<50	<50	<50	<50
52-4M	*No core collected*	---	---	7,960	<50	<50	<50	<50
52-5M	Silty, clayey sand with gravel (SC-SM)	0.38	116.9	8,230	<50	<50	<50	<50
52-6M	Silty sand with gravel (SM)	0.38	107.1	9,220	<50	<50	<50	<50
52-7S	Silty sand (SM)	0.48	114.2	10,400	<50	<50	<50	<50
52-7M	*No core collected*	---	---	9,900	<50	<50	<50	<50
52-7D	*No core collected*	---	---	8,750	<50	<50	<50	<50
52-8S	*No core collected*	---	---	7,810	<50	<50	<50	<50
52-8M	Clayey gravel with sand (GC)	0.39	107.7	9,390	<50	<50	<50	<50
52-8D	*No core collected*	---	---	6,830	<50	<50	<50	<50
52-9S	Clayey sand with gravel (SC)	0.38	122.9	12,500	**2,740**	**475**	<250	**3,210**
52-9M	*No core collected*	---	---	14,200	<50	<50	<50	<50
52-9D	*No core collected*	---	---	10,200	**52**	<50	<50	**52**
52-10S	Clayey gravel with sand (GC)	0.35	129.4	11,400	**69**	<50	<50	**69**
52-10M	*No core collected*	---	---	11,500	**3,170**	**598**	<250	**3,770**
52-10D	*No core collected*	---	---	8,220	<50	<50	<50	<50
52-11S	Silty, clayey sand with gravel (SC-SM)	0.41	119.0	11,800	**1,140**	<50	<50	**1,140**
52-11M	*No core collected*	---	---	12,400	**252**	**138**	<50	**390**
52-11D	*No core collected*	---	---	8,200	<50	<50	<50	<50
52-12S	*No core collected*	---	---	13,400	**1,210**	**251**	<50	**1,460**
52-12M	*No core collected*	---	---	17,200	**1,790**	<50	<50	**1,790**
52-12D	Clayey sand with gravel (SC)	0.36	118.5	8,760	**357**	<50	<50	**357**
52-12E	*No core collected*	---	---	8,800	<50	<50	<50	<50

USCS = Unified Soil Classification System; TOC = Total Organic Carbon; TPH = Total Petroleum Hydrocarbons

Table G-4. *Soil Sampling Summary for Gulf Coast Region Salt Cavern Well*

Sensor ID	USCS Designation	Porosity	Bulk Density (pcf)	TOC (mg/Kg)	TPH (mg/Kg)			
					>C12-C28	>C28-C35	C6-C12	C6-C35
1	Clayey gravel (GC)	0.52	115.8	**2,860**	<50	<50	<50	<50
2	*No core collected*	NC	NC	**1,340**	<50	<50	<50	<50
3	Fat clay (CH)	0.57	99.9	**1,960**	<50	<50	<50	<50
4	*No core collected*	NC	NC	NC	NC	NC	NC	NC
5	Clayey sand with gravel (SC)	0.61	108.5	**3,600**	<50	<50	<50	<50
6	*No core collected*	NC	NC	**3,150**	<50	<50	<50	<50
7	*No core collected*	NC	NC	**2,680**	<50	<50	<50	<50
8	*No core collected*	NC	NC	**3,620**	<50	<50	<50	<50
9	*No core collected*	NC	NC	**3,970**	<50	<50	<50	<50
10	*No core collected*	NC	NC	**4,030**	<50	<50	<50	<50
11	*No core collected*	NC	NC	**1,900**	<50	<50	<50	<50
12	*No core collected*	NC	NC	**4,750**	<50	<50	<50	<50
13	*No core collected*	NC	NC	**5,260**	<50	<50	<50	<50
14	Fat clay (CH)	0.53	113.4	**3,350**	<50	<50	<50	<50
15	*No core collected*	NC	NC	**2,460**	<50	<50	<50	<50
16	*No core collected*	NC	NC	**5,400**	**120**	**132**	<50	**252**
17	*No core collected*	NC	NC	**3,870**	<50	<50	<50	<50
18	*No core collected*	NC	NC	**2,940**	<50	<50	<50	<50

USCS = Unified Soil Classification System; TOC = Total Organic Carbon; TPH = Total Petroleum Hydrocarbons